Austrian Journal of Technical and Natural Sciences

№ 1–2 2018
January – February

PREMIER
Publishing

Vienna 2018

Austrian Journal of Technical and Natural Sciences

Scientific journal

№ 1–2 2018 (January – February)

ISSN 2310-5607

Editorial office Premier Publishing s.r.o.
Praha 8 – Karlín, Lyčkovo nám. 508/7, PSČ 18600

E-mail: pub@ppublishing.org

Homepage: ppublishing.org

Austrian Journal of Technical and Natural Sciences is an international, German/English/Russian language, peer-reviewed journal. It is published bimonthly with circulation of 1000 copies.

The decisive criterion for accepting a manuscript for publication is scientific quality. All research articles published in this journal have undergone a rigorous peer review. Based on initial screening by the editors, each paper is anonymized and reviewed by at least two anonymous referees. Recommending the articles for publishing, the reviewers confirm that in their opinion the submitted article contains important or new scientific results.

Premier Publishing s.r.o. is not responsible for the stylistic content of the article. The responsibility for the stylistic content lies on an author of an article.

Instructions for authors

Full instructions for manuscript preparation and submission can be found through the Premier Publishing s.r.o. home page at:
http://www. ppublishing.org.

Material disclaimer

The opinions expressed in the conference proceedings do not necessarily reflect those of the Premier Publishing s.r.o., the editor, the editorial board, or the organization to which the authors are affiliated.

Premier Publishing s.r.o. is not responsible for the stylistic content of the article. The responsibility for the stylistic content lies on an author of an article.

Included to the open access repositories:

Typeset in Berling by Ziegler Buchdruckerei, Linz, Austria.
Printed by Premier Publishing s.r.o., Vienna, Austria on acid-free paper.

Section 1. Medicine

Hudojberdiev Olloqul Isoqovich,
pro-rector, Tashkent pharmaceutical institute,
Hadzhieva Umida Abdulxaevna,
senior research associate,
Uzbek chemico-pharmaceutical scientific and research institute,
Madzhitova Dildora Umarkhanovna,
junior research associate,
Uzbek chemico-pharmaceutical scientific and research institute,
Azizov Umarkhon Mukhtorovich,
deputy director, professor.
Uzbek chemico-pharmaceutical scientific and research institute,
E-mail: shodman@mail.ru

WORKING OUT OF THE METHODS OF QUALITY CONTROL AND STANDARDIZATION OF THE DIURETIC PREPARATION OF "EKUSTIM" CAPSULES

Abstract: "Ekustim" capsules have been standardized according to the requirements VFM on such indicators as the description, authenticity, solubility, average weight, desintegration ability, microbiological cleanliness and quantitative definition. On the basis of the results of conducted researches the project of worldwide officinal article is made.

Keywords: a dry extract and capsules of "Ekustim", quality monitoring methods, standardization, average weight, desintegration ability, dissolution, microbiological cleanliness, quantitative definition and metrological characteristics.

Synthetic medical products which applied now as diuretics and sell in chemist's network of the ROU basically are delivered on import and are expensive.

Necessity of working out new diuretic preparations are caused by a great demand of public health services for the cheap domestic medical products which have no side effects.

In this respect phytogenesis preparations are more preferable, as they affect more softly, they are better tolerance, in most cases do not cause an allergy and may be applied long without side effects. However, an essential lack of these preparations is low concentration of yaayceшtпп beginning in those recommended medicinal forms (teas, infusions, broths) and accordingly, small efficiency in clinical practice. In this connection obtain of dry extracts from plants with allocation of the basic effecting substances allows to remove the specified lacks. Reception of dry extracts from medicinal vegetative raw materials provides the big profitability and rationality of its use as the maximum output of dietary supplements in this case is reached, pharmacotherapeutic efficiency of

preparations raises at the expense of possibility of its dispensing.

Earlier we had been developed technology of reception of a dry extract "Ekustim" (Urostim) consisting of a mix of dry extracts of the following 8 herbs: grasses of alhagi false, grasses of erva woolly, grasses of a field horsetail, grasses of ground burnut, florets of silvery yarrow, seeds of cucumbers, columns with corn silk and naked licorice, for getting capsular medicinal form [1–2].

Now we developed the technology of getting of "Ekustim" capsules in the form of a capsule by 0.35 gram, in following structure:

Dry extract "Ekustim"	– 0.350 g;
Microcrystalline cellulose	– 0.095 g;
calcium stearate	– 0.005 g;
Average weight	– 0.450 g.

Research objective. The purpose of the present research is working out of a quality monitoring methods and standardization of "Ekustim" capsules.

Experimental part. An investigated preparation standardized according to the requirements of GF XI on the following indicators: description, authenticity, average weight, desintegration time, dissolution, microbiological cleanliness, quantitative definition. Capsules of "Ekustim" represent the firm of gelatinous capsules in the size "0" containing deep brown granule with a specific smell.

Authenticity establishment was conducted on qualitative reactions to the basic acting substances: the sum of flavonoidsов and hardening agents.

450 mg of a powder of contents of capsules of a preparation are placed into a measured flask by volume of 25 ml, add 10 ml of water, mix and lead the volume by purified water to a mark and filtered through the paper filter of GOST(120226–76) (solution A). To 2 ml of the received filtrate add 5–6 drops of 5% spirit solution of iron (III)-chloride; a green coloring occur (tannins).

450 mg of a powder of contents of capsules of a preparation are boiled during 5 minutes with 20 ml of water and is filtered. To 5 ml of a filtrate add 3 ml of 1% spirit solution of aluminum chloride; flavovirent colouring occur (flavonoids).

Average weight and deviation from average weight of contents of capsules. The average weight of contents of one capsule should be from 405 mg to 495 mg. The deviation from average weight of separate capsules contents should be ± 10% at 18 capsules and ± 25,0% (but no more) at 2 capsules. During the conducted tests it is established, that all capsules meet these requirements.

Definition of desintegration time of capsules were conducted by a technique described in GF XI edit [2, P. 24]. Thus all tested capsules withstand general requirements of GF XI and of have completely broken up within 15 minutes.

One of the basic indicators of quality of capsulated medical products is the test for dissolution which simulates destiny of a preparation in a gastroenteric path.

Definition of solubility of a preparation was conducted according to the requirements of GF XI, edit. [2, P. 159].

By one capsule are placed to each of 6 baskets, a basket was immersed in the vessel containing 500 ml of purified water, with temperature $(37 \pm 1)^{\circ}$C and switch on the device. After 45 mines pass select test from the vessel centre and filter through the paper filter "Dark blue tape". To 250 ml of a filtrate add 25 ml of anilic sulpho-acids and titrated with 0,02 mol/l solution of $KMpO_4$ up to golden-yellow coloring.

Control experience is conducted in parallel. 500 ml of water, 25 ml of anilic sulpho-acids. 1 ml 0.02 pier/l of solution of $KMпO_4$ corresponds to 0.004157 g of tannins in recalculation to tannin.

The content of tannins (X), in% conversion is calculated as per the following formula:

$$X = \frac{(V - V_1) \cdot 500 \cdot 4.15 \cdot K \cdot 100}{17.5 \cdot 250}$$

Where:

V – Volume of a solution of potassium permanganate (0,02 mol/l), spent to titration of the examined solution, ml;

V_1 – Volume of a solution of potassium permanganate (0.02 mol/l), spent to titration in control experiment, ml;

4.15 – the quantity of tannins corresponding to 1.0 ml of 0.02 mol/l of $KMnO_4$ solution;

17.5 – the declared quantity of tannins in one capsule, mg;

K – correction factor.

The quantity which has passed to the medium of dissolution of tannins should be not less than 75%.

Loss in weight drying was defined on GF XI. Nearby 1.0 g (exact weighed portion) of granules of capsules contents was dried at temperature 100–105 °C to constant weight. Loss in weight makes 3–5%.

Microbiological cleanliness of preparation was estimated under the requirements of GF XI, edit. [2, P. 193] "Methods of microbiological control of medical products" and amendments № 2 dated 25.09.20056 a category 3B at these experiments conducted in five series the satisfactory results corresponding to specified requirements were received.

Quantitative definition of sum of flavonoids were conducted by the technique described in XI, edit [2, P. 324].

450 mg (exact weighed portion) of the powder of contents of capsules are placed in a flask with capacity of 100 ml, add 50 ml of 50% of a solution of hot ethyl spirit and mixed. After cooling at a room temperature, solution volume lead up by the same solvent to the mark and filter through the paper filter (solution A). 3.0 ml of a solution place in a flask by capacity of 25 ml, add 3.0 ml of 2% chloride aluminum, 1 drop of the diluted acetic acid and lead up volume of a solution of 96% ethyl spirit to the mark. A solution is mixed and placed in a dark place. After 40 minutes pass, optical density of the received solution is measure on spectophotometer at length of a wave of 400 nanometers, in a ditch with thickness of a layer of 10 mm. The solution prepared in the same way, but without adding of a solution of chloride aluminum is used as a comparison solution.

Optical density of a rutin solution of the standard sample (*SS*), prepared similarly to the tested solution is measured in parallel.

The sum of flavonoids content (X), in mg in one capsule, in equivalent to rutin is calculated as per the formula:

$$X = \frac{D_1 \cdot a_0 \cdot 100 \cdot 25 \cdot 1 \cdot b \cdot 1000}{D_0 \cdot a_1 \cdot 3 \cdot 100 \cdot 25} = \frac{D_1 \cdot a_0 \cdot b \cdot 333.3}{D_0 \cdot a_1},$$

Where:

D_1 – optical density of a solution of tested sample;

D_0 – optical density of a solution of the standard sample of rutin;

a_1 – Weight of weighed portion of tested sample, in mg;

a_0 – Weight of weighed portion of the standard sample of rutin, in mg;

b – Average weight of contents of one capsule, in mg.

Note. *Preparation of a solution of the standard sample of rutin.* About 0.05 g (exact weighed portion) of rutin (FC42 Uz-0137–2007), preliminary dried up at temperature (130–135° C) during 3 hours is placed in a measured flask with capacity of 100 ml and dissolved in 85 ml of 96% of ethyl spirit at heating on a water bath. After cooling at a room temperature solution volume lead up by the same solvent to a mark and mixed. 1.0 ml of the received solution is placed in a measured flask with capacity of 25 ml and further make the same way, at preparation of the tested solution beginning from words "… add 3.0 ml of a solution of 2% aluminum chloride …" to "… without adding a solution of aluminum chloride. A period of storage of a solution is1 month.

Preparation of a solution of 2% aluminum chloride.

2.0 g of aluminium chloride (GOST 3759–75) is placed in a measured flask by a capacity of 100 ml, dissolved in 96% of ethyl spirit and lead up solution volume by the same solvent to the mark. A period of storage of a reactant is 3 months.

Results of the analysis are given in table 1.

Table 1.– Metrological characteristics of a technique of quantitative definition of the sum ща flavonoids of "Ekustim" capsules

Content of a sum of flavonoids,%	metrological characteristics
5.8	$f = 4$; $X_{ср} = 5.88$; $S^2 = 0.007$; $S = 0.0837$
5.9	$S_x = 0.0374$
6.0	$T(95\%.4) = 2.78$
5.8	$\Delta X = 0.2326$; $\Delta X_{ср} = 0.1040$; $\varepsilon = 3.95\%$
5.9	$\varepsilon_{ср} = 1.77\%$

Apparently from (table 1), Content of flavonoids fluctuates in one capsule within 5.8–6.0 mg. Therefore not less than 4.5 mg was fixed as the norm of the content of the sum of flavonoids in one capsule.

Content of tannins. 450 mg (exact weighed portion) of a preparation is placed into a measured flask by capacity of 250 ml, add 100 ml of water, dissolved, lead up to a mark by water, mix. 25 ml of the received solution is transferred to a conic flask by capacity of 1 liter, add 750 ml of water, 25 ml of a solution of anilic sulpho-acid and titrate at mixing with 0.02 mol/l solution of $KMnO_4$ up to golden-yellow color.

Control experiment are held in parallel. 750 ml of water, 25 ml of anilic sulpho-acid.

The content of tannins (X), in% conversion are calculated as per the formula:

$$X = \frac{(V - V_1) \cdot 0.004157 \cdot 250 \cdot 100}{a \cdot 25},$$

Where: V – Volume of a solution of potassium hypermanganate (0,02 pier/l), spent for titration of the tested solution, ml;

V_1 – Volume of a solution of potassium hypermanganate (0.02 pier/l), spent for titration in control experiment, ml;

a – mass of weighed portion of a preparation in gram;

0.004157 – content of tannins corresponding to 1 ml 0.02 mol/l of $KMnO_4$ solution, g.

Apparently from (table 2), the content of tannins in one capsule fluctuates within 6.3–6.5%, Therefore the norm of the content of tannins has been fixed not less than 5%.

Table 2.– Metrological characteristics of a technique of quantitative definition of the sum ща flavonoids of "Ekustim" capsules

Content of sum of tannic,%	metrological characteristics
6.3	$f = 4$; $X_{ср} = 6.38$; $S^2 = 0.007$; $S = 0.0837$
6.5	$S_x = 0.0374$
6.4	$T(95\%.4) = 2.78$
6.4	$\Delta X = 0.2326$; $\Delta X_{ср} = 0.1040$; $\varepsilon = 3.64\%$
6.3	$\varepsilon_{ср} = 1.63\%$

Table 3.– Numerical indicators of "Ekustim" capsules

Name of index	Norm for "Ekustim" capsules
1	***2***
Description	Hard gelatin capsule of size 0. Contents of capsule granule deep brown with characteristic smell.
Identity	Reaction with 1% spirit solution of aluminum of chloride there is a flavovirent coloring (flavonoids). Reaction with 5% spirit solution of iron (III)-chloride; there is a green coloring (tannins)

1	*2*
average weight and deviation from average mass of capsules content.	Should be from 405mg to 495 mg
desintegration time	No more than 20 minutes
solubilization	No more than 75%
content flavonoids in equivalent to rutin	Not less than 4.5 mg
content of hardening agent	Not less than 5%

Proceeding from results of the analysis of "Ekustim" capsules we establish the norms of numerical indicators regulating its quality (tab. 3).

Expiration date of "Ekustim" capsules is studied according to OST 42–2–70 in natural conditions and it is established, that it makes more than 2 years. On the basis of the given experiments, the project of time of officinal articles on "Ekustim" capsules is developed.

References:

1. Azizov U. M., Hadzhieva U. A., Madzhitova D. U., Hudojberdiev O. I. / Standardization of a dry extract "Urostim" // Pharmaceutical magazine.– Tashkent,– 2017.– No. 2.– P. 51–54.
2. Azizov U. M., Hadzhieva U. A., Madzhitova D. U., Hudojberdiev O. I. / Creation and working out of the technology of "Urostim" diuretic agent on the basis of a combination of local herbs // Pharmaceutical magazine.– 2017.– No. 3.– P. 98–102.

Section 2. Food industry

Ashurov Furqat Baxromovich,
Bafoyeva Guljamol Nusratovna,
teachers of Bukhara engineering technological institute, Uzbekistan.
Abduraxmonova Saidakbar Abduraxmonovich,
teacher of Tashkent chemical, technological institute, Uzbekistan.
Hamroyev Elmurod Ortiqnazarovich,
Karshi Engineering Economics Institute
E-mail: elmur.1990@mail.ru

COMPATIBILITY OF COTTON CONFECTIONARY FAT WITH NATURAL COCOA BUTTER

Abstract: The article deals with themethods ofhydrogenationand perietherification, the opportunity ofobtainingcocoa oil substitute, which is close to the natural cocoa oil in its physical and chemical dualities as its freezing and melting temperature, solidity, the content of triglycerids offractionandetc. New scientific, experimental and practical resultsof obtainingcocoa oil substitute have been presented.

Keywords: cotton palmitin, hydrogenation, salomas, cocoa, cocoa oil, perietherification, fatty acid content, triacylglycerids, modification, solidity, its freezing and melting temperature, transisomers, hydrogenate.

Introduction.Due to the raise in price of cocoa butter on the world market, at present many countries produce it's alternate materials on basis of various natural oils (palm, soy and others).

In Uzbekistan the main type of vegetable oil is cotton seed, which is in contrast to other types of oil contains up to 24% of palmitin ($C_{16:00}$) acid. Analogic fatty acid is contained in significant amount in natural cocoa butter [1].

Therefore, obtaining the alternate materials of cocoa butter, particularity confectionary fat, by means of catalytic hygrogenization of cotton seed oil is considered rational.Here with, it is needed to get hydrogenizate(salomas) enriched with 2-oleosaturated triglyceride, as natural cocoa butter contains more than 80% oftriglycerides.Such triglycerides impart to cocoa butter specific properties, high hardness and fusibility (fluidity).

In present time, substitution of cocoa butter for confectionary fat is defined according to the type of producing product (glaze, chocolates ant etc.)

For example, confectionary industry adds to natural cocoa butter up to 25% of alternate materials, as farther increase of the lost worsens the property and quality of the derivable products. Mostly, the content of confectionary fat in choco-

late glazes doesn'ttranscend 15%, that is shown by bloom on the surface and the reducing its storage stability [2].

It is known, that confectionary fat obtaining by hydrogenation of vegetable oils, differs from cocoa butterwith butter-fat acid and triglyceride composition. It contains up to 65% of transisomerisized nosaturated fat acids, that change the type of coagulate and structural – mechanical indicator of cocoa butter, as triglycerides of such fats atcoagulate combine with triglycerides cocoa butter eutectic mixtures, differwith lowlevel ofdilatometricindicatorsand thetemperatureof coagulate [3].

Materials and methods: That's why, we chose for hydrogenization refined cotton oiland cotton palmitin, on the basis which got confectionaryfatand alternate material of cocoa butter, which indicators are shown on the (table 1).

Table1.– Comparative indicators of natural cocoa butter, cotton confectionary fat and alternative materials of cocoa butter got on the basic of palmitin

Names of oils and fats	Melting temperature, ºC	Moisture temperature, ºC		Congelation point, ºC	Butter fat acid composition						Triglecerid composition,%					Mass fraction of trans isomers,%
		15º C	20º C		$C_{14:0}$	$C_{16:0}$	$C_{18:0}$	$C_{18:1}$	$C_{18:2}$	$C_{20:0}$	C_{48}	C_{50}	C_{52}	C_{54}	C_{56}	
Natural cocoa butter (control)	32.9	1100	910	29.8	–	26.0	35.2	35.0	2.8	1.0	0.7	18.8	46.0	33.1	1.4	–
Cotton confectionary fat	37.8	570	350	30.5	0.4	21.0	6.0	64.5	8.1	–	1.8	14.4	29.5	54.0	0.3	63.0
Alternative materials of cocoa butter	37.2	750	530	31.0	0.3	24.1	5.2	62.4	8.0	–	1.7	15.0	29.0	54.1	0.2	58.7

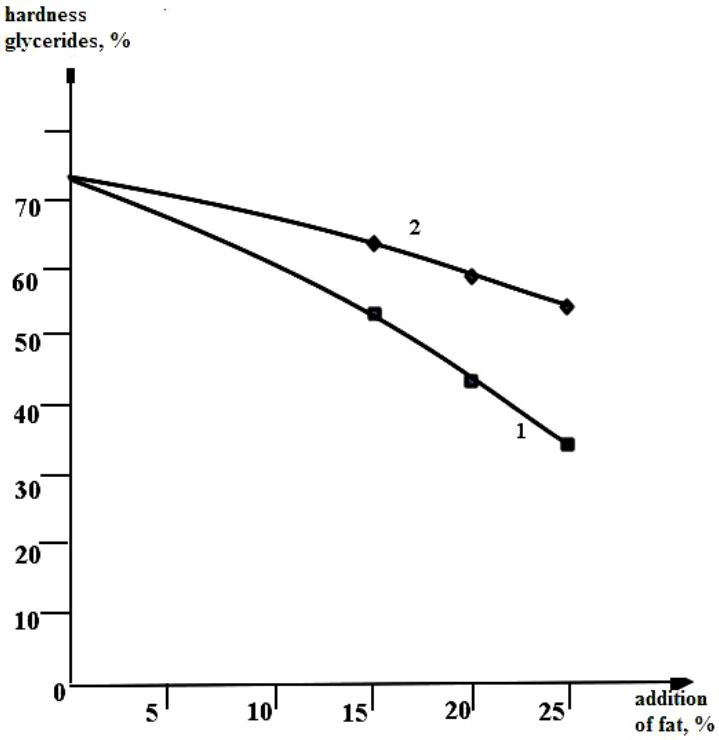

Figure 1. Dilametric characteristics ofisohard mixtures of confectionary fat [1] and alternative material of cocoa butter [2] with cocoa butter

Comparative indicatorsof natural cocoa butter, cotton confectionary fat and alternative materials of cocoa butter got on the basic of palmitin.

It's seen on the (table 1), that producing by oil –fat industry confectionary fat on the basis of hydrogenization of cotton seed oil differs much from natural cocoa butter with fat-acid and triglyceride content. If in the last one there is no transizomers, that in confectionary fat their portion is 63%.

At that, the temperature of melting of confectionary fat in accordance with natural cocoa butter increase 5.1° C and in the contrary, its hardness is about 2 times lower than the last ones.

Considering this, cotton palmitin hard fraction of cotton oil, rich (till 24%) in palmitin ($C_{16:00}$) acid [4].

It is seen on the table.1, that alternative material of cocoa butter, gotten by means of hydrogenization of cotton palmitin in comparison with cotton seed confectionary fat, it has more high (750 at 150 ° C) hardness and comparatively low temperature of melting. Differential indicators exist in fatty acid and triglyceride composition of offered alternative material of cocoa butter, in comparison with confectionary fat and natural cocoa butter.

We were studied the compatibility of cotton confectionary fat and offered alternativematerial of cocoa butter with cocoa butter means of their introduction till 25%.In this, there defined the dilatometric characteristic and the temperature of congelation of gotten mixtures in Jenson's apparatus.

It is shown on (fugure 1), that changes of the content of hard triglycerides in the mixtures at definite temperature visually characterizes compatibilities of cotton confectionary fat and offered alternative material of cocoa butter with cocoa butter. As it is seen, the addition to the last ne the confectionary fat and alternative material of cocoa butter bring to different decreases of the content of hard glycerides at 20 and 25 ° C. For example, at 20 ° C the confectionary fat has coexistence 8% that is not enough in our opinion.

With the addition to the mixture the confectionary fat for substitution 25% of cocoa butter, fraction of total mass of hard glycerides reduces from 73.2% till 38.7%, thatis not reasonably for the climate of Uzbekistan. Conversely, the usage of offered alternative material of cocoa butter in such amount brings to the reducing of fraction of total mass of hard glycerides from 73.2% till 55.4% that is considered acceptable from the point of their coexistence with cocoa butter.

Table 2. – Dilatometriccharacteristicsofmixturesofcottonconfectionaryfa tandalternativematerialofcocabutterwithnaturalcocoabutter

Names and fat composition	**Content,%**	**Indicators of dilatation at ° C**							**Indicators of hardening of Jenson**			
		10	**15**	**20**	**25**	**30**	**35**	**40**	t_{max}, ° C	t_{min}, ° C	**Temperature rise, ° C (Δt).**	**The duration of the pour, min.**
Natural cocoa butter (control)	100	60.9	64.5	57.4	72.0	44.0	3.5	1.0	29.8	25.2	4.6	45
Mixtures:												
Cotton confectionary fat	15	60.1	57.8	51.6	42.5	16.9	4.0	3.5	27.5	24.0	3.5	57
Natural cocoa butter	85											
Alternative material of cocoa	15	62.4	62.3	57.5	45.3	17.0	2.2	2.0	28.2	24.2	4.0	48
Natural cocoa butter	85											

We've investigated dilatometric characteristics of explored mixtures of fats at temperature from 0°C till 40 ° C gotten results are shown on (table 2). With this, for evaluating the influence of input of additive compounds of fat on technological properties of natural cocoa butter was investigated changes of its congelation in Jenson's apparatus.

Dilatometric characteristics of mixtures of cotton confectionary fat and alternative material of cocoa butter with natural cocoa butter.

In confectionary industry for introducing the technological process of enrobing, its necessary that the temperature of congelation no more than 60 min.

As its seen in the (table 2) in comparison with natural cocoa butter for investigated mixtures of fats typically decreasing of temperature beginning of crystallization (t_{min}) and finishing of crystallization (t_{max}) exactly, congelation temperature, but at this temperature rise practically doesn't change (Δt). According to continuation of crystallization, all investigated mixtures satisfy a claim, but their congelation temperature below 28 ° C.

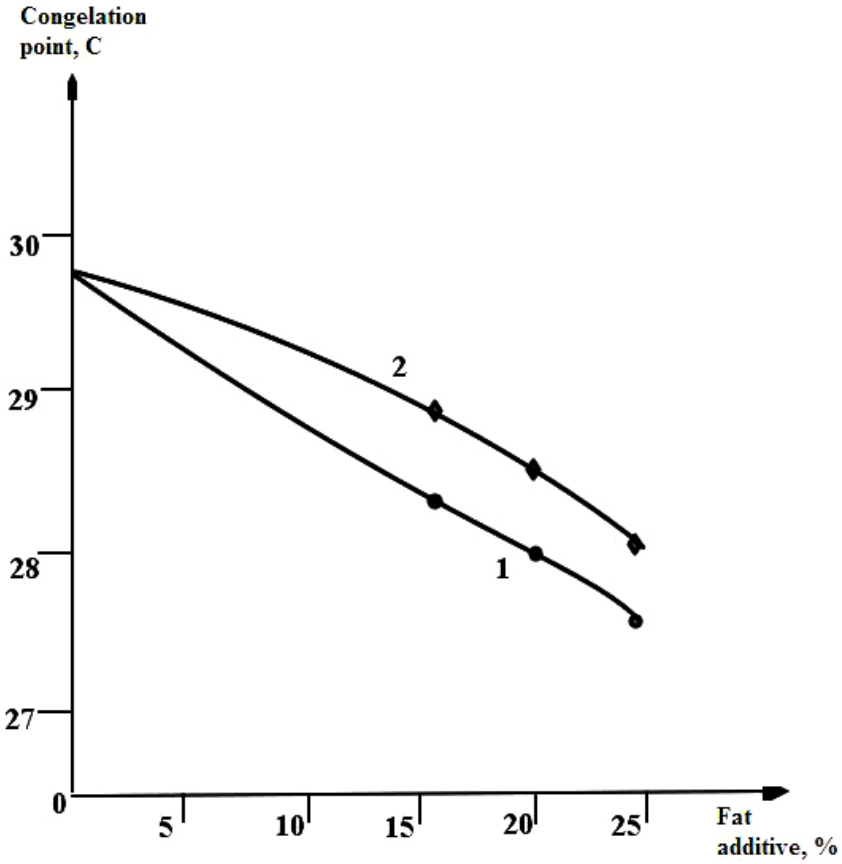

Figure 2. Changes of crooked freering of cotton confectionary fat [1] and alternative material of cocoa butter [2] depending on their content in the mixture with natural cocoa butter

Changes of congelation temperature of investigated mixtures of fats depending on composition of additive compounds are shown on the (Figure 2).

From the (Figure 2) it is shown that, the addition to natural cocoa butter the cotton confectionary fat and alternative material of cocoa butter brings to reasonable decrease of congelation temperature of the first one. Here with, it's not discovered correlation of crooked congelation of temperature of mixtures of fats from composition trans-isomerized fatty acids in cotton confectionary fat and alternative cocoa butter.

Results and Discussion: So, investigations showed that the addition of cotton confectionary fat and alternative material of cocoa butter to the mixture composition with natural cocoa butter brings to the changes of physic-chemical and technological properties of the last one. At that, change that is more significant is observed at addition of 25% the mixture mass of cotton confectionary fat to composition of natural oil that offered alternative material of cocoa butter. That's why its recommended to substitute part of cocoa butter for cotton confectionary fat with the amount till 15% and offered alternative material of cocoa butter till 25% from getting mass of fatty mixture.

References:

1. Majidov K. H., Vasiyev M. G. "Getting the grease mass for confectionary fats" Oil-fat industry,– 1982.– No. 9.– P. 2–4.
2. Pavlova I. V., Belova A. B., Nosovitskaya F. P. "Alternative materials of cocoa butter and confectionary fats." Technological requirements. TR9140–23600334534–99. St.: VNIIF,– 1999.– 15 p.
3. Pavlova I. V. Alternative materials of cocoa butter and confectionary fats. Monography. St.: VNIIF.– 2000.
4. Arutyunyan N. S., Arisheva E. A., Yanova L. I., Zaharova I. I. Melamud N. A. "Technology of oil refinery" // – M.: Agropromizdat,– 1985.– 358 p.
5. Shumateva N. F., Bizhanov F. B. Obtaining confectionery fats, analogues and substitutes for cocoa butter. Alma-Ata: Science,– 1986.– 63 p; Normanova R. D., Ermakova T. P., Redko T. S. Solid fats used in confectionery production abroad.– Moscow: TsNTIITIEipishcheprom,– 1976.– No. 11.– P. 1–7.
6. Redko T. V., Smirnova A. T., Grauerman L. A. Manufacture of a cocoa butter substitute abroad.– M. TSNIIITEIPP,– 1974.– 16 p.
7. Manufacture of cocoa butter substitutes for the confectionery industry from vegetable raw materials / Redko T. V., Pavlova N. V.– Moscow: AgroNIIETEIpP,– 1989. Issue 12.– P. 1–32.
8. Tillaeva G. U. Development of technology for obtaining a cocoa butter substitute from cotton salomi by crystallization in a solvent. Author's abstract of the Candidate of Science.– Tashkent, Tash PI,– 1989.– 24 c.
9. US Pat. No. 4268527 Method for the production of a cocoa butter substitute / Matsuo Jakaharu, Sawamura Norio, Hashimoto Vu Kio, Hoshida Wataru // Declared 7.11.79.Op.19.05.81. Priority 21.11.78. № 53–144736. Japan. RJK,– 1982–5.R.7417. P. 14.
10. Bafoyeva G. N., Ashurov F. B., Abdurakhimov S. A. Cotton palmitin is a valuable raw material for obtaining a cocoa butter substitute // Oil and fat industry.– 2012.– No. 1.– With. – P. 29–30.

Section 3. Rolnictwo

Tukhtaeva Khabiba Toshevna,
Teacher, Tashkent institute of irrigation
and agricultural mechanization engineers
of the Bukhara branch, Uzbekistan, Bukhara city
E-mail: Habiba1078@mail.ru

MOBILIZING LOCAL WATER RESOURCES FOR THE DEVELOPMENT OF LOCAL DESERT IRRIGATION SYSTEMS

Abstract: The questions of land and water resources of the Central Kyzyl Kum. Undrained basins Kizilkum become places reset collector drain, resulting in large areas of pastures and hayfields are subject to flooding, flooding in and out of traffic. The above packages of measures under the conditions of their implementation will contribute to the optimization of the environment, prevention of desertification and improve the productivity of desert ecosystems.

Keywords: Geoinformation monitoring, Kyzyl Kum, water resources, land resources, yield, drainage basin, irrigation.

Central Kyzyl natural geographical study of the area is carried out in the framework of regional-scale studies may be considered. This area is different from all other regions of the natural geographical aspects. Its internal structure, some parts of the gap between it and the ground to natural geographic areas to identify and compare the structure and main features of the latter will be achieved through small areas of the landscape. At the same time, we are in a particular landscape, multi-component and the presence of many factors considered emerging dynamic geosystem. Its internal structure, vertical and horizontal, in connection with the forward and reverse, once known natural geographer B. S. Preobrajenskiy idea of mono- and polisystem reflected in the graphical model.

Landscape with a taxonomic value, that is, of course, the area is small, and at the same time as Tract understand morphological unit of geosystem. These geosystems Central Kyzyl district Wednesday formation and development.

Information about regional and typological approach dispersed in various publications and cartographic materials and fragmented. We have reviewed and summarized the results of its application to physical and geographical regionalization and landscape mapping of the Central Kyzyl Kum. Particular attention is paid to the methods and ways of using this approach, representatives of various schools of thought.

To develop the capacity of regional-typological approach developed structural-logic, which summarizes and systematizes the basic idea of it. The contents of this scheme reveals the spectrum of known and potential opportunities for exploring and mapping of geosystems. It seems that the development of regional and typological maps using structural and logic can be seen not only as a result of logical operations, preferring one way or another their preparation, but also as a system of analysis and synthesis of territorial differentiation and integration of geosystems of various types and grades.

Regional and typological approach extends and complements the cartographic method of research, and its structural logic reveals the methodology of creation and the use of regional and typological maps for landscape sphere of knowledge and solutions on this basis in various applications.

In Kyzyl Kum, occupying nearly a quarter of the area of the country, inhabited by more than 30% of the population. It produces the bulk of the gold country, graze more than 20% of sheep and 35% of the total herd of karakul sheep. Initiated the development of phosphorite deposits.

Under these conditions, the most important measure to reduce the social, socio-political tensions could be the solution to the problem of water supply and water beautification desert and pasture areas, as well as the adoption of measures to improve the economy of livestock farms.

Land Fund desert and pasture areas suitable for irrigation of more than 1.5 million hectares Water resources are estimated at over 1 billion. m^3, including withdrawals from. Amuriver. However, most of the available water resources, including enhanced mineralization, with appropriate water treatment and the development of specific technologies can be used for drinking purposes and irrigation and water suppley.

Solving the problem of the use of local water resources is particularly important for the creation in each of the areas of Kyzyl Kum at least 1–2 thousand ha. Irrigated land fund for the production of fruits and vegetables and fodder for livestock.

Irrigated agriculture in the artesian wells is limited to no more than 2 thousand ha. While not common irrigated soil, and random, which turned order, stretches of sand, shallow gray – brown soils of ground and even education. In the Central Kyzyl Kum projected groundwater reserves are 836.37 thousand. m^3/day; are approved by 516.79 thousand. m^3/day. They are mainly concentrated in Minbulak and Kanimekh areas.

At the moment of drainage water disposed to the development of territories, including natural and anthropogenic water lakes are about 1.2 billion. m^3/year. Commercial use of these water resources will contribute to the development of plant and other industries in the Central Kyzyl Kum.

To dramatically increase the efficiency of the use of temporary surface runoff is necessary (as the base for calculations) to know the conditions of formation and modes of this flow. At the same time, the data of the flow alone are not enough to solve the problem. Need to develop improved methods for the concentration of runoff in localized areas and water conservation techniques, providing the opportunity to use it with respect to the motor.

Temporary runoff is formed when the intensity of rainfall in the catchment area is greater than the absorption capacity of the soil cover and the accumulation of moisture in micro relief. Ceteris paribus, the greater the intensity of rainfall and the number and the smaller absorption capacity of soils, the larger the surface runoff. Runoff in watersheds begins to form, depending on the degree of hydration and mechanical composition of the soil, the amount and intensity of rain. As well as the size of the catchment area and the terrain.

To improve the efficiency of the use of temporary surface runoff is necessary (as a base for calculation) to examine the conditions of formation and treatment of runoff. But there is not enough data, should develop improved methods of concentration drain on localized areas and water conservation techniques, providing the possibility of relatively long-term use.

To this end, we performed a morphological analysis of the territory on topographic maps and satellite images. This will highlight the positive and negative elements of the relief with the altitude and slope areas. In Kizilkum allocated system representing the watersheds of different orders; clearly limited area of their formation, transit and accumulation that allows you to identify components of their migration flows. For the Central Kyzyl Kum mapped plastics relief which can determine the formation of an in-

terim surface runoff catchment area, the potential reserves of these waters.

Method allows you to display on the map ordered, genetically informed systemic structure of the earth's surface, the actual structure of the soil cover, the other components of nature. And lithodynamic flows, areas of their formation, transit and accumulation of soluble components.

On pastures where there is fresh groundwater is divided into three areas:

1. District undrained (slope 0–5°), where soils are composed of sandy and sandy sediments, groundwater strongly mineralized, with precipitation per 15 mm rain runoff is formed, there is flooding pastures unreasonabley.

2. The area of the scattered drain (slope-sided, above 5°), where soils are composed of loamy sediments. Watershed runoff temporary unilateral, with precipitation at a rain of 5 mm with the intensity of 0.075 mm / min, humidity 15% loamy soil runoff begins, clay it occurs at an intensity of 5 mm to 0.01 mm/min.

3. The area of concentrated runoff (slope from two sides above 5°), where soils are composed of loamy and clayey sediments, temporary catchment runoff with two slopes, a closed-sided flow direction. During precipitation one 5mm rain intensity 0,075 mm/min, at a humidity of 15% loam soil runoff begins and clay-at 0.01 mm/min.

Calculations catchment, located in the area have shown that the amount of surface runoff in a single rain (total precipitation – 10 mm, the average rainfall intensity of 0.05 mm/min) with a catchment area of 270 km^2, loamy deposits is about 518 thousand. m^3 of water with the same area with rain intensity of 0.1 mm/min. You can collect up to 1296 thousand. m^3 of water. Similar calculations were performed for sites with different lithological structure, with different amounts of precipitation for rain, varying intensity and different in footprint watersheds in different geomorphological conditions of the Central Kyzyl Kum.

The use of even a small fraction of the potential water resources would improve, and in some desert areas with sustainable drinking water and pasture by storing water in the underground natural reservoirs and surface vessels.

References:

1. Reteyum. Geographical zoning and allocation of geosystems questions of geography.– Moscow.– 1975.– 98 p.
2. Stepanov I. Time and space science of soils. Nedokuchaevskaya soil science.– Moscow: Science,– 2003.– 184 p.
3. Sochava V. B. Introduction to the Study of the ecosystems.– Novosibirsk: Nauka,– 1978.– 317 p.

Section 4. Technical science

Agzamova Hilolahon Avazovna,
JSC "UzLITIneftgaz", engineer,
Laboratory "Industrial safety"
Khaitov Odiljon Gafurovich,
Tashkent State Technical University,
Head of the department "Mining",
Candidate of Geological-mineralogical Sciences.
E-mail: javokhir.toshov@yandex.ru

STATUS AND PROSPECTS ASSOCIATED GAS UTILIZATION AT THE FIELD UZBEKISTAN

Abstract: The article provides information about the projects and the ongoing work on the utilization of associated gas and reduce emissions of harmful substances into the atmosphere in the fields of Uzbekistan.

Keywords: oil and gas, hydrocarbon, transported, utilization, process.

In the years of independence, as in most countries of the world, environmental protection has legislatively been put in the rank of state policy. Adopted policy documents and legislation to improve the environmental situation, including the laws of the Republic of Uzbekistan "On Environmental Protection" (1992). "On Environmental Impact Assessment" (2000.) and others.

Uzbekistan joined the international institutions of the UN, OSCE and others, ratified more than 9 environmental conventions and related protocols of their development, has signed 12 international agreements on cooperation in the field of environmental protection, including the "Greenhouse Gas" (1993). And "Kyoto Protocol" (1999). As you know, Uzbekistan is the largest country in terms of population in Central Asia with a vibrant economy [1, P. 72–75].

The energy potential of Uzbekistan is mainly associated with significant resources and reserves of oil and gas. Mining and gas reserves, Uzbekistan ranks third among the CIS countries, and is one of the largest of its exporters. Development of oil and gas industry relies on a good raw material base, which allows the country to provide not only the needs at the expense of their resources, but also contractual commitments to export natural gas in the near and far abroad.

Currently in the territory of Uzbekistan five oil and gas regions are known (Ustyurt, Bukhara-Khiva, Surkhandarya, Hissar and Fergana) and two promising (Khorezm and Mid-Syr Darya). These oil and gas regions as of 01.01.2012 discovered 242 oil and gas fields, of which 104 are in development, 66 prepared for the development of 72-in intelligence 121. Of the 68 producing fields contain deposits of oil, more than half belong to the category of oil and gas or gas-oil, ie contain gas caps. Reduction in reservoir pressure and gas lift wells on translation method of operating on the main fields of the Republic, such as Kokdumalak, North Urtabulak, Crook, South Kemachi, Umid and others led to the increase in the

volume of produced gas. Up to 2005. a significant amount of gas (about 5 billion cubic meters) flared, increasing emissions of air pollutants and greenhouse gas emissions.

It should be noted that the impact of global climate change is becoming a big challenge for the world. It is estimated that every year in the world burned 140 billion cubic meters of associated gas. In this regard, the utilization of associated gas produced in order to prevent negative impacts on the environment of emissions and resource has become one of the priorities of many oil-producing countries, in particular the implementation of investment projects in the oil and gas industry of Uzbekistan [2, P. 16–22]. In the preparation and implementation of these investment projects significant impetus was the liberalization of legislation in terms of attracting foreign investment. So, in 2000. was issued Presidential Decree "On measures to attract foreign direct investment in the exploration and production of oil and gas", would grant benefits to investors to compensate for their geological risks, in 2001. Law "On Production Sharing Agreements (PSA)", expands the rights of investors. In 2005. enacted important to stimulate investment law "On additional measures to stimulate the attraction of direct foreign investments", significantly broadens the scope of application of tax and other benefits.

The first investment project for utilization of associated gas was supplied to the gas condensate field Kokdumalak providing basic oil and condensate Republic. During the preparation of oil and gas condensate allocated petroleum gases and gases weathering flared polluting the atmosphere and increasing greenhouse gas emissions. In order to reduce flaring of associated gas and reduce harmful emissions into the atmosphere, as well as additional volumes of marketable gas and liquid hydrocarbons, in accordance with the decree of the Cabinet of Ministers of the Republic of Uzbekistan beat a joint venture "Kokdumalakgaz" for the investme [nt project "Disposal of produced gas Kokdumalak the field". Implementation of the project was carried out in three stages: Stage 1 (2005).– Construction and commissioning of DCS (booster station) –1 line with the turbo-compressor units with a total capacity of 32 MW with a daily utilization of associated gas 3.25 million cubic meters; Stage 2 (2007).– Expansion of BCS-1 line and construction of a new BCS-2 with a total capacity of 64 MW with a daily utilization of associated gas in the volume of 9,000,000 cubic meters; Stage 3 (2009).– Construction of BAC –3 line with a total capacity of 48 MW, with a daily utilization of associated gas in the volume of 6.75 million cubic meters.

In the field Kokdumalak gas collection made on collection points, where it comes to the headworks, which is pumped to the inlet pressure complex gas at 10 MPa. At this setting, recycled gas is quenched, where stands a liquid (condensate). The purified gas is supplied to the Mubarek gas processing plant, which is processed and then transported through the main gas pipelines in the direction of exports domestic market. The condensate is fed to the condensate stabilization unit for stabilizing the discharge of condensate and LPG. Stable condensate is sent to Bukhara refinery.

The implementation of the investment project "Disposal of produced gas field Kokdumalak" significantly reduced the volume of flared associated gas, gas degassing units of oil and gas condensate and collection points, to increase the yield of marketable gas, LPG and condensate. The project is an environmental concern and its implementation will significantly reduce emissions of harmful substances into the atmosphere and greenhouse gas emissions. Achieved a reduction in annual emissions of carbon monoxide from 30,643.18 to 3,686.204 tons of nitrogen dioxide from 4752.2 to 1516.606 tons of sulfur dioxide from 4316.99 to 727.246 tons of soot from 2815.34 to 256.196 tons of nitrogen oxide 1190.34 up to 379.545 tons of hydrocarbons 1053.52 to 377.323 tons.

To solve the problems associated gas utilization in the fields of Uzbekistan are also widely used

technical and technological solutions. For example, in the oil and gas fields in the North Shurtan Shakarbulak and by changing the composition of the system design and process equipment utilized by more than 1 million cubic meters of associated gas. In these fields the transition to the joint operation of oil and gas condensate field units allowed to dramatically increase the rate of selection of oil (more than 2 times). At the same time there was a natural increase in GOR and increased volumes of associated gas produced along with oil due to the inflow of gas from the gas-condensate part of the deposit. In the initial gas saturation of the reservoir oil 305 m^3/t exceeded more than 5000 cubic meters per 1 ton of oil, and the wellhead pressure wells 1.5–6 MPa increased to 15.8–21.6 MPa. Height wellhead pressure in the wells allowed oil treatment plants installed and put into operation unit separator for separation and gas under its own pressure (10 MPa) at GS "Shurtan". To block separators were well connected with high wellhead pressure. This allowed only in 2009. of the total volume of associated petroleum gas produced at the field Shakarbulak in the amount 422.3 million cubic meters, disposed of 367 million cubic meters, or more than 86.9%.

At the beginning of 2013 in the fields of Uzbekistan reached recycle up to 75% of produced gas. Work carried out in Uzbekistan on utilization of associated gas and reduce harmful emissions into the atmosphere has been approved by the Global Partnership on burning flare gas reduction GGFR (Global Gaz Flaring Reduction a Publik-Private Partnership). Regional Conference for which the countries of Europe and Central Asia was held in Tashkent on 14–16 June 2012., Where it was considered the experience of Uzbekistan associated gas utilization and implementation of CDM projects in the oil and gas industry.

According to preliminary estimates of consultants GGFR a number of projects for utilization of associated gas categorized perspective, including:

– Utilization of associated gas fields in the North Shurtan, Garmiston, Shakarbulak, Kumchuk and headworks "Shurtan", with the volume of utilization of associated gas 0.69 billion cubic meters per year;

– Utilization of gas processing at the Mubarek gas processing plant, with a projected volume of waste acid gases to 0.7 billion cubic meters per year;

– Utilization of associated gas at a group of fields Arniez, Zevardy, Sardoba, Zheynov with the volume of gas utilized to 0.25 billion cubic meters per year.

These investment projects have been prepared on the basis of the decision of the President of the Republic of Uzbekistan № 1111–525 from 06.12.2006. "On Measures for the implementation of investment projects under the Clean Development Mechanism of the Kyoto Protocol" and in accordance with the Regulation "On the procedure for the preparation and implementation of investment projects under the CDM of the Kyoto Protocol", approved by the Cabinet of Ministers of 10.01.2007g. As a result of the above investment projects planned utilization of associated gas in the oil and gas industry of the Republic of Uzbekistan by the end of 2015 brings to 95%.

References:

1. Hegay L. I. Decrease in ecological risks-a condition of sustainable development of oil and gaz sector of Uzbekistan // Uzbek journal of oil and gaz of Uzbekistan. Special edition. May – 2011.– P. 72–75.
2. Abdullaev G. S., Nurmatov M. R. Greation of reliable raw-material base of hydrocarbons on long-term prospect. Innovations in the field of prospecting works // Uzbek journal of oil and gaz of Uzbekistan. Special edition. May – 2012.– P. 16–22.

Askerova R. I.
Azerbaijan State Oil and Industry University
E-mail: rahimova_mahluqa@mail.ru

RESEARCHES OF OPERATION MODES OF THE FLOW LINES ON THE CASPIAN SEA FIELDS

Abstract: The modes of operation of the flow lines on the "Bulla-Deniz" field (Azerbaijani sector of the Caspian Sea) are investigated. For identifications complications in flow lines, they were grouped in factor productivity, selections from each group were composed and statistically processed. As a result of carried out researches consistent statistical relationship between the indicators of the gas factor and performance has been revealed.

Key words: salt depositions, flow lines, gas factor, line productivity.

Operation modes of flow lines in the system of field storage of well products have always been the subject of scientific and field researches in the direction of the efficiency increase of "layer-well" system — oil storage center. Optimal choice of their operation modes for all distance beginning from oil producing wells to product storage center is very significant for regulating oil extraction and increase of efficiency of oil storage center. Thus, change of pressure in the flow lines.

Alteration of pressures involves change on the wellhead and in its turn it brings to change of extraction indices.

Urgency of the researches of operation modes of flow lines also increases due to various complications taking place in them (precipitation of solid particles, sedimentation of paraffin, salt depositions, initiation of gaseous and aqueous locks and others). The main reasons of appearance of these complications are from one side wrong choice of operation modes of flow lines, from other side inopportune reveal and carrying out engineering measures on the liquidation.

The abovementioned determines significance of the carrying out operative control of operation modes of flow lines in the fields. In the industry practice the work on the cleaning of flow lines is carried out with considerable delay because of lack of effective methods on diagnoses of complications in the earliest phase of their appearance. As a result, of the carried analysis of many years field data, capacity of flow lines practically either isn't restored or is out of order and extra expenditures are required for construction of new lines [1, 2, 3]. Proceeding from it, general researches on storage systematization and analysis of field indices on flow lines operation modes have been carried out to liquidate complications, restore, and possibility of increasing outlet capability of flow lines.

As the object of research 23 flow lines of the "Bulla — deniz" field (Azerbaijan) have been taken and dynamics of the change of average values of the following indices have been analyzed: oil consumption, gas consumption, pressure at the beginning and end of the line, gas factor, average temperature of the flow and productivity of the flow line. All these indices are presented in the Table. Studied lines were divided into two groups due to their productivity on the basis of hyperbolic value of distribution to reveal the flow lines in the operation of which complications occurred [4]. Flow lines with $q_{oil}/\Delta P<92$ *t/day/MPa* productivity refer to the first group, indices with $q_{oil}/\Delta P>92$ *t/day/MPa* productivity were collected to the second group.

After division into groups we proceeded with big probability that complications have occurred in the

lines with small productivity. That's why flow lines have been separately taken on each group: № 9, 65, 43 and 122 — from the first group line; № 61, 57 and 48 — from the second group line. Samples on monthly indices of oil consumption; gas factor and line productivity have been prepared individually. These indices have been processed for establishing static relations between existing methods of data analysis.

The results of data processing have revealed definite regularity in the behavior of the dependence curves of flow line productivity on the gas factor. Thus, for the flow lines of the second group where occurrence of complications doesn't observed (lines N61, 57 and 48) gas factor weakly influences oil consumption change at the same pressure drops. By the other words points plotted on the coordinates of flow line productivity ($q_{oil}/\Delta P$, *t/day/MPa*) and gas factor index (q) are located on the straight line rather accurately (figure, a). As it is seen from the figure increase of gas factor index doesn't considerably influence flow line productivity decreases. Together with it, analysis of dependency of productivity on the gas factor index for flow lines of the group (lines 9, 62, 43 and 122) not showing occurrence of complications has revealed the following stable regularity. In these lines productivity considerably decreases by the increase of gas factor (figure, b).

It can be explained by that due to the complications occurred in the lines, oil consumption decreases, part of the gas dissolves in the sediments and as a result productivity of flow lines reduces.

The result of the carried out researches allow us to determine the following main conclusion that considerable decrease the productivity by gas factor increase is the diagnostic criterion for early revealing of the occurrence of complications in the flow lines and carrying out engineering works on their in-time liquidation.

Table 1.– Dynamics of average values of operational parameters of the flow lines

Flow lineshjjhjhjh Flow lines lineslineslines	*Diameter of line D, m*	*Length of line L, m*	*Rate of oil, q_{oil} tons per day*	*Rate of gas, q_{gas} Cubic meters per day*	*The pressure at the beginning, P_1, MPa*	*Gas factor, q cubic meters per ton*	*The pressure at the end, P_2, MPa*	*Average temperature, S*	*Output of line, t/day/MPa*
1	*2*	*3*	*4*	*5*	*6*	*7*	*8*	*9*	*10*
9	0,102	1250	253	76	5,8	300	2,2	50	70,3
60	0,102	1500	462	72	7,2	156	2,2	45	92,4
67	0,102	1700	410	30	4,5	143	0,8	57	110,8
57	0,102	1500	285	25	6,3	88	4,2	58	135,7
65	0,102	1000	200	46	9,6	230	4,7	44	40,8
62	0,102	1800	150	28	4,4	187	2,0	43	62,5
61	0,102	1250	300	44	6,8	98	3,0	40	107,1
71	0,102	1250	385	44	5,8	114	2,0	47	101,3
34	0,102	1000	450	36	6,0	120	2,2	49	118,4
48	0,102	1250	210	45	3,9	110	1,9	38	105,0
43	0,102	1750	190	21	5,0	110	0,8	37	45,2
122	0,102	1200	181	80	7,0	442	2,0	35	36,2
100	0,102	1200	310	53	4,4	170	2,1	55	134,8

1	*2*	*3*	*4*	*5*	*6*	*7*	*8*	*9*	*10*
84	0,102	1350	220	22	5,1	100	2,0	45	70,9
80	0,102	1250	255	65	4,0	254	1,8	53	115,3
32	0,102	1500	250	47	3,5	188	0,9	53	96,1
45	0,102	1650	225	20	4,7	88	1,2	59	64,3
85	0,102	1750	150	40	4,9	266	3,5	35	107,0
76	0,102	1750	140	38	5,9	271	4,5	29	100,0
39	0,102	1500	60	6	3,7	100	2,3	54	42,8
36	0,102	1400	180	25	4,4	140	2,8	32	112,5
105	0,102	1300	320	39	6,4	310	3,0	42	94,1
17	0,102	1300	230	57	6,0	250	3,5	40	92,0

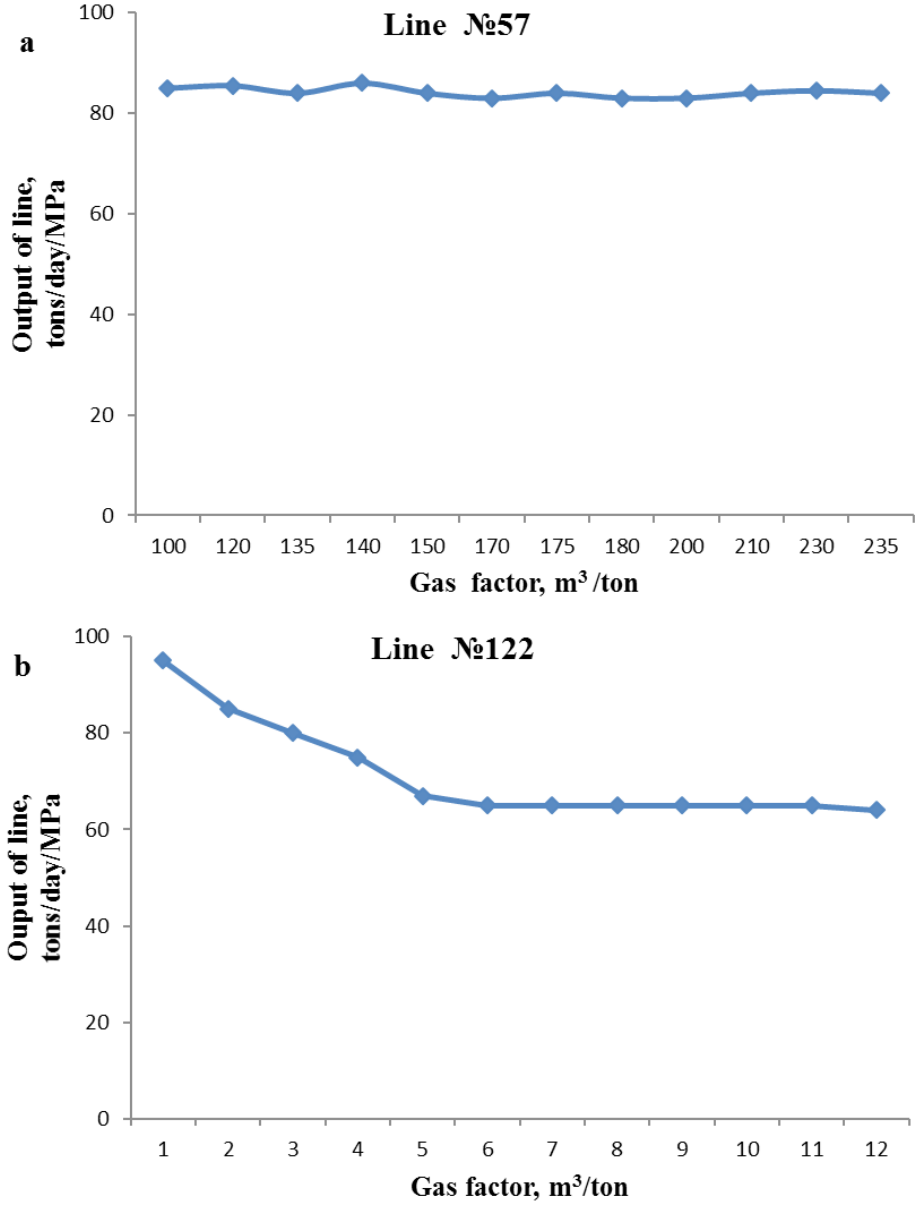

Fiqure 1. The curves of the influence of the gas factor on the output of the flow lines

References:

1. Control of the complications in the storage and preparing of the oil wells products – Collection of scientific works of the Ministry of oil and gas industry SSSR, Ufa, 1989. P. 32.
2. Grisenko A. N., Klapchuk O, V., Xharchenko Y. A.– "Hydrodynamics of gas – liquid mixtures in the wells and pipelines" M. Nedra, 1994. P. 312.
3. Gumerov A. G., Medvedev A. P., Khudyakova L. P. and et all – "Development conception of the system of technical diagnosis of field pipelines" – oil economy N1, 2005. P. 78.
4. "Transport and storage of oil and gas" edited by N. N. Konstantinova, M., Nedra, 1975. P. 175.
5. Gumpator G. G. "Study of the process of storage, transport and prepare of oils in the condition of offshore fields of Azerbaijan." Baku, 1996. P. 235.

Isakov Hayatulla,
candidate of technical sciences, assistant professor of the
Department of Chemistry, Andijan State University
Uzbekistan, Andijan,
E-mail: xayotilla.isakov@bk.ru

ABOUT COORDINATED COMPOUNDS OF ACETATES OF DIVALENT CO, CU AND ZN WITH FURFURYLDICARBAMIDE

Abstract: In this paper, the results are presented by synthesizing the study of complex compounds of divalent cobalt acetate, copper and zinc with furfuryldicarbamide.

Keywords: furfuryldicarbamide, metal acetates, furfural, IR spectrum, complex compounds, derivatogram, thermolysis, thermal effect.

Numerous studies in the literature have been devoted to the synthesis and study of the properties of coordination compounds of various metal salts with carbamide and its derivatives [1; 2]. Coordination of the apical ligands is in many cases carried out through the oxygen atom of the carbonyl group. The furfuryl- dicarbamide molecule contains 7 donor atoms – three oxygen atoms and four nitrogen atoms of primary, secondary amine groups and can form complexes, with metal salts exhibiting a competitive ability for coordination of the metal with acidoligands and water molecules [3].

Objects and methods of research

This report describes the results of the synthesis and study of the physicochemical properties of coordination compounds of acetates of bivalent cobalt, copper and zinc with furfuryl dicarbamide (L).

Synthesis of coordination compounds was carried out by the interaction of saturated aqueous solutions of the corresponding metal acetates and furfury ldicarbamide in a molar ratio I: I with subsequent precipitation of powder precipitates.

Analysis of synthesized compounds on the content of metals was carried out according to [4], nitrogen by micromethod DUMA [5], carbon and hydrogen by burning in an oxygen current.

To establish the individuality of the complexes, radiographs were taken on a DRON-2 installation with a C-antikatode [6].

IR absorption spectra of furfuryldicarbamide and the resulting compounds in the 400–4000 cm^{-1} region were recorded on an IR-Fourier spectrophotometer system 2000, firm Perkin Elmer using the method of pressing samples with KBr.

The thermal analysis was carried out on a derivatograph of the Paulik-Paulik-Erdei system, at a rate of 10 deg / min with a 0.1 g sample with a sensitivity of T-900, TT-100, DTA-1/10, and DTG-1/10 galvanometers. The holder was a platinum crucible with a diameter of 7 mm without a cover. Al_2O_3 was used as a reference.

Results and their discussion

The results of the elemental analysis of complex compounds are given in (Table 1).

Table 1.– Results of elemental analysis

Compound	M%		N%		C%		H%	
	Found	Calcu.	Found	Calcu.	Found	Calcu.	Found	Calcu.
1	*2*	*3*	*4*	*5*	*6*	*7*	*8*	*9*
Furfuryldicarbamide (L)	–	–	28.41	28.28	42.53	42.42	5.11	5.05

1	*2*	*3*	*4*	*5*	*6*	*7*	*8*	*9*
$Co(CH_3COO)_2 \cdot L \cdot 3H_2O$	13.69	13.77	12.95	13.08	31.03	30.84	5.16	5.14
$Cu(CH_3COO)_2 \cdot L \cdot H_2O$	16.04	15.97	13.99	14.07	33.40	33.17	4.39	4.52
$Zn(CH_3COO)_2 \cdot L \cdot 2H_2O$	15.80	15.68	13.51	13.43	31.70	31.65	4.77	4.84

Comparison of X-ray diffraction patterns of compounds shows that they differ from those of the initial metal acetates and furfuryldicarbamide, therefore, the complexes have individual crystal structures.

Some vibrational frequencies in the IR absorption spectra of the uncoordinated furfuryldicarbamide molecule and its complexes with Co (II), C (II) and Zn (II) acetate are given in Table 2.

The assignment of the absorption bands of the furfuryldicarbamide molecule was carried out according to [7–10].

Comparison of the free molecule of furfuryldicarbamide and its complexes with metal acetates shows, that in the transition to complexes an essential change is observed in the bands of valense vibrations of the ether bond –C-O-C- furan ring.

The high-frequency shift of the valence vibration of $\vartheta(-C-O-C)$: by 7–9 cm The sixth coordination site is filled with a water molecule^{-1} and the preferential valence vibration of the C = O bond by 3–4 cm^{-1} indicates a simultaneous participation in the coordination of the oxygen atom of the furan ring and two nitrogen atoms of substituted amine groups.

Analysis of the values of the frequency $\vartheta(C-C)$ acetate group shows that in the complexes each group is coordinated monodentately with the participation of a ring oxygen atom in the hydrogen bond. The sixth coordination place is filled with a water molecule.

Derivatographic data of the thermolysis of furfuryldicarbamide of its complexes with cobalt, copper and zinc acetates are given in (Table 3).

The endothermic effects at 142, 220 and exothermic effects at 165, 200, 320, 490, 590, 650 °C appear on the heating curve of the derivatogram of furfuryl dicarbamide.

The first one corresponds to the melting of an organic ligand. The presence of subsequent thermal effects is due to the stepwise decomposition and combustion of the thermal decomposition products of substituted carbamide molecules.

Conclusion

The thermal behavior of coordination compounds depends on the nature of metals and is characterized by dehydration, deactivation, stepwise decomposition and burning of thermal decomposition products.

On the basis of elemental, X-ray phase, derivatographic analysis and spectroscopic data, the following possible structure should be proposed:

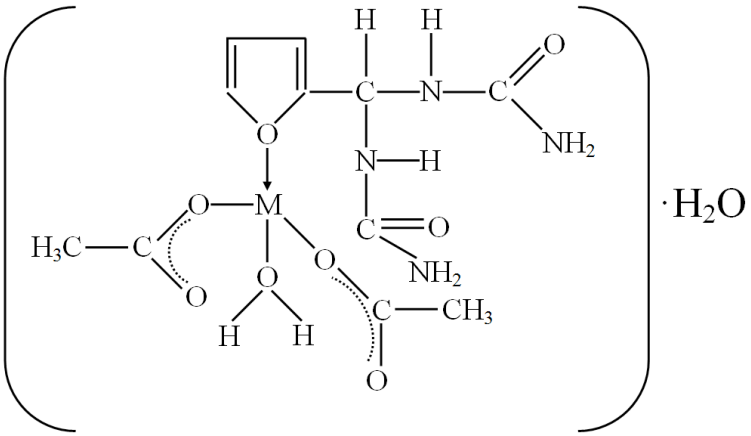

Table 2. – Some characteristic frequencies (cm^{-1}) in IR absorption spectra of furfuryldicarbamide and its complexes with acetates of divalent cobalt, copper and zinc

Furfuryldi-carbamide – L		**$Co(CH_3COO)_2 \cdot L \cdot 3H_2O$**		**$Cu(CH_3COO)_2 \cdot L \cdot H_2O$**		**$Zn(CH_3COO)_2 \cdot L \cdot 2H_2O$**	
fre-quen-cies	**absorption**	**fre-quen-cies**	**absorption**	**fre-quen-cies**	**absorption**	**fre-quen-cies**	**absorption**
3449	$\vartheta_{as}(NH_2)$	3536, 3424	$\vartheta_{as}(OH)H_2O$, $\vartheta_{as}(NH_2)$	3570, 3470	$\vartheta_{as}(OH)H_2O$, $\vartheta_{as}(NH_2)$	3530, 3460	$\vartheta_{as}(OH)H_2O$, $\vartheta_{as}(NH_2)$
3348	$\vartheta_{s}(NH_2)$	3348, 3257	$\vartheta_{s}(OH)H_2O$, $2\delta(NH_2)$	3424, 3335	$\vartheta_{s}(OH)H_2O$, $2\delta(NH_2)$	3430, 3335	$\vartheta_{s}(OH)H_2O$, $2\delta(NH_2)$, $\vartheta(NH_2)$
3140	$\vartheta(CH)_{f.r.}$	3112	$\vartheta(CH)_{f.r.}$	3110	$\vartheta(CH)_{f.r.}$	3111	$\vartheta(CH)_{f.r.}$
1666	$\vartheta(CO)$, $\delta(NH_2)$	1670	$\vartheta(CO)$, $\delta(NH_2)$	1669	$\vartheta(CO)$, $\delta(NH_2)$	1670	$\vartheta(CO)$, $\delta(NH_2)$
1631	$\vartheta(CO)$, $\delta(NH_2)$	1628	$\delta(NH_2)$, δ (HOH)	1627	δ (HOH), $\delta(NH_2)$	1629	δ (HOH), $\delta(NH_2)$
1594		1574	$\delta_{к}$, $\vartheta_{as}(COC)$	1479	$\vartheta_{к}$, $\vartheta_{as}(COO)$	1601	$\vartheta_{as}(COO)$
1536	$\delta_{к}$			1603	$\vartheta_{as}(COO)$	1557	$\vartheta_{к}$
1466	$\vartheta(CN)$	1441, 1436 1417	$\vartheta(CN)+\vartheta_3(COO)$	1436 1416	$\vartheta(CN)$	1456 1417	$\vartheta(CN)$, $\vartheta_s(COO)$
1377	δ (CH)	1344	δ (CH)	1355	δ (CH)	1378	δ (CH)
1310	δ (CH)						
1253 1229	ϑ (–C-O-C-)	1256 1236	ϑ (–C-O-C-)	1258 1236	ϑ (–C-O-C-)	1257 1238	ϑ (–C–C-C-)
1149	$\beta(NH_2)$	1158	$\beta(NH_2)$	1181	$\beta(NH_2)$	1180	$\beta(NH_2)$
1077	ϑ (CN)+	1057	ϑ (CN),	1049	ϑ (CN)+	1047	ϑ (CN)+
1010	$+\vartheta$ (–C-O-C-)	1023	ϑ (–C–C-C-)	1032	$+\vartheta$ (–C-O-C-)	1018	$+\vartheta$ (–C–C-C-)
		960	ϑ (CC) acet.	950	ϑ (CC)acet.	953	ϑ (CC) acet.
884	ϑ к (fur.r.)	895	ϑ к (fur.r.)	893	ϑ к (fur.r.)	895	ϑ к (fur.r.)
744	$\delta(NH_2)$	753	$\delta(NH_2)$	783	$\delta(NH_2)$	780	$\delta(NH_2)$
		671 617	δ (COO)	685	δ (COO)	692	δ (COO)
559	δ (C)	527	δ (NCN)	629, 615 549	δ (NCN)	622 551	δ (NCN)

Table 3. – Derivatographic data of thermolysis of furfuryldicarbamide and its complexes with acetates divalent cobalt, copper and zinc

Compound	Temperature effect interval, °C	Peak effect, °C	Loss of mass, Cu,%	Total weight loss, Cu,%	Nature effects	The resulting compound
1	*2*	*3*	*4*	*5*	*6*	*7*
Furfuryldicarbamide (L) Removal of the hydrate molecule of water	130–143	142	0.05	0.05	endothermic	furfuryldicarbamide
	143–182	165	2.27	2.32	exothermic	decomposition start
	182–205	200	5.68	8.00	exothermic	intensive decomposition
	205–280	220	32.95	40.95	endothermic	thermolysis
	280–420	320	30.11	71.06	exothermic	Thermolysis and combustion of thermolysis products
	420–542	490	21.59	92.65	exothermic	decomposition
	542–595	590	6.80	99.45	exothermic	decomposition
	595–770	650	0.40	99.85	exothermic	Burning thermolysis products
$Co(CH_3COO)_2 \cdot L \cdot 3H_2O$	60–105	90	3.52	3.52	endothermic	Removal of the hydrate molecule of water
	105–160	120	8.69	12.21	endothermic	Removal of coordinated molecules
	160–180	175	2.72	14.93	endothermic	The decomposition of the anhydrous complex began
	180–212	210	1.96	16.89	endothermic	decomposition
	212–258	245	2.72	19.61	endothermic	decomposition
	258–320	300	7.06	26.67	endothermic	decomposition
	320–380	350	17.39	44.06	exothermic	decomposition with combustion of
$Cu(CH_3COO)_2 \cdot (L) \cdot 0{,}5H_2O$	380–510	465	22.28	66.34	exothermic	decomposition with combustion of thermolysis products
	510–890	880	3.05	69.39	endothermic	decomposition of cobalt carbonate
	100–130	125	2.06	2.06	endothermic	dehydration
	130–155	150	2.50	4.56	endothermic	dehydration complex
	155–185	170	7.60	12.21	endothermic	the beginning of decomposition of anhydrous complex
$Zn(CH_3COO)_2 \cdot (L) \cdot 2H_2O$	185–235	230	34.78	46.99	endothermic	intensive decomposition
	235–275	278	13.04	60.03	exothermic	decomposition
	275–325	290	–0.30	59.73	exothermic	oxidation of thermal decomposition products
	325–380	345	–0.60	59.13	exothermic	oxidation of thermolysis products

1	*2*	*3*	*4*	*5*	*6*	*7*
$Zn(CH_3COO)_2 \cdot \cdot(L)\cdot 2H_2O$	380–500	440	-0.50	58.63	exothermic	oxidation of thermolysis products
	100–140	130	9.00	9.00	endothermic	of education $Zn(CH_3COO)_2 \cdot L$
	140–182	150	11.58	20.58	endothermic	the beginning of decomposition of anhydrous complex
	182–250	210	19.28	39.85	endothermic	intensive decomposition
	250–320	258	24.68	60.54	endothermic	thermolysis
	320–410	380	6.02	66.56	exothermic	thermolysis of a combustion product decomposed
	410–480	430	2.89	69.45	exothermic	Thermolysis and formation of zinc oxide

References:

1. Sulaimankulov K. "Compounds of carbamide with inorganic salts" – Frunze: Илим.– 1976.– 223 p.
2. Azizov T. A., Mahmudov Zh.U., Sharipov H. T., Beglov B. M. and others "Synthesis and study of complex compounds of divalent metal acetates with methylenedicarbamide" // Journal Inorganic chemistry – 1990.– P. 35.– No. 8.– P. 2030–2033.
3. Askarov I. R., Isaev Yu.T., Makhsumov A. G., Kirghizov Sh.M. // Organic chemistry. Uzbekistan.– Tashkent.– 2012.
4. Пришбл П. "Complexes in chemical analysis" // – Moscow.: – ИЛ.– 1960.
5. Klimova V. A. "Basic micromethods of analysis of organic compounds" // – Moscow.: Chemistry.– 1967.– 19 p.
6. Kovba L. M., Trunov V. N. "X-ray Phase Analysis" // – Moscow: Moscow State University – 1976–232 p.
7. Varlomov G. D., Jalilov A. T., "Chemistry and technology of furfuramide and its derivatives" // – Uzbekistan – Tashkent.– Fan.– 1990.– P. 8–9.
8. Spinter E. "The vibration spectra and structures of the hydrochlorides of urea, thiourea and acetamide. The basic properties of amides and thioamides" // Spectrochim. Acta.– 1959.– No. 12.– P. 95–100.
9. Saito Y., Machida K., Uno T. "Infrared spectra of partially deyterated ureas" // Spectrochim. Acta.– 1971.– V. 27 A.– P. 991–1002.
10. Abdurakhimova N., Isakov H., Askarov I. R., Usmanov S., Azizov T. A. // "Coordination compounds of furfuramide with acetates of bivalent cobalt, zinc and copper" // Universum: Technical science: electronic scientific journal.– Moscow.– 2017. December.– № 12 (45).

Lavrentyeva Irina Viktorovna,
Doctor of economy, associate professor,
Russian Presidential Academy of National Economy
and Public Administration, Chelyabinsk branch,
Chelyabinsk, Russia.
E-mail: astralavr@mail.ru

Sergienko Polina Grigoryevna,
master, Russian Presidential Academy
of National Economy and Public Administration,
Chelyabinsk branch, Chelyabinsk, Russia
E-mail: corn-serg@mail.ru

Arefyev Stepan Anatolyevichssia,
master, Russian Presidential Academy
of National Economy and Public Administration,
Chelyabinsk branch, Chelyabinsk, Russia
E-mail: astralavr@mail.ru

STATE CULTURAL POLICY AS PREPOTENT FACTOR OF ECONOMIC DEVELOPMENT

Abstract: The factor of influence of culture on forward economic development in the state is analyzed In the presented article. The thesis is substantiated that, economic problems have primarily a spiritual dimension, the material and value aspects are interrelated. The facts are given, indicating the regularity of the influence of cultural state policy and economy. The thesis of the insolvency of the cultural policy oriented to pragmatic principles of market relations, the main dominant of which is the realization of the concept of economic Darwinism, the cult of money is substantiated. The facts of destruction in the economic, social, demographic continuums of the state structure are given. Attention on negative trends in the formation of cultural values among young people is focused. The author substantiates the conclusion about the need to reformat the life of society through a new state cultural policy based on human values.

Keywords: cultural policy, culture, economic factor, economic basis, spiritual dominant.

The discussions, that were so popular in the last century and which have not lost their relevance in our time – the dominance of the material (basis) and the ideal (superstructure) – have not been much closer to understanding the fact that state cultural policy is fundamental to the economic development of society.

From numerous definitions of culture as "forms of vital activity and the integral integration of large communities that distinguish the existence of people in the natural environment and the animal world" [13], we can distinguish the principle of controllability of economic science, the foundation of which is the world outlook and cultural values.

The practice of living in market conditions (since the last century to this day) has shown the presence of a large number of studies confirming the patterns of mutual influence of the economy and culture. A

number of scientists, in their studies, pointed to the dominant influence of culture on different sides of society and the state:

- dominance of cultural factors above the achievement of personal gain [1; 3; 4];
- connectivity between the pace of economic development and the country's cultural systems [9];
- Insufficiency of setting up of economic incentives in entrepreneurial activity and building up production relations [5];
- definition of economic (business) activity through the totality of mental properties and functions that accompany the management [6];
- relationship between the moral and emotional state of society and the development of the population economy [11; 12; 13; 14];
- consideration of capitalist relations as a cultural and spiritual phenomenon [7];
- capitalist spirit as a concentrate of human sins and passions and the factor of the decline of mankind [8].

The main message of numerous studies on the interrelation between culture and economy points to a "proportional" relationship between the state of culture and the economy – the fact that the economic behavior of the population is affected by the level of culture that dominates the society. In turn, culture, as is known, is variable and depends on the level of morality inherent in it and can contribute to either impede the evolutionary development of mankind.

The cultural policy of the present is built according to the pragmatic principles of the era of market relations, the main dominant of which is the realization of the concept of economic Darwinism, the revival of the cult of money, the unrestrained growth of capital in pursuit of profit, the ignoring of moral values. The economic confrontation of world systems forced states to work actively in the ideological field.

Market ideology, declaring the multiplying and protecting its own wealth and power, redirected all its power into the sphere of material interests: all for the sake of money, in the name of money, through money. Cultural-information "memes" that introduce the consciousness of the younger generation and the adult population through movies and plays, literature, etc., form the behavior of a person with an animal, a robotic and demonic type of psyche, immoral in nature. The consumer society born under this cultural diktat has the grounds and purpose of satisfying parasitic needs leading to the degradation of the individual, and then, mediating through the economic behavior of the population, to the degradation of the country, which has been repeatedly confirmed by history.

Not transferred genetically, but formed by external factors (religious, ideological, educational, political, etc.), culture, depending on the dominant type of worldviews, can have a colossal influence on the course of the history of state development, as was repeatedly pointed out by the great minds of the past and the present-the dominant influence ideological, religious, educational and cultural factors are inevitable.

From studies of the interrelationship between culture and economics, it becomes clear that economic problems are primarily a spiritual dimension, the material and value aspects are interrelated, and economic growth depends on the moral atmosphere and emotional state of society, the level of culture in society. The problem of economic growth and increasing GDP is the problem of the formation of values and worldview. Repeated ignoring of the factor of culture or its use in a destructive key always led to economic collapses.

Particularly disturbing is the influence of the cultural factor on the younger generation. Powerful impact through media channels – television, Internet technologies, advertising – form a "narrow sense horizon with a value space, defined primarily by entertainment media, mass culture and gloss, a magical mirage of 'big money", the formation of vague and conflicting political orientations and preferences, pragmatic attitude to the West as a

source of material wealth, employment and recreation opportunities [15].

The consequence and the main reason for the impact not only on youth, but also on the general population is the phenomenon of "ekonocyde" (Silaste G. G.), associated with the collapse of employment in the labor market, a reduction in savings, increasing risks of crediting [12]. So, from 2013 by 2018 the average per capita income of Russian residents increased by 5547 rubles (from 25928 to 31475 rubles per month), but the inflation accumulated during this time "ate all the accumulations". Every third citizen of working age earns less than 15,000 rubles a month, and more than 5 million people have a salary at the level of SMIC, and 13% of the population lives below the poverty line [16]. According to Rosstat, real disposable incomes of the population of Russia declined in 2017 by 1.7% [17].

Defining the law of spiritual determination, a number of researchers [10; 11] point to the relationship between spiritual ill-being and the dynamics of births and deaths of labor resources and reveal the spiritual and cultural collapse in the dominant cause of depopulation. The predicted values of the population's vitality ratios (ratio of fertility rates to mortality) tend to decrease to year 2031. According to the demographic forecast of Rosstat, the natural population decline will increase and from 2025 will exceed 400 thousand people annually; the slowdown in population decline is projected only closer to the 2030s. International migration (according to the forecast, the inflow of migrants will be less than 300 thousand people per year) in the long term will not be able to compensate for population decline [18].

While analyzing economic phenomena and processes, the majority of economists ignore the cultural factor, in the long-term perspective, the interrelationship of the dynamic laws of the mutual influence of culture on the economy is obvious. Culture should be perceived by society as a fundamental institution of economic, demographic, social development. The primary task of reformatting a society with the means of a cultural factor from destructive to constructive development of society is a task that requires a decision at the state level both in strategic and tactical plans.

References:

1. Смит А. Теория нравственных чувств Серия Библиотека этической мысли. Издательство «Республика» – 1997.– 352 с.
2. Guiso Luigi, Paola Sapienza, and Luigi Zingales. "Does Culture Affect Economic Outcomes?" Journal of Economic Perspectives, 20(2).– 2006.– P. 23–48.
3. Милль Дж. С. Речь об университетском воспитании, произнесенная в Университете С.-Андрью (в Шотландии) Джоном Стюартом Миллем, ректором университета Электронный ресурс Режим доступа URL: http://abuss.narod.ru/study/su/mill_university.pdf
4. Юманс Э. Новейшее образование: его истинные цели и требования. Милль Дж. С. Речь об ниверситетском воспитании / Пер. с англ. М. А. Антоновича. СПб.: Русская книжная торговля,– 1867.– С. 5–71.
5. Вебер М. Протестанская этика и дух капитализма Изд-во Центр гуманитарных инициатив.– 2018.– 656 с.
6. Зомбарт В., Буржуа. Этюды по истории духовного развития современного экономического человека Электронный ресурс Режим доступа URL: http://www.nehudlit.ru/books/detail8728.html
7. Катасонов В. Ю. Религия денег. Духовно-религиозные основы капитализма.– М.: Кислород,– 2014.– 408 с.

8. Вальцев С. В. Закат человечества. Почему человечество вырождается? – М.: Книжный мир,– 2008.– 352 с.
9. Benfield E C. The Moral Basis of the Backward Society. The Free Press.– Glenkoe,– 1958.– 308 p.
10. Гундаров И. А. «Духовное неблагополучие и демографическая катастрофа» // Общественные науки и современность – 2001.– № 5.– С. 58–65.
11. Якунин В. И., Багдасарян В. Э., Сулакшин С. С. Идеология экономической политики: проблема российского выбора. Монография – М.: Научный эксперт,– 2008.– 288 с.
12. Силласте Г. Г. Эконоцид – социальные последствия финансового кризиса // Мониторинг общественного мнения № 2 (102), март-апрель – 2011.– С. 132–142.
13. Астафьева О. Н., Аванесова Г. А. Развитие национальной культуры и культурная политика в Российской империи и СССР: сравнительный анализ [Текст] Ярославский педагогический вестник – 2015.– № 4.– С. 206–216.
14. Гольц Г. А. Культура и экономика: поиски взаимосвязи Общественные науки и современность,– 2000.– № 1.– С. 23–35.

Pirniayzova Periuza Mambetniyazovna,
Linguestic colleg by
Kazakh University of the world Language
E-mail: aydanushka@list.ru

ANALYTICAL SOLUTION OF DIFFUSION PROBLEMS IN THE SIMULATION OF IMPURITY DIFFUSION AND OBTAINING AN EXACT SOLUTION

Abstract: In this article given in demonstrative way, it is considered decision of a one-dimensional and two-dimensional problem of diffusion, by a recurrently operational method, which describes process of distribution of harmful impurity along a watercourse.

The received numerical results on the computer, where it is possible to define what time there is a distribution and river clarification. The received results are illustrated in drawings.

Keywords: distribution process, harmful impurity, the differential equation, the diffusion equation, problem Kashi.

The process of transporting pollutants to river water is described by diffusion equations. In many monographs, the solution of these models is given only with the use of numerical methods of difference schemes, and a number of questions arise related to the choice of methods for solving a number of various problems on which the practical realizability, accuracy and duration of the solution on the computer depend. In particular: a) an analytic description of a plane or spatial domain for which diffusion equations and boundary conditions are studied, i.e. analytical description of coastlines and river bottom; b) an analytical description of the dependence of the coefficients of the equation on the spatial coordinates; c) an analytical description of the dependence of the spatial coordinates and time of inhomogeneous parts of the solved diffusion equation, i.e. from sources of pollution; d) the correct choice in the difference scheme of the relationship between the spatial steps of the gird, and also between them and the step of discretization of time.

In the work considered by us, the solution of these equations is given by analytical, where practical realization gives an exact solution. We consider the solution of a one-dimensional, two-dimensional, three-dimensional differential equation of parabolic type diffusion. One-dimensional production, as a special case of the three-dimensional diffusion equation, the coefficients of which determine the physical processes of interest to us, in particular the spread of pollution along the width of the watercourse and the infinite speed of propagation, and a number of other physical processes are determined by analogous equations, among them the potential flow, diffusion transfer of mass, flow through a porous medium and some fully developed currents in channels.

Integro-differential operators are introduced in the form of a special numbers with constant coefficients determined from the recurrence parity associated with the differential equation under consideration. The particular solutions obtained in this case have a simpler from than in other papers, since they are constructed on the basis of one recurrence relation, which leads to simpler differentiation formulas. With this approach, the general solutions are expressed in terms of arbitrary functions and are not related to the solution of the other equation. The resulting form of general solutions makes it possible to apply the method of initial functions for solving boundary value problems, since arbitrary analytic

functions foe functions entering into general solutions can be expressed in terms of the initial functions given by the condition. From these formulas of general solutions, it is easy to find all particular solutions, it is easy to find all particular solutions in various classes of analytic functions.

Such a recurrent-operator method is very effective in constructing the solution of the equation of the theory of heat conduction. The solution of the equation of the two-dimensional diffusion problem is the same as in the solution of the one-dimensional diffusion problem, that is, the solution is also sought with the introduction of an integro-differential operator in the form of a special series with constant coefficients, determined from the recurrence relation [4]

$$\left(\partial_t + a_{02}\partial_x^2 + a_{01}\partial_x + a_{00}\right)q(x,t) = f(x,t), \quad (1)$$

$$a_{02} = k_x;\ \ a_{01} = v_x;\ \ a_{00} = \alpha,$$

Where $q(x,t)$ is the concentration of emissions; pollutant NO_3 – nitarate ion; v_x – is the time – averaged velocity component along the x – axis; k_x – is the diffusion coefficient, α – is the rate of destruction of the substance; $f(x,t)$ is the source function.

The solution of equation (1) is obtained in the form

$$q = \sum_{i=0}^{\infty}\sum_{j=0}^{\infty} Q_{i,j}t^{i!}\partial_x^j g(x) \quad (2)$$

Substituting solution (2) into (1), we obtain the following recurrent equation:

$$Q_{i,j} = -a_{0,2}Q_{i-1,j-2} - a_{01}Q_{i-1,j-1} - a_{00}Q_{i-1,j} \quad (3)$$

Under the initial conditions $Q_{0,0} = 1$, $Q_{i,j} = 0$, at $i < 0$ or $j < 0$

$$Q_{0,0} = 1,\ \ Q_{0,1} = 0;\ \ Q_{1,0} = -a_{00};$$
$$Q_{2,0} = a_{00}^2;\ \ Q_{1,1} = -a_{01};\ \ Q_{0,2} = 0; \quad (4)$$
$$Q_{3,0} = -a_{00}^3;\ \ Q_{2,1} = 2a_{01}a_{00};\ \ Q_{12} = -a_{02};\ \ Q_{0,3} = 0.$$

Writing out the first terms of the numbers (2), we have

$$q(t,g(x)) = g + [-a_{00}tg(x)] + \left[a_{00}^2 t^{2,!}g(x) - a_{01}tg'(x)\right] +$$
$$+\left[-a_{00}t^{3,!}g(x) + 2a_{00}a_{01}t^{2,!}g'(x) - a_{01}tg''(x)\right] +$$
$$+\left[a_{00}^4 t^{4,!}g(x) - 3a_{00}^2 a_{01}t^{3,!}g'(x) + (2a_{00}a_{02} + a_{01}^2)t^{2,!}g''(x)\right] + \quad (5)$$
$$\left[\begin{array}{c} -a_{00}^5 t^{5,!}g(x) - 4a_{00}^3 a_{01}t^{4,!}g'(x) - \\ -3(a_{00}^2 a_{02} + a_{01}^2 a_{00})t^{3,!}g''(x) + 2a_{02}a_{01}t^{2,!}g'''(x) \end{array}\right] + \ldots .$$

A function satisfying the initial conditions for $t_0 = 0.1$, the next:

$$g(x) = \frac{N}{2w\sqrt{\pi a_{20}t_0}}e^{\left(-\frac{(x-a_{10}t_0)^2}{4a_{20}t_0} - a_{00}t_0\right)} \quad (6)$$

Substituting (6) in(5), we have

$$g(t,g(x)) = Ce^{-\left(\frac{(x-a_{10}t_0)^2}{4a_{20}t_0} + a_{00}t_0\right)} + \left[-a_{00}t\left(Ce^{-\left(\frac{(x-a_{10}t_0)^2}{4a_{20}t_0}\right)}\right)\right] +$$
$$+\left[a_{00}^2\frac{t}{2!}g(x) - a_{10}t\left(Ce^{-\left(\frac{(x-a_{10}t_0)^2}{4a_{20}t_0} + a_{00}t_0\right)}\right)'\right] + \ldots .$$

This series is collapsed into a function

$$g(x) = \frac{N}{2w\sqrt{\pi a_{20}(t_0+t)}}e^{\left(-\frac{(x-a_{10}(t_0+t))^2}{4a_{20}(t_0+t)} + a_{00}(t_0+t)\right)}$$

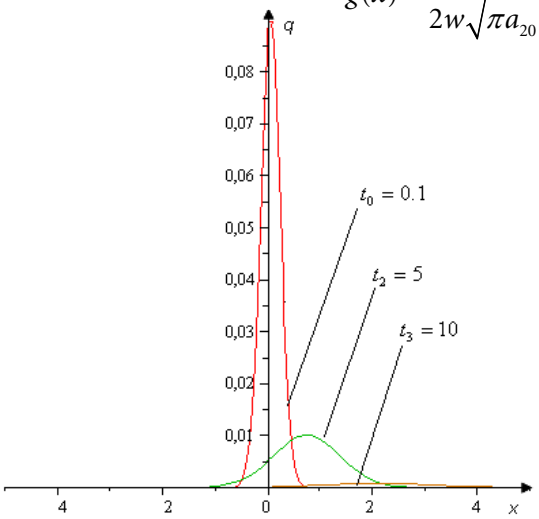

Figure 1. Process of distribution of emission of harmful during the initial moment of time

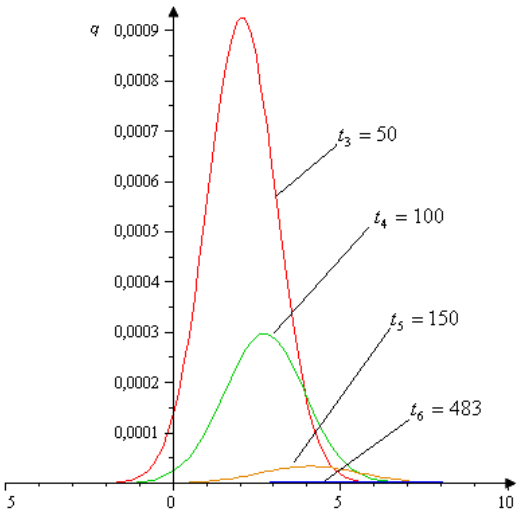

Figure 2. Process of distribution of harmful impurity in time

Given the function $g^*(t,g(x))$ to the values $t=t_1$, $t=t_2$, $t=t_3$... we construct a combined graph of the function $g_1^*, g_2^*, g_{3,}^*$...

In the recurrent-operatror method, the solution is obtained in the form (5), while and the authors of K, I, Kachiashvili, D. G. Gordeziyani obtained

$$g(x,t)=\frac{N}{2w\sqrt{\pi K_x(t_0+t)}}e^{\left(-\frac{(x-V(t_0+t))^2}{4K_x(t_0+t)}-\alpha(t_0+t)\right)}$$

By the same algorithm for solving the problem of a simulation one-dimensional diffusion equation, a solution is obtained for two-dimensional diffusion equation

$$\frac{\partial q}{\partial t}=k_x\frac{\partial^2 q}{\partial x^2}+k_y\frac{\partial^2 q}{\partial y^2}-u_x\frac{\partial q}{\partial x}-\alpha q+f(x,y,t) \quad (7)$$

At the initial and boundary conditions

$$q(x,y,t)\big|_{t=0}=\frac{N}{2w\sqrt{\pi k_x k_y(t_0+t)}}e^{\left(-\frac{(x-u_x(t_0+t))^2}{4k_x(t_0+t)}-\frac{y^2}{4k_y(t_0+t)}-\alpha(t_0+t)\right)}$$

Boundary conditions

$$\frac{\partial q(x,y,t)}{\partial x}\Big|_{x=0}=\frac{\partial q(x,y,t)}{\partial x}\Big|_{x=l_1}=\phi(y,t);$$

$$0\le y\le l_2,\quad 0\le t\le T$$

$$\frac{\partial q(x,y,t)}{\partial y}\Big|_{y=0}=\frac{\partial q(x,y,t)}{\partial y}\Big|_{y=l_2}=\psi(x,t)$$

$$0\le x\le l_1,\quad 0\le t\le T;$$

For convenience, finding the coefficients of the series that rewrote equation (7) in the form

$$(\partial_x^2+a_1\partial_y^2-a_2\partial_x-a_3\partial_t-a_4)q(x,y,t)=f(x,y,t) \quad (8)$$

Where $a_1=\frac{k_y}{k_x}$; $a_2=\frac{u_x}{k_x}$; $a_3=\frac{1}{k_x}$; $a_4=\frac{\alpha}{k_x}$;

We seek the solution of this equation in the form of a series

$$q_r(x,y,g_r)=\sum_{i=0}^{\infty}\sum_{j=0}^{\infty}\sum_{k=0}^{\infty}Q_{i,j,k}x^{(i+j+k+r)!}\partial_y^{j+2}\partial_t^k(g_r(y,t));r=0,1 \quad (9)$$

Substituting equation (9) into equation (8) and making the appropriate mixing of the indices and talking the common factor in parenthesis and equating the expressions in parenthesis to zero, we obtain the following recurrence equation

$$Q_{i,j,k}=-a_1Q_{i,j-2,k}+a_2Q_{i-1,j,k}+a_3Q_{i-1,j,k-1}+a_4Q_{i-2,j,k} \quad (10)$$

Under the initial $Q_{0,0,0}=1$, $Q_{i,j,k}=0$ by $i<0$ or $j<0$, or $k<0$ (11)

From the recurrence relation (10) we find coefficients of the series (9). Then changing the order of summation in (9), we obtain a solution of equation (8) in the from

$$q_r=\sum_{i=0}^{\infty}x^{i+j+k!}\Big(\sum_{j=0}^{i}\sum_{k=0}^{j}Q_{i,i-j,j-k}\Big)\frac{\partial^{i-j}}{\partial y^{i-j}}\frac{\partial^{j-k}}{\partial t^{j-p}}g_r(y,t),r=0,1. \quad (12)$$

We next write out the first few terms of the series (3) substituting the coefficients

$$q_0=g_0+a_3xg_0+[(a_2^2+a_4)g_0^{''}-a_1g_0^{''}+a_3g_0^{'}]\frac{x^2}{2!}+$$

$$+[a_2(a_2^2+a_4)g_0^{''}+2a_2a_3g_0^{''}+(-2a_1a_2)g_0^{'}]\frac{x^3}{3!}+\ldots$$

$$q_1=a_3g_0+[(a_2^2+a_4)g_0^{''}-a_1g_0^{''}+a_3g_0^{'}]x+$$

$$+[a_2(a_2^2+a_4)g_0^{''}+2a_2a_3g_0^{''}+(-2a_1a_2)g_0^{'}]\frac{x^2}{2}+\ldots$$

The particular solution of the inhomogeneous equation (8) in accordance with the recursion-operator method [5] has the form

$$q^*(f)=\sum_{i=0}^{\infty}\sum_{j=0}^{\infty}\sum_{k=0}^{\infty}Q_{i,j,k}\frac{\partial^{-(i+j+k+2)}}{\partial x^{-(i+j+k+2)}}\frac{\partial^j}{\partial y^j}\frac{\partial k}{\partial t^k}f(x,y,t),$$

Thus, the general solution of the cranes (8) will be

$$q(x,y,t)=q_0(x,y,g_0)+q_1(x,y,g_1)+q^*(f). \quad (13)$$

Solving the Cauchy problem foe equation (1) with $f(x,y,t)=0$, for an instantaneous point source of a unit mass of a pollutant with an initial condition

$$q(x,y,t)\big|_{t=0}=\frac{N}{2w\sqrt{\pi k_x k_y(t_0+t)}}e^{\left(\frac{(x-u_x(t_0+t))^2}{4k_x(t_0+t)}-\frac{y^2}{4k_y(t_0+t)}-\alpha(t_0+t)\right)},$$

N – the capacity source of pollution for the river (mg/s); w – is the area if the rivers live section (m^2). Substituting this function in a numbers

$$q_r(x,y,g_r)=\sum_{i=0}^{\infty}\sum_{j=0}^{\infty}\sum_{k=0}^{\infty}Q_{i,j,k}\frac{x^{(i+j+k+r)}}{(i+j+k+r)!}\partial_y^j\partial_t^k(g(y,t));$$
$$r=0,1$$

by $t=0$, we find that $q_0=g_0$, we obtain a power numbers that depends on the variable t_0. This numbers converges into an elementary function $q(x,y,t)=\frac{N}{2w\sqrt{\pi k_x k_y t}}e^{\left(-\frac{(x-u_x t)^2}{4k_x t}-\frac{y^2}{4k_y t}-\alpha t\right)}$, which coincides with the results of the authors of K. I. Kachiashvili, D. G. Gordesiyani, D. I. Melikzhanyan, obtained by a finite-difference method.

According to (Figure 5), with the passage of time the intensity of emission of harmful impurities decreases, and according to the graph it is possible to determine the values $x=l$, $y=m$ meaning that the concentration reaches the maximum allowable emission rate. The results obtained coincide with the results of other authors.

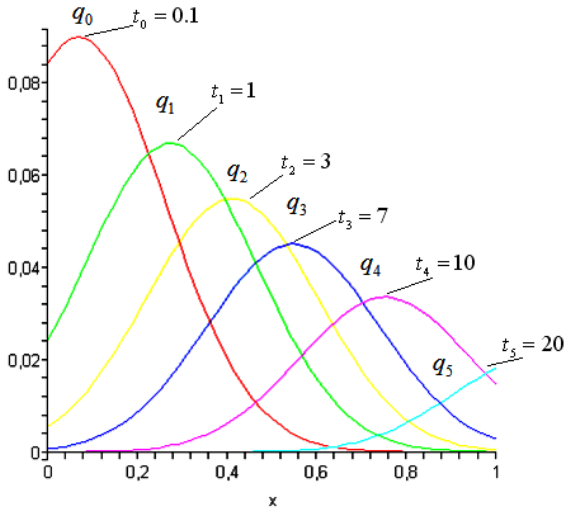

Figure 3. Process of distribution of harmful impurity

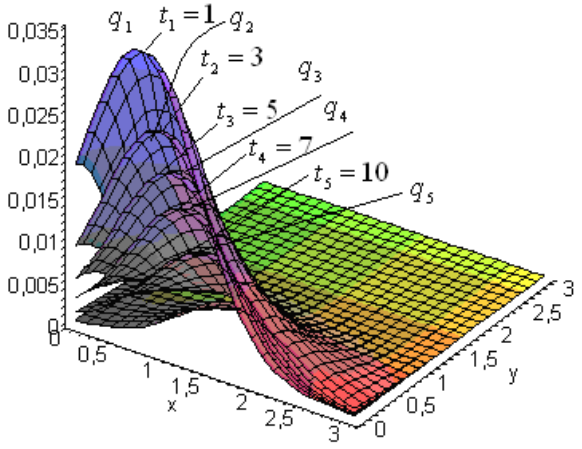

Figure 4. Process of distribution of emission of harmful impurity on an axis x impurity to axes x, y

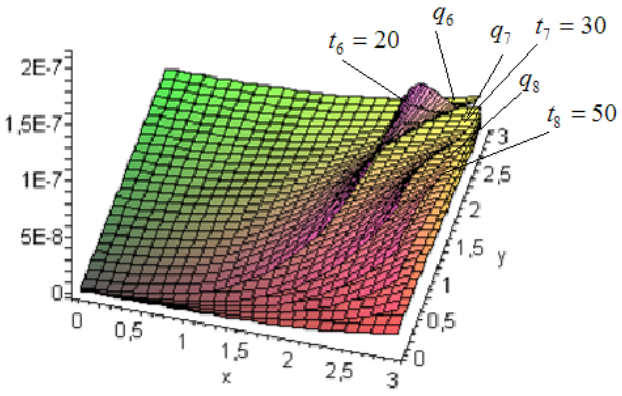

Figure 5. The process of distribution of harmful impurities over time

References:

1. Berlyand M. E. Modern problems of atmospheric diffusion and air pollution. -Leningrad: Gidrometeoizdat,– 1975.– 447 p.
2. Bondarenko B. A., Pirniyazova P. M. Normalized systems of functions and their applications to the solution of the problems for the equations diffusions / Questions Calculus and Applied mathematics.– Tashkent,– Institute of Mathematic and Information Technology of academy Science of RUz.– 2008.– No. 119.– P. 5–12.
3. Ivaknenko A. G. Inductive method of self-organization of models of complex systems.– Kyiv.: Naukova dumka,– 1982.– 296 p.
4. Kachaishvili K. I., Gordesiani D. G., Melikzhanyan G. I. Modern modeling and computer technologies for research and quality control to river water.– Tbilisi. GTU,– 2007.– 251 c.
5. Spivakov U. L. Special classes of solutions of linear differential equations and their application in an anisotropic and inhomogeneous theory of elasticity.– Tashkent: FAN,– 1987.– 296 p.
6. Frolov V. N. Special classes of functions in the anisotropic theory of elasticity.– Tashkent.: FAN.– 1981.– 224 c.
7. Pirniyazova P. M. Mathematical modeling of the process of distribution of harmful impurities in the river by a recurrent – operator method // Advances in ecological research.– United States.: Academic Press.– 2016.
8. Pirniyazova P. M. About solving single-measure problem of diffusion // The Uzbek Magazine “The Problem of Informatics and Power Science”.– Tashkent,– 2005.– № 4.– P. 97–101.
9. Pirniyazova P. M. The decision of the general problem of one-dimensional diffusion by a recurrently-operational method // The Uzbek Magazine “The Problem of Informatics and Power Science”.– Tashkent,– 2005.– № 5.– P. 89–94.

Radjabov Telman Dadaevich,
Graduate student, of the Tashkent
University of information technologies
Faculty of Telecommunications technology
Professor, Doctor of Physics and Mathematics
Rakhimov Bakhtiyorjon Nematovich,
Graduate student, of the Tashkent
University of information technologies
Faculty of Telecommunications technology
Atadjanov Sherzod Shuxratovitch,
Doctor of Technical Sciences,
Tashkent University of Information Technologies,
head of the department for educational and methodical
works with regional branches, applicant University
Maxsudov Ravshan Baxtiyor ugli,
Graduate student, of the Tashkent
University of information technologies
Faculty of Telecommunications technology
E-mail: umb@tuit.uz, tatuumb@mail.ru

DEVELOPMENT OF CRITERIA FOR DETERMINING THE PROBABILITY OF ERROR IN DIGITAL TELEVISION

Abstract: In this paper, we propose a method for determining and analyzing the probability of a PB error and estimating the noise immunity of signals based on the likelihood theory. The method is relatively simple in estimating the signal-to-noise ratio for signals with quadrature modulation types (for QAM example), it makes it possible to determine the probability of a bit (symbol) error with a sufficiently high accuracy from a small sample and without the need for any reference sequences in the signal, modulation type.

Keywords: modulation, keying, digital television, error probability, orthogonal signal, credibility, equal probability, communication channel, noise.

Digital television typically uses spectrally effective type modulation methods, PSK phase shift keying, FSK frequency shift keying, amplitude shift keying ASK, modulation without breaking phase CPM, differential phase shift keying DPSK, quadrature amplitude modulation QAM, orthogonal modulation with frequency multiplexing of COFDM signals. When all the modulation methods are used, errors occur in the transmission of the bits of the PB. However, as it is known [1, 196–202], the higher the order of the constellation, the higher requirements are imposed on the transmission channel. Therefore, an adaptive approach to the operation of the communication system as a whole is used in the digital television (also in the GPRS system). The type of modulation is

selected as the result of a trade-off between the desired data rate and the quality of the communication channel. In addition, all digital communication systems have a threshold effect when the system operates on the verge of the corrective power of the channel decoder and a minimal deterioration in the quality of the signal may lead to a disconnection. Therefore, evaluating the proximity of the system to such a breakdown threshold will avoid unexpected effects.

1. Criteria for determining the probability of error P_B in digital TV. For channels AWGN, binary symmetric channel (BSC), discrete memoryless channel (DMC) and Q-nary symmetric channel (QSK), the digital signal transmitted during the interval (0, T) is represented as follows:

$$s_i(t) = \begin{cases} s_1(t) & 0 \le t \le T \text{ for the symbol } 1 \\ s_2(t) & 0 \le t \le T \text{ for the symbol } 0 \end{cases} \quad (1)$$

The received signal $r(t)$ is distorted due to the noise effect n (t), as well as the non-ideal impulse response of the channel $h_c(t)$, and is described by the following formula:

$$r(t) = s_i(t) * h_c(t) + n(t) \quad (2)$$

when $h_c(t)$, which does not degrade the quality of the waveform $r(t)$ can be simplified:

$$r(t) = s_i(t) + n(t) i = 1,\ 2. \quad 0 \le t \le T \quad (3)$$

The model for demodulation and detection of a digital signal is shown in (Fig. 1). In this case, demodulation is defined as the restoration of a signal (into an undistorted video pulse), and detection is defined as the decision process regarding the digital value of this signal.

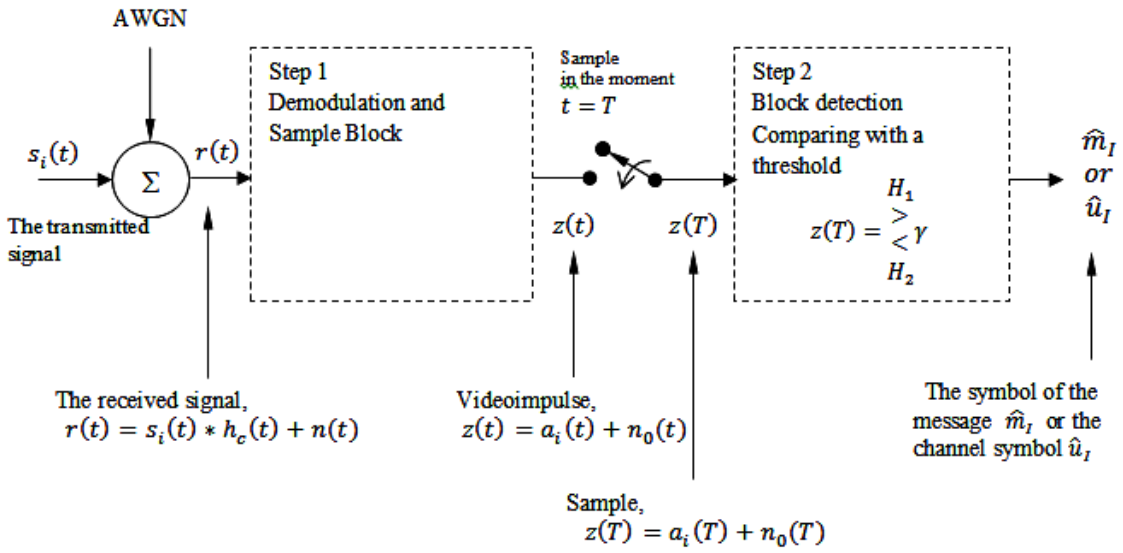

Figure 1. Model of demodulation and detection of a digital signal

The demodulation and sampling unit performs signal reconstruction as a preparation for the next necessary step – detection.

At the output of the filter, the noise is AWGN, then the output of step 1 can be described by the following expression.

$$z(T) = a_i(T) + n_0(T) i = 1,2. \quad (4)$$

where $a_i(T)$ is the desired signal component, and a $n_0(T)$ is the noise. The expression (4) can be represented in simplified form as $z = a_i + n_0$, where n_0 is the noise component – a random Gaussian variable with zero mean, therefore $z(T)$ – is a random Gaussian variable with an average useful signal a_1 or a_2, depending on, a binary zero or binary one was transmitted. It is known that the probability density of random Gaussian noise n_0 can be expressed as follows [1, 137–138]:

$$p(n_0) = \frac{1}{\sigma_0\sqrt{2\pi}} \exp\left[-\frac{1}{2}\left(\frac{n_0}{\sigma_0}\right)^2\right], \quad (5)$$

where σ_0^2 – is the noise variance. Using the expressions (4) and (5), we can express the densities of conditional probabilities $p(z|s_1)$ and $p(z|s_2)$:

$$p(z|s_1)=\frac{1}{\sigma_0\sqrt{2\pi}}\exp\left[-\frac{1}{2}\left(\frac{z-a_1}{\sigma_0}\right)^2\right] \quad (6)$$

and

$$p(z|s_2)=\frac{1}{\sigma_0\sqrt{2\pi}}\exp\left[-\frac{1}{2}\left(\frac{z-a_2}{\sigma_0}\right)^2\right]. \quad (7)$$

These densities of conditional probabilities are shown in (Fig. 2). The density $p(z|s_1)$, shown on the right is called the likelihood s_1 and shows the probability density of the random variable $z(T)$ under the condition of the s_1 symbol transfer, the function $p(z|s_2)$ is the likelihood s_2 and shows the probability density $z(T)$ the symbol s_2. The abscissa, $z(T)$, represents the full range of possible sampling values taken during phase 1 (Fig.1).

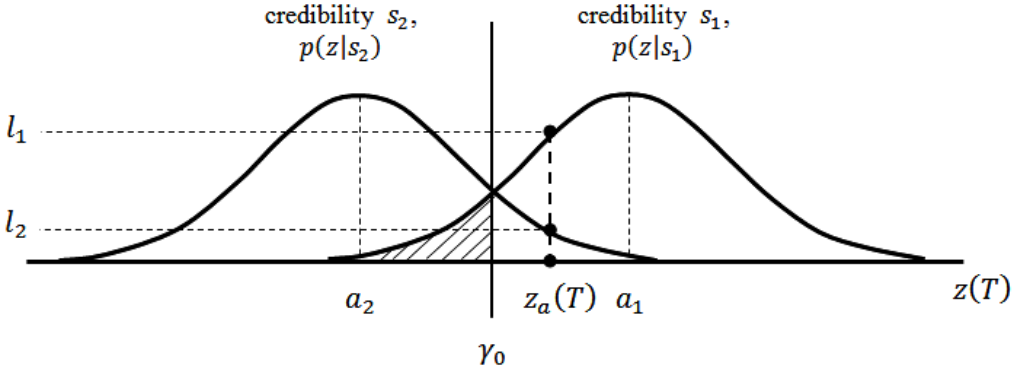

Figure 2. Densities of conditional probabilities: $p(z|s_1)$ and $p(z|s_2)$

In Step 2, detection is performed by selecting a hypothesis that is a consequence of a threshold measurement.

$$z(T)=\begin{matrix}H_1\\ >\\ <\\ H_2\end{matrix}\gamma \quad (8)$$

where H_1 and H_2 are two possible (binary) hypotheses. The choice of H_1 is equivalent to the signal $s_1(t)$ being transmitted, the result of the detection is a digital unit, also H_2 is equivalent to the transmission of the signal $s_2(t)$, and hence the result of the detection is a digital zero.

2. Rationing of the functional to evaluate the quality criterion for signal transmission in digital TV

In digital television, the normalized version of the ratio of the average signal power to the average noise power (S/N or SNR) – E_b/N_0 is used as the criterion for the quality of transmitted signals.

E_b is the energy of the bit, it can be described as the signal power S multiplied by the transmission time of the bit T_b. N_0 is the spectral power density of noise, because it can be expressed as the noise power N divided by the bandwidth W. Since the bit transmission time T_b and the bit rate R_b are mutually inverse, T_b can be replaced by $1/R_b$:

$$\frac{E_b}{N_0}=\frac{ST_b}{N/W}=\frac{S/R_b}{N/W} \quad (9)$$

An important parameter used in digital television is the data transfer rate in bits per second. To represent the bit rate, instead of writing R_b for simplicity, R is written for simplicity. Taking into account (9), it is seen that the ratio E_b/N_0 is the S/N ratio normalized to the bandwidth and bit rate:

$$\frac{E_b}{N_0}=\frac{S}{N}\left(\frac{W}{R}\right) \quad (10)$$

Therefore, one of the most important quality metrics in digital television is a graph of the probability of occurrence of an erroneous bit P_b from E_b/N_0, i.e. the graph of the functional $P_b(E_b/N_0)$, the smaller the required ratio is E_b/N_0, the more effective is the detection process at a given error probability.

3. Develop criteria for maximum likelihood of receiving signals in digital TV

The decision criterion used in stage 2 (Fig.1) was described by the formula (8) as follows:

$$z(T) = \begin{matrix} H_1 \\ > \\ < \\ H_2 \end{matrix} \gamma$$

The criterion for choosing the threshold γ for making a binary solution in expression (8) is based on minimizing the error probability. The calculation of this minimum value of the error $\gamma = \gamma_0$ begins with a relationship record of the ratio of the densities of conditional probabilities and the ratio of the priori probabilities of the appearance of the signal. Since the density of the conditional probability $p(z|s_i)$ is also called the likelihood function s_i, formula

$$\frac{p(z|s_1)}{p(z|s_2)} = \begin{matrix} H_1 \\ > \\ < \\ H_2 \end{matrix} \frac{P(s_2)}{P(s_1)} \qquad (11)$$

there is the likelihood ratio criterion functions. In this inequality $P(s_1)$ and $P(s_2)$ are priori probabilities of $s_1(t)$ and $s_2(t)$ signal transmission. It follows from formula (11) that if the ratio of the truth-likeness functions is greater than the ratio of priori probabilities, then hypothesis H_1 should be chosen. For $P(s_1) = P(s_2)$ and symmetric right-hypothetical functions $p(z|s_i), (i = 1, 2)$, the substitution of formulas (6) and (7) in (11) yields

$$z(T) = \begin{matrix} H_1 \\ > \\ < \\ H_2 \end{matrix} \frac{a_1 + a_2}{2} = \gamma_0 \qquad (12)$$

where a_1 is the signal component of $z(T)$ in the transmission $s_1(t)$, and a_2 is the signal component of $z(t)$ for $s_2(t)$. The threshold γ_0, represented by the expression $(a_1 + a_2)/2$ – is the optimal threshold for minimizing the probability of making the wrong decision in this important particular case. This approach is called the minimum error criterion.

For equiprobable signals, the optimal threshold γ_0, as shown in (Fig. 2), passes through the intersection of the likelihood functions. From formula (12), it is clear that the decision-making stage consists in an effective choice of the hypothesis corresponding to the signal with the maximum likelihood. If the sample value of the received signal is $z_a(T)$, then the decision criterion can be considered as a comparison of the likelihood functions $p(z_a|s_1)$ and $p(z_a|s_2)$, that is, the more probable value of the transmitted signal corresponds to the largest probability density, while the detector chooses $s_1(t)$ if

$$p(z_a|s_1) > p(z_a|s_2) \qquad (13)$$

Otherwise, the detector selects $s_2(t)$.

4. Analytical aspects of error probability estimation and its optimization in digital TV

Theorem. The error probability P_B when receiving and transmitting digital signals depends on the energy of the received bit and the power spectral density of the noise, but not on the specific waveform.

Proofs of the theorem. In the process of making a binary solution, shown in (Fig. 2), there are two possible errors. An error *e* will appear when $s_1(t)$ is transmitted, if, due to the channel noise, the level of the transmitted signal $z(t)$ falls below γ_0. The probability of this is equal to the following [1, 149–151]:

$$P(e|s_1) = P(H_2|s_1) = \int_{-\infty}^{\gamma_0} p(z|s_1)dz \qquad (14)$$

Similarly, the error occurs when $s_2(t)$ is transmitted, if, due to the channel noise, the level of the transmitted signal $z(t)$ rises above γ_0:

$$P(e|s_2) = P(H_1|s_2) = \int_{\gamma_0}^{\infty} p(z|s_2)dz \qquad (15)$$

The probability of an error is equal to the sum of the probabilities of all the possibilities of its appearance. For the binary case, the probability of an erroneous bit can be expressed as follows:

$$P_B = \sum_{i=1}^{2} P(e, s_i) = \sum_{i=1}^{2} P(e|s_i)P(s_i) \qquad (16)$$

Combining formulas (14) – (16), we obtain

$$P_B = P(e|s_1)P(s_1) + P(e|s_2)P(s_2) \qquad (17)$$

or,

$$P_B = P(H_2|s_1)P(s_1) + P(H_1|s_2)P(s_2) \qquad (18)$$

i.e., when $s_1(t)$ is transmitted, the error occurs when H_2 is selected, or when $s_2(t)$ is transmitted, the error occurs when H_1 is selected. For equal priori probabilities (i.e. $P(s_1) = P(s_2) = 1/2$), we have the following:

$$P_B = \frac{1}{2}P(H_2|s_1) + \frac{1}{2}P(H_1|s_2) \qquad (19)$$

Using the symmetry of probability densities, we obtain the following:

$$P_B = P(H_2|s_1) = P(H_1|s_2) \qquad (20)$$

The probability of an erroneous bit, P_B, is numerically equal to the area under the "tail" of any likelihood function, $p(z|s_1)$ or $p(z|s_2)$ that "fills" the "wrong" side of the threshold. Thus, to compute P_B, the function $p(z|s_1)$ is integrated from – ∞ to γ_0 or $p(z|s_2)$ from γ_0 to ∞:

$$P_B = \int_{\gamma_0=(a_1+a_2)/2}^{\infty} p(z|s_2)dz \qquad (21)$$

Here $\gamma_0 = (a_1 + a_2)/2$ is the optimal threshold from equation (12). replacing the likelihood function $p(z|s_2)$ by its Gaussian equivalent of formula (7), we have

$$P_B = \int_{\gamma_0=(a_1+a_2)/2}^{\infty} \frac{1}{\sigma_0\sqrt{2\pi}} \exp\left[-\frac{1}{2}\left(\frac{z-a_2}{\sigma_0}\right)^2\right]dz \qquad (22)$$

We make the substitution $u = (z - a_2)/\tilde{A}_0$. Then $\tilde{A}_0 du = dz$, for $z = \gamma_0$ the boundary of the interval $u = (z - a_2)/\sigma_0 = (a_1 - a_2)/2\sigma_0$ and

$$P_B = \int_{u=(a_1-a_2)/2\sigma_0}^{u=\infty} \frac{1}{\sqrt{2\pi}} \exp\left(-\frac{u^2}{2}\right)du = Q\left(\frac{a_1-a_2}{2\sigma_0}\right) \qquad (23)$$

$Q(x)$ is the error integral in the AWGN channel and is used to describe the probability with a Gaussian distribution density. This function is defined as follows:

$$Q(x) = \frac{1}{\sqrt{2\pi}} \int_x^{\infty} \exp\left(-\frac{u^2}{2}\right)du \qquad (24)$$

$Q(x)$ can not be calculated in an analytical form, it can be calculated by approximation, for $x > 3$, the approximation function $Q(x)$ is calculated by the following formula:

$$Q(x) = \frac{1}{x\sqrt{2\pi}} \exp\left(-\frac{x^2}{2}\right). \qquad (25)$$

Suppose that the input of a linear, time-invariant filter, followed by a discredit device (Fig.1), is fed with the known signal *s(t)* plus the noise of the AWGN *n(t)*. At time $t = T$, the output signal of the sampling device $z(T)$ consists of the signal component a_i and the noise component n_0. The dispersion of the noise at the output (average noise power) is written as σ_0^2. The ratio of the instantaneous noise power to the average noise power, $(S/N)_T$, at time $t = T$ outside the sampling device in step 1 is equal to the following:

$$\left(\frac{S}{N}\right)_T = \frac{a_i^2}{\sigma_0^2}. \qquad (26)$$

The problem consists of determining the transfer function of the filter $H_0(f)$ with the maximum ratio $(S/N)_T$. The signal at the filter output can be expressed in terms of the filter transfer function *H(f)* (before optimization) and the Fourier transform of the signal at the input

$$a_i(t) = \int_{-\infty}^{\infty} H(f)S(f)e^{2\pi ift}df \qquad (27)$$

where $S(f)$ is the Fourier transform of the signal at the input, $s(t)$. If the two-way spectral noise power density at the input is $N_0/2$, then the output noise power can be written as follows:

$$\sigma_0^2 = \frac{N_0}{2}\int_{-\infty}^{\infty} |H(f)|^2 df \qquad (28)$$

Combining formulas (26) and (28), we obtain an expression for $(S/N)_T$:

$$\left(\frac{S}{N}\right)_T = \frac{\left|\int_{-\infty}^{\infty} H(f)S(f)e^{2\pi ift}df\right|^2}{N_0/2\int_{-\infty}^{\infty}|H(f)|^2 df} \qquad (29)$$

The case $H(f) = H_0(f)$ is determined, at which $(S/N)_T$ reaches a maximum. To do this, we use the Schwarz inequality, one of the forms of which is presented below:

$$\left|\int_{-\infty}^{\infty} f_1(x)f_2(x)dx\right|^2 \le \int_{-\infty}^{\infty}|f_1(x)|^2 dx \int_{-\infty}^{\infty}|f_2(x)|^2 dx \qquad (30)$$

Equality is achieved with $f_1(x) = kf_2^*(x)$, where k is an arbitrary constant, and the symbol "*" denotes a complex conjugate value. If the Schwarz inequality is applied to formula (29) with the substitution of values, we obtain the following inequalities:

$$\left|\int_{-\infty}^{\infty} H(f)S(f)e^{2\pi ift}df\right|^2 \le \int_{-\infty}^{\infty}|H(f)|^2 df \int_{-\infty}^{\infty}|S(f)|^2 df \quad (31)$$

$$\left(\frac{S}{N}\right)_T \le \frac{2}{N_0}\int_{-\infty}^{\infty}|S(f)|^2 df \quad (32)$$

or

$$\max\left(\frac{S}{N}\right)_T = \frac{2E}{N_0}, \quad (33)$$

where the energy E of the input signal $s(t)$ is equal to

$$E = \int_{-\infty}^{\infty}|S(f)|^2 df. \quad (34)$$

To optimize P_B in the channel environment and the receiver with the AWGN noise shown in (Fig. 1), we need to select the optimal receiving filter in step 1 and the optimal decision threshold in step 2. For the binary case, the optimal decision threshold is already selected and given by formula (12), and in formula (1.23) it is shown that the error probability at such a threshold is $P_B = Q\left[(a_1 - a_2)/2\sigma_0\right]$. For a minimal P_B, in general, you need to select a filter (matched) with the maximum argument of the function $Q(x)$. Therefore, you need to determine the maximum $(a_1 - a_2)/2\sigma_0$, which is equivalent to the maximum

$$\frac{(a_1 - a_2)^2}{\sigma_0^2}, \quad (35)$$

where $(a_1 - a_2)$ is the difference of the desired signal components at the output of the linear filter at time $t = T$, and the square of this difference signal represents its instantaneous power. In the derivation given in equations (26)–(34), it was shown that 100 matched filters give the maximum possible signal-to-noise ratio equal to $2E/N_0$. Let us assume that the filter matches the input difference signal $\left[s_1(t) - s_2(t)\right]$. Therefore, for the time $t = T$, the signal-to-noise ratio at the output:

$$\left(\frac{S}{N}\right)_T = \frac{(a_1 - a_2)^2}{\sigma_0^2} = \frac{2E_d}{N_0} \quad (36)$$

and

$$E_d = \int_0^T\left[s_1(t) - s_2(t)\right]^2 dt \quad (37)$$

is the energy of the difference signal at the input of the filter. Equation (36) does not represent the signal-to-noise ratio for any particular transmission, $s_1(t)$ and $s_2(t)$, this ratio gives the metric of the difference of signals at the filter output.

Combining equations (23) and (36), we obtain the following:

$$P_B = Q\left(\sqrt{\frac{E_d}{2N_0}}\right). \quad (38)$$

Equations (38) are important intermediate result involving the energy of the difference signal at the input of the filter. From this equation, we can derive a more general relationship for the energy of the received bit. First, we determine the time correlation coefficient ρ, which we will use as a measure of the similarity of the two signals $s_1(t)$ and $s_2(t)$. We have a classical correlation expression

$$\rho = \frac{1}{E_b}\int_0^T s_1(t)s_2(t)dt \quad (39)$$

and

$$\rho = \cos\theta, \quad (40)$$

where $-1 \le \rho \le 1$. If we consider $s_1(t)$ and $s_2(t)$ as signal vectors $\mathbf{s}_1$ and $\mathbf{s}_2$, then the more convenient representation ρ is the formula (40). A vector representation allows you to obtain convenient graphic images. The vectors $\mathbf{s}_1$ and $\mathbf{s}_2$ are separated by an angle θ; at a small angle, the vectors are sufficiently similar (strongly correlated), and at large angles they differ. The cosine of the angle θ gives the same normalized correlation metric as the formula (39).

Writing out the expression (37), we obtain the following:

$$E_d = \int_0^T s_1^2(t)dt + \int_0^T s_2^2(t)dt - 2\int_0^T s_1(t)s_2(t)dt. \quad (41)$$

The first two terms in the formula (1.41) represent the energy associated with the bit, E_b:

$$E_b = \int_0^T s_1^2(t)dt = \int_0^T s_2^2(t)dt \qquad (42)$$

Substituting equations (39) and (42) into the formula (1.41), we obtain the following:

$$E_d = E_b + E_b - 2\rho E_b = 2E_b(1-\rho). \qquad (43)$$

Substituting equation (43) into (38), we obtain the following

$$P_B = Q\left(\sqrt{\frac{E_b(1-\rho)}{N_0}}\right). \qquad (44)$$

Based on the value of the cross-correlation coefficient, there are three cases of determining the error probability P_B in a real system:

1. $\rho = 1$. If the signals are represented as vectors, the angle between them will be zero. Since, in a real system, communication signals (alphabet elements) should be as incommensurable as possible so that they can be easily distinguished (detected). This value of ρ is practically not used;

2. $\rho = -1$. The angle between the signal vectors is 180° and these signals are called antipodal (Fig.3, *a*).

3. $\rho = 0$. The angle between the vectors is 90°, such signals are called orthogonal (Fig. 3, *b*). In order for the two signals to be orthogonal, they should not be correlated during the symbol transmission time, i.e. the following condition must hold:

$$\int_0^T s_1(t)s_2(t)dt = 0. \qquad (45)$$

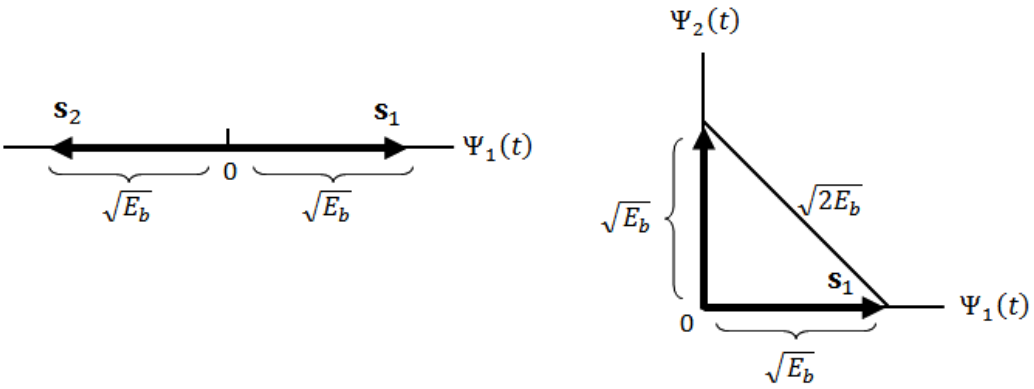

a) b)

Figure 3. Vectors of digital signals: a) antipodal; b) orthogonal

When detecting antipode signals $(\rho = -1)$ using a matched filter, equation (44) can be written as follows:

$$P_B = Q\left(\sqrt{\frac{2E_b}{N_0}}\right) \qquad (46)$$

Similarly, when detecting orthogonal signals $(\rho = 0)$:

$$P_B = Q\left(\sqrt{\frac{E_b}{N_0}}\right) \qquad (47)$$

Therefore, the error probability P_B is dependent on the energy of the input bit and the noise power spectral density, but not on the specific waveform. **The theorem is proved.**

5. The Energy Advantage Under Canal Coding

For definition of efficiency in the beginning for the circuit 16-level PSK without channel encoding pays off, how much greater (concerning accessible 18.5 dB) value E_b/N_0 is required for reception $P_B = 10^{-10}$. This additional E_b/N_0 is demanded efficiency of channel encoding. Using the following formula it is found E_s/N_0 without use of encoding which will give probability of occurrence of mistake $P_B = 10^{-10}$.

$$P_B \approx \frac{P_E}{\log_2 M} \approx \frac{2Q\left[\sqrt{\frac{2E_s}{N_0}}\sin\left(\frac{\pi}{M}\right)\right]}{\log_2 M} = 10^{-10} \qquad (48)$$

Calculation of the equation (48) with a trial and error method rather E_s/N_0, will give value for system without channel encoding $E_s/N_0 = 518.25$ (27.15 dB) and as each symbol consists from $\log_2 16=4$ the bit's, demanded E_b/N_0 (without encoding) = = 518.25/4 = 129.6 (21.13 dB). From the equation

$$\frac{E_s}{N_0} = (\log_2 M)\frac{E_c}{N_0} = (\log_2 M)\left(\frac{k}{n}\right)\frac{E_b}{N_0}, n = 127, k = 106 (49)$$

it is known, $E_s/N_0 = 236.4$ (23.74 dB), and therefore, with channel encoding, E_b/N_0 (with encoding) = = 236.4/4 = 59.1 (17.72 dB). Efficiency of channel encoding is defined by the following formula:

$$G\ (\text{дБ}) = \left(\frac{E_b}{N_0}\right)_{without\ encoding} (\text{dB}) - \left(\frac{E_b}{N_0}\right)_{with\ encoding}$$

$$(\text{dB}) = 21.13\ \text{dB} - 17.72\ \text{dB} = 3.41\ \text{dB}$$

For estimation of efficiency of the canal coding compare the attitude E_b/N_0 energy, happening to on one bit, to spectral density of the powers of the noise in system with coding and in base system without coding and define the difference in importance E_b/N_0 under given probability of the error (fig. 4). This difference measured in decibel and named energy advantage of the code (EAC), can be used for comparison of the different codes.

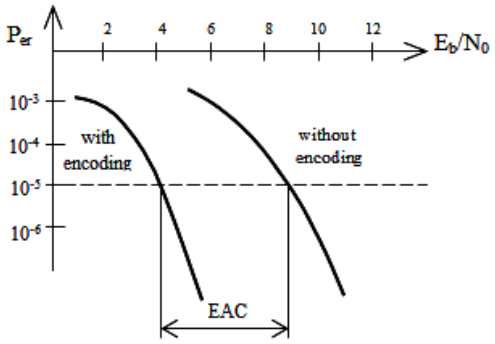

Figure 4. The mark of EAC

In (table 1) is brought resulting advantage of the coding is brought resulting advantage of the coding for different combination internal and external codes under two importance's of probability of the error – 10^{-5} and 10^{-8}.

Table 1.– EAC for different codes and combination of the codes [8]

Variant of the coding/ decoding	EAC, dB	
	10^{-5}	10^{-8}
1. Rid-Solomon+Viterbi	6.5…7.5	8.5…9.5
2. Rid-Solomon +biorthogonal	5…7	7…9
3. Rid-Solomon+short block	4.5…5.5	6.5…7.5
4. Viterbi	4…5.5	5…6.5
5. Block code (hard decision)	3…4	4.5…5.5
6. Convolution code (decoding on threshold)	1.5…3	2.5…4.0

The conclusion

The final criterion for the quality of the digital television system is often the current bit value (BER) or symbolic error (SER). Their measurement is performed either on the basis of the analysis of the reference sequences that are transmitted together with the signal, or on the basis of data on the occurring errors received from the channel decoder.The technique proposed above can be used not only to determine the signal-to-noise ratio (SNR), but also to calculate the probability of a bit (or symbol) error for all types of digital modulation.

From the method suggested above, it becomes clear that in digital television the probability of error P_B does not depend on the type of modulation and on the specific waveform, but only depends on the energy of the input bit and the spectral power density of the noise.

The system of modulation in digital television and the question of the application of one or the other modulation methods is universal. The quality of the work depends only on technological and probability-energy parameters of the system.

The method allows to determine the current value of the bit error in the receiver much faster and with less error than traditional methods.

References:

1. Sklyar B. Digital communication.– M.: Publishing house "Williams",– 2003.
2. Kanakov V. A. New measurement technologies in digital transmission channels of information: textbook.-method. mater. in progr. the qualification "Modern system for mobile digital communication, the problems of noise immunity and protection of information". Nizhny Novgorod,– 2006.
3. Measurement guide lines for DVB systems, ETSITR101290,– 2001.
4. Popov D. I. Statistical theory of radio engineering systems: textbook / Ryazan state radio engineering University, Ryazan,– 2009.
5. Rozhkov I. T. The synthesis of the measure of the signal/noise of the received radio signals.– Saratov: Publishing house Sarat. University press,– 1990.– 166 p.
6. Digital Transmission: Carrier-to-Noise Ratio, Signal-to-Noise Ratio, and Modulation Error Ratio. WhitePaper, Cisco,– 2006.
7. Dubov M. A., Polyanin V., Stoyanov D., Bryukhanov Yu. a. Estimation of probability of bit error of reception of signals quadrature modulation petalonia methods // proc. 14-th Intern. Conf. "Digital signal processing and its applications – DSPA-2012".– M.,– 2012.– Vol. 1.– P. 173–177.
8. Lokshin B. A. "Digital broadcasting: from aspic to viewer".– Moscow. Company SAYRUS SISTEMS,– 2001.

Radjabov Telma,
Professor, Doctor of Physics and Mathematics
Tashkent University of information technologies,
Faculty of Telecommunications technology,
Rakhimov Bakhtiyorjon,
Doctor of Technical Sciences,
Tashkent University of information technologies,
Faculty of Telecommunications technology
Fayzullayev Narzulla,
Student, Tashkent University of information technologies,
Faculty of Telecommunications technology,
E–mail: b.rahimov@tuit.uz, brah2008@rambler.ru)

OPTOELECTRONIC SENSOR SOLID SURFACE COLOR ANALYZER

Abstract: A surface color analyzer consisting of a sensor and an electronic unit is described. An embodiment of the sensor in the form of a hemisphere is presented, in which three pairs of Y–shaped supply and outgoing optical fibers are installed.

Keywords: analyzer, color, colors, LED, light-emitting diode, optical fibers, RGB-system.

1. Introduction

At present, optoelectronic methods of control are successfully used for quantitative and qualitative analysis of various substances, for example, for determining the parameters of liquid semitransparent media (oil products, vegetable oil, glycerin, juices, drinks, urine, blood, etc.). Compared to other physicochemical methods of analysis, they have significant advantages such as high accuracy, sensitivity and economy. The essence of optoelectronic monitoring is that any substance reflects, absorbs, or emits light. Depending on the chemical composition of the substance and the quantitative ratio of its constituent elements, the intensity of light, the absorption coefficient, the reflection angle, and other characteristics of the interaction of light radiation and matter change [1].

2. Analyzer of solid materials

Further in this chapter the optoelectronic automatic analyzer for measurement of color parameters of the surface of solid materials, for example, metals, plastic, glass, paper, etc., in those areas of the industry where color is one of the main indicators of quality of production is described.

Filter colorimeters containing light sources, correcting light filters (X), (Y), (Z) and a photocell are known.

However, this device controls on the principle of passage, analyzes the colors of only translucent fluids, and also has a complex design.

The surface color analyzer of solid materials consists of an electronic unit containing a master oscillator and a trigger switch, a sensor containing three pairs of measuring LEDs and three pairs of compensating light emitting diodes, three measuring instruments, and a measuring system. According to the invention, three triggers connected to the trigger switch are connected to it, three identical optical radiation receivers are located behind the sensor in the signal path, three comparison units that receive signals from the

respective optical radiation receivers, a photoelectric signal processing unit that is connected to the three comparison units and a memory associated with the processing unit, in addition, the sensor is in the form of a hemisphere, with an attached annular casing of soft rubber to which is attached Three pairs of optical fibers disposed at an angle, for example 45°, relative to each other and symmetrically with respect to the normal to the test surface at the reflection point.

In (Fig. 1) is a block diagram of the device for analyzing the color of the surface of solid materials, and in (Fig. 2) – one of the embodiments of the sensor. The color analyzer consists of a sensor and an electronic unit. The sensor is made in the form of a hemisphere 1, in which are installed three pairs of Y–shaped supply 2–4 and withdrawing 5–7 optical fibers.

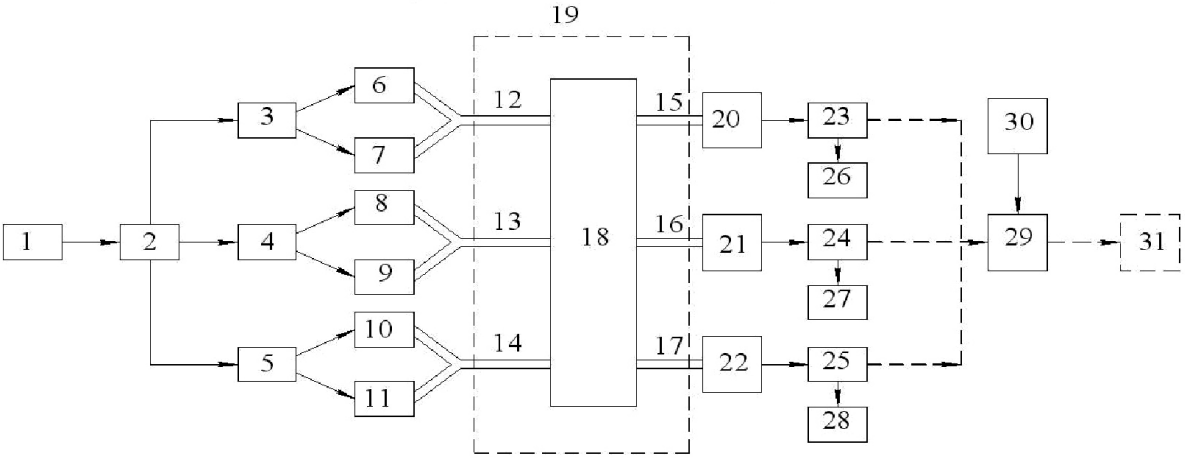

Figure 1. Structural schematic of color analyzer of the solid surface

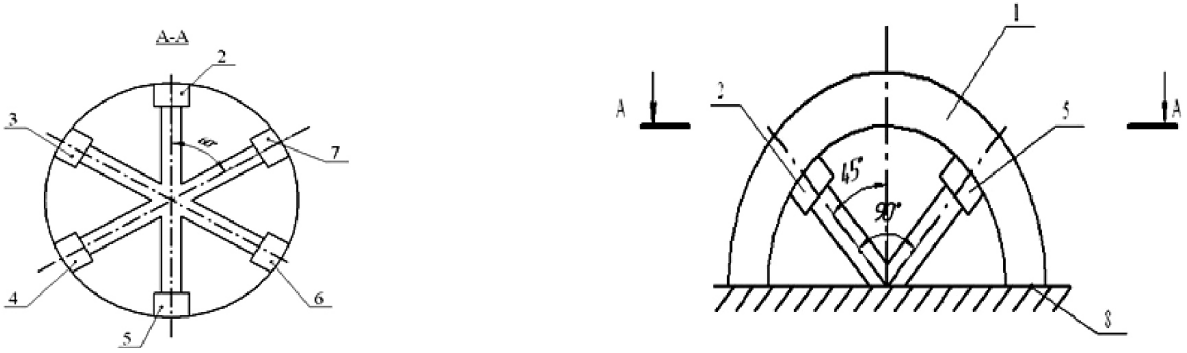

Figure 2. One embodiment of the sensor

Narrow beam radiation, which allows control of parameters is beeped and received due to the flow of the light through the leading 2–4 and offtake 5–7 fiber optic.

The device of the analyzer of the surface color of solid materials in fig. 15, and in (fig. 1) – one of options of sensor performance. The analyzer of color consists of the sensor and the electronic block. The sensor is executed in the form of a hemisphere, 1 in which three couples of Y figurative bringing 2–4 and taking away 5–7 optical fibers are established.

Physical meaning consists of the following: color parameters are detected as an objective features of the subject developing in spectral composition outcoming from them (transmitted and attracted) radiation and perceived as visual sensation.

3. The device works as follows

The master oscillator 9 generates pulses that are supplied to the input of the switch 10. The sepa-

rating pulses are fed to the input of three identical flip–flops 11–13, three outputs of which are connected to three measuring LEDs 14, 16, 18, the second three outputs are equipped with compensation LEDs 15, 17, 19 pulses from the triggers are fed to the corresponding LEDs. Each optocoupler is responsible for monitoring a particular parameter.

The monitored surface 8, which is enclosed in the hemisphere 1, is irradiated by two optical fluxes (measuring and compensating) through the supply optical fibers 2–4.

Optoelectronic pairs are enclosed in a soft rubber casing for the necessary orientation of the sensor and optical isolation of the optical channel and are located at an angle of, for example, 45°, relative to each other and symmetrically with respect to the normal to the monitored surface at the reflection point.

The optical radiation is reflected from the monitored surface and the outgoing optical fibers 5–7 are fed to optical radiation receivers 20–22 operating at wavelengths $\lambda_1 = 680nm$, $\lambda_2 = 560nm$, $\lambda_3 = 450nm$ and converting the optical signals into electrical ones. Due to the passage of light through the supply and discharge optical fiber, a narrow beam of radiation is fed and received, which makes it possible to control the parameters.

Further, the signal falls on its comparison unit 23, 24, 25, the ratio of the two signals (measuring and compensating) is taken and further the measuring system 26, 27, 28 determines shades of three colors. The measurement process at this stage can be completed. Or, three signals can be fed to the photoelectric signal processing unit 29, where they are matched to any of a series of exemplary stored in the memory 30. Then both signals or their ratio are applied to the measurement system or to the computer 31.

The physical meaning is as follows: color parameters are defined as an objective property of objects, which is manifested in the spectral composition of the radiation emitted from them (transmitted, reflected) and perceived as a conscious visual sensation. In this definition, two aspects are given- physical and psycho-physiological, inextricably linked to each other.

The modern theory of color recognition is based on the uniquely established fact of human eye trichromatic, i.e. the visual apparatus contains three types of receptors, each of which predominantly reacts to red, green or blue.

4. Characterization

According to this, the color parameter is mathematically expressed by a vector in three–dimensional color space, and the beginning of this vector coincides with the beginning of the color coordinate system (CCS). If we use the unit vectors of three colors of red r_n, green g_n and blue b_n as the primary colors, then any color can be expressed as:

$$Y = R_{r_n} + G_{g_n} + B_{b_n}$$

where R, G, B are the qualities of the corresponding colors.

In (Fig. 3) the curves for the addition of colors of the systems RGB (a) and XYZ (b) are shown. RGB–system is empirical, which is used as the primary colors of pure spectral radiation of red ($\lambda = 700$ nm), green ($\lambda = 546.1$ nm) and blue ($\lambda = 435.8$ nm) colors. And XYZ is a phenomenological system. The meaning of these systems is that the spectrally pure color with $\lambda = 600$ nm nm is perceived by the eye as consisting of a red and green component in a 14: 3 ratio, radiation with $\lambda = 450$ nm is perceived as a ratio of 7.5: 1: 35 red, green and blue colors respectively.

In the RGB system, the curves of red r_n, green g_n and blue b_n are constructed so that for each of the three primary colors only the ordinate of one curve differs from zero. The main disadvantage of these addition curves is the presence of a negative section near the curve. When measuring color coordinates, color subtraction cannot be realized, therefore, in colorimetric this system is not applied.

Thus, the task of controlling color parameters based on the XYZ system is carried out in three ways. The first is a visual comparison of the measured color with the reference one. The standard is chosen from a pre-compiled color atlas or by

computer programming of each of the colors. The second is the spectrophotometry of the observed radiation and the calculation of the X, Y, Z coordinates. The third is the direct measurement of the X, Y, Z coordinates using three reference optical radiation receivers, the spectral functions whose sensitivities exactly correspond to the Y_x, Y_y, Y_z curves. This method is undoubtedly the most promising, since it meets the requirements of the technological process.

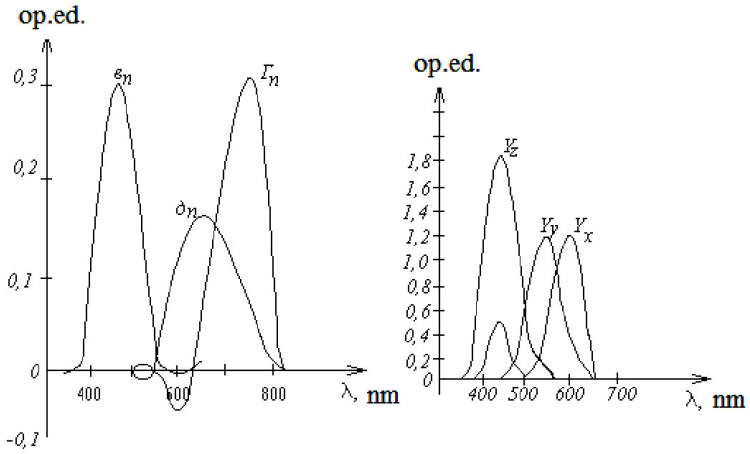

Figure 3. Characteristics of sensors a color analyzer of the surface of solid materials

To develop this method, the device must perform the following operations:

– the isolation of the analyzing radiation at three wavelengths (red, green and blue);

– receiving the radiation fluxes reflected from the monitored object and converting them into a photoelectric signal;

– processing and comparison of the photoelectric signal.

The purpose of each of the three optocouplers is explained as follows: the monitored surface is irradiated with two light streams with wavelengths λ_1 and λ_2, one of which is measurement radiation, and the other is compensatory radiation.

Let the light flux f_0 fall on the monitored surface. The illuminated layer will divide the light flux incident onto it into three parts:

1) f_{λ_1} – reflected from the surface and incident on the receiver of optical radiation, from which came the falling stream;

2) f_{λ_2} – reflected from the surface and not incident on the receiver of optical radiation;

3) f_{λ_3} – absorbed stream, which in the substance of the layer will turn into heat or another form of energy.

In accordance with the law of conservation of energy, the sum of the light fluxes is equal to the incident flux:

$$f_{01} = f_{\lambda 1} + f_{\lambda 2} + f_{\lambda 3}$$

or

$$\frac{f_{\lambda 1}}{f_{01}} + \frac{f_{\lambda 2}}{f_{0\lambda}} + \frac{f_{\lambda 3}}{f_{0\lambda}} = 1$$

For colored substances, these coefficients depend on the spectral composition of the incident radiation. For monochromatic radiation with a certain wavelength (as the emission spectrum of a light–emitting diode), we denote $\rho(\lambda)$, $\tau(\lambda)$, and $a(\lambda)$.

$$\lambda \mp \frac{1}{2}\delta\lambda$$

The spectral dependence of these coefficients is conveniently depicted graphically[2].

The conclusion

The proposed device has improved color recognition accuracy due to three opt couplers that control three color parameters corresponding to the parameters X, Y, Z.

The device has increased accuracy of control due to three–dimensional measurement with wave-

lengths λ_1 = 680 nm, λ_2 = 560nm, λ_3 = 450 nm, when multi–color photo resistors are used as standard optical radiation receivers.

If necessary, the signal from the output of the photoelectric signal processing unit can be fed into the automatic control system.

References:

1. Rakhimov B.N., Ushakov O.K., Larina T.V., Kutenkova E.Yu. The analyzer of color of a surface of firm materials//the Scientific and technical magazine "Devices and the technician of experiment". – Moscow, – 2012. – No. 3. – P. 131–132.
2. Pat. № 2429456 of the Russian Federation. Analyzer of the color of the surface of solid materials / Rakhimov B.N., Kutenkova E.Yu., Larina T.V., Ushakov O.K. // 20.09.2011. Bul. No. 26.

Isakov Hayatulla,
candidate of technical sciences, assistant professor of the
Department of Chemistry, Andijan State University
Uzbekistan, Andijan
E-mail: xayotilla.isakov@bk.ru

Abdurahimova Nodira,
master of Andijan State University,
Uzbekistan, Andijan

Askarov Ibrahim Rahmanovich,
doctor of Chemical Sciences, Professor,
Department of Chemistry, Andijan State University
Uzbekistan, Andijan

Usmanov Sulton,
doctor of technical sciences, professor, head of laboratories
JSC AB Bekturov Institute of Chemical Sciences,
Kazakhstan, Almaty

Azizov Tohir Azizovich,
doctor of Chemical Sciences, Professor, Head of Laboratory
Institute of General and Inorganic Chemistry.
Uzbekistan, Tashkent

COMPLEX COMPOUNDS OF ACETATES OF DIVALENT COBALT, COPPER AND ZINC WITH TRIMETHYLOLTHIOCARBAMIDE.

Abstract: In this paper, the results are presented by synthesizing the study of complex compounds of divalent cobalt acetate, copper and zinc with trimethylolthiocarbamide.

Keywords: Trimethylolthiocarbamide, metal acetates, IR spectrum, synergistic effect, derivatogram, thermolysis, peak, thermal effect.

Introduction

The creation of new chemicals for the use of agriculture is one of the topical problem of chemists – inorganics. Thiocarbamide its derivatives have biologically active effects, in particular, stimulate plant growth. Due to the synergistic effect of the complexes of microelements with thiocarbamide, its derivatives have a higher activity than the sum of the original components.

Previously, we studied the complex compound of cobalt, copper and zinc acetates with dimethylolthiocarbamides.

Objects and methods of research

In the present work, the results of synthesis and investigation of coordination compounds of acetates of divalent cobalt, copper and zinc with trimethylolthiocarbamide are given. Trimethylolthiocarbamide is obtained by reacting thiourea with formaldehyde at pH 8.0–8.5 according to [4].

Coordination compounds of cobalt, copper and zinc acetates were synthesized by the interaction of saturated aqueous solutions of metal acetates and trimethylolthiovcarbamide at a molar ratio of 1: 1, followed by precipitation at room temperature. The

precipitate formed is filtered off, dried in a vacuum desiccator over P_2O_5.

The obtained compounds were analyzed on an atomic-absorption spectrophotometer of the Perkin-Eller firm of the 3030 model, on the Carlo Erba analyzer 1108 (Italy). IR absorption spectra were used to determine the individuality of the synthesized isolated complexes using a two-beam infrared spectrophotometer of the Zeiss IR-20 in the 400–4000 cm^{-1} region.

IR absorption spectra were used to determine the individuality of the synthesized allocated complexes using a two-beam infrared spectrophotometer of the Zeiss IR-20 in the 400–4000 cm^{-1} region. Samples were prepared in the form of tablets compressed with KBr.

The thermal analysis was recorded on the derivatograph of the Paulik-Paulik-Erdei system [5–6] at a rate of 10 deg / min. and samples – 0.10 g with the sensitivity of galvanometers T-900, TG-100 DTA-1/10, DTG-1/10. The recording was carried out under atmospheric conditions with a constant removal of the gaseous medium by means of a water jet pump. The holder was a platinum crucible with a diameter of 7 mm without a cover. Al_2O_3 was used as a reference.

Results and their discussion

The results of elemental analysis are given in Table 1.

Table 1.– Results of elemental analysis

Compound	M%		N%		S%		C%		H%	
	Found	Calcu.	Found	Calcu.	Found	Calcu.	Found	Calcu.	Found	Calcu.
Trimethylolthiocarbamid (L)	–	–	17.01	16.87	20.02	19.87	29.04	28.91	5.97	6.02
$Co(CH_3COO)_2 \cdot L \cdot H_2O$	16.29	16.33	7.81	7.76	8.93	8.87	26.41	26.59	5.02	4.99
$Cu(CH_3COO)_2 \cdot L \cdot H_2O$	17.29	17.38	7.57	7.66	8.88	8.76	26.31	26.27	4.86	4.92
$Zn(CH_3COO)_2 \cdot L \cdot H_2O$	17.91	17.80	7.69	7.63	9.01	8.72	25.96	26.16	5.01	4.90

Some vibrational frequencies (cm^{-1}) in IR absorption spectra of trimethylolthiocarbamide (L) and its complexes with cobalt, copper and zinc acetate are shown in (Table 2).

Table 2.– Some vibrational frequencies (cm^{-1}) in the IR absorption spectra of trimethylolthiocarbamide and its complexes

Trimethylolthiocarbamide (L)	$Co(CH_3COO)_2 \cdot L \cdot H_2O$	$Cu(CH_3COO)_2 \cdot L \cdot H_2O$	$Zn(CH_3COO)_2 \cdot L \cdot H_2O$	Absorption
1	*2*	*3*	*4*	*5*
	3483			ϑ (OH)H_2O
3359	3286	3294	3305	ϑ (OH)alcohol
	3272	3243	3258	ϑ (NH)+2 δ (NH)
3044	3098	3143, 3097	3115	
2955	2922	2972	2973	ϑ (CH)
2897		2843		
	1643 crooked	1654	1636 crooked	δ (NH), δ (OH)
1621	1614	1634		
	1560	1557	1584	ϑ_{as}(COO)
1542	1539	1550	1574,1552	

1	*2*	*3*	*4*	*5*
1521	1521	1540	1538	
1457	1447	1464	1452	ϑ_s(COO)
		1399	1405	ϑ_s(N-C-N)
1423	1417			ϑ (C-N)
1364	1350	1350	1343	$\delta_S(CH_3)$
1300	1300	1303		
1250	1226	1264		ϑ (C=S)amide n
1157	1166	1179	1176	δ (NH)
1064			1081	ϑ (CN)
1026			1022	ϑ (COH)
988			990, 963	$p(CH_2)+\vartheta$ (C–C)$_{ац}$
	897	923	901	
939		853	887, 847	ϑ (C–C)+ $p(CH_2)$
913	804, 720	737	742	$p(CH_2)$
676	673	679	682	δ (COO)
626	623		621	
579	532	562	508	δ (N-C=S), δ (NH)

Comparison of the IR spectra of free trimethylolthiocarbamide and the investigated complex compounds shows that the frequencies of valence vibrations of OH bonds are mixed into the low-frequency region by 54–73 cm^{-1}. While the assumed C = S bond band at 1250 cm^{-1} in the case of cobalt decreases by 24 cm^{-1}, and 14 cm^{-1} is reported for copper, and in the case of zinc disappears. However, the low-frequency band at 579 cm^{-1} attributed to $\overset{N}{\underset{N}{}}C=S$ the deformation vibration of the bond in all cases decreases by 17–71 cm^{-1}. These changes indicate that in coordination both the oxygen atoms of the alcohol groups and the sulfur atom of the thioamide group participate.

Derivatographic data of thermolysis of trimethylolthiocarbamide and its complexes are given in Table 3. The temperature intervals, the peak of thermal effects, the loss of mass of each effect, the nature of thermal effects and the resulting compounds after each process were determined. It is shown that the thermal behavior of complexes depends on the nature of the metal and the composition of the compounds.

Table 3.– The derivational data of the thermolysis of trimethylolthiocarbamide and its complexes with acetates of divalent cobalt, copper and zinc

Compound	**Temperature range of effect ° C**	**Peak effect ° C**	**Weight loss**	**Nature of effect, ° C**	**Formed compounds**
1	*2*	*3*	*4*	*5*	*6*
Trimethylolthiocarbamide (L)	135–150	135	5.00	endothermic	The thermolysis product L
	150–200	160	14.00	endothermic	The thermolysis product L
	200–288	230	40.00	endothermic	The thermolysis product L
	288–310	292	5.00	endothermic	The thermolysis product L

1	*2*	*3*	*4*	*5*	*6*
Trimethylolthiocarbamide (L)	310–370	355	5.00	exothermic	The thermolysis product L
	370–420	400	3.00	exothermic	The thermolysis product L
	420–515	480	6.00	exothermic	The thermolysis product L
	515–595	570	16.00	exothermic	Among the decomposition products L
$Co(CH_3COO)_2 \cdot L \cdot H_2O$	90–130	120	5.11	endothermic	$Co(CH_3COO)_2 \cdot L$
	130–200	150	18.59	endothermic	The thermolysis product $Co(CH_3COO)_2 \cdot L$
	200–242	215	8.97	exothermic	The thermolysis product $Co(CH_3COO)_2 \cdot L$
	242–252	250	18.90	exothermic	The thermolysis product $Co(CH_3COO)_2 \cdot L$
	252–300	270	9.62	endothermic	The thermolysis product $(CH_3COO)_2 \cdot L$
	300–490	415	8.33	exothermic	The thermolysis product $Co(CH_3COO)_2 \cdot L$
	490–610	585	3.20	exothermic	The thermolysis product $Co(CH_3COO)_2 \cdot L$
	760–920	820	14.10	exothermic	Co_2S_3
$Cu(CH_3COO)_2 \cdot L \cdot H_2O$	60–120	90	4.85	endothermic	$Cu(CH_3COO)_2 \cdot L$
	120–165	140	3.13	endothermic	The thermolysis product $Cu(CH_3COO)_2 \cdot L$
	165–198	190	5.73	exothermic	The thermolysis product $Cu(CH_3COO)_2 \cdot L$
	198–215	200	7.29	endothermic	The thermolysis product $Cu(CH_3COO)_2 \cdot L$
	215–262	235	17.81	exothermic	The thermolysis product $Cu(CH_3COO)_2 \cdot L$
	262–360	285	7.60	endothermic	The thermolysis product $Cu(CH_3COO)_2 \cdot L$
	360–450	425	2.60	exothermic	The thermolysis product $Cu(CH_3COO)_2 \cdot L$
	450–550	520	7.55	exothermic	The thermolysis product $Cu(CH_3COO)_2 \cdot L$
	550–585	560	–1.56	exothermic	Oxidation of the thermolysis product $Cu(CH_3COO)_2 \cdot L$
	700–770	750	3.43	endothermic	$CuS+CuSO_3$
$Zn(CH_3COO)_2 \cdot L \cdot H_2O$	90–130	110	4.89	endothermic	$Zn(CH_3COO)_2 \cdot L$
	130–180	150	11.31	endothermic	The thermolysis product $Zn(CH_3COO)_2 \cdot L$

1	*2*	*3*	*4*	*5*	*6*
$Zn(CH_3COO)_2 \cdot L \cdot H_2O$	180–280	235	26.73	endothermic	The thermolysis product $Zn(CH_3COO)_2 \cdot L$
	280–380	340	11.90	endothermic	The thermolysis product $Zn(CH_3COO)_2 \cdot L$
	380–520	425	6.55	endothermic	The thermolysis product $Zn(CH_3COO)_2 \cdot L$
	520–600	580	7.74	exothermic	Education ZnS
	600–760	740	–2.14	exothermic	Oxidation ZnS
	760–840	820	2.38	endothermic	Education ZnO

Conclusion

The synthesis conditions were developed, three complex compounds of acetates of divalent cobalt, copper, and zinc with trimethylolthiocarbamide were isolated in a solid state. With the help of elemental, derivatographic analysis, vibrational spectroscopy, the composition, thermal behavior and methods of coordination of the molecule of trimethylolthiocarbamide and the acetic acid ion are proved. The central atom is surrounded by six oxygen atoms and has a geometric configuration of a distorted octahedron.

References:

1. Isakov H., Usmanov S., Gorbunov V. V. "IR absorption spectra of coordination compounds of zinc, cobalt (II), copper (II) with dimethylolthiourea and methylene dithiourea" // Uzb. chem. Journal – 1994.– No. 6.– P. 6–9.
2. Isakov H. Complex compounds of some d-metals with dimethylolthiourea // Rept. AS. Rept. Uzb.– 1996.– No. 1, 2.– P. 40–42.
3. Askarov I. R., Isaev Yu.T., Makhsumov A. G., Kirghizov Sh.M. // Organic Chemistry. Tashkent.– 2012.– 572 p.
4. Kadawaki BiLL Chem, Sec, g Japan – 1936. VII.– 248 p.
5. Isakov H. "X-rayg raphic and thermogravimetric studies of thiourea-formaldehyde oligomers" Rept. AS. Rep. Uzb.– 1996.– No. 8.– P. 32–35.

Egamberdiev Elmurod Abdukodirovich,
Doctoral, candidate of the chair
"Technology of cellulose and woodworking"
Tashkent chemical-technological institute
Email: el.0919@mail.ru

Rakhmanberdiev Gappar Rakhmanberdievich,
Professor, of the department
"Technology of cellulose and woodworking"
Tashkent chemical-technological institute
Email: raxmanberdiev@mail.ru

Mardonov Asror Khasanovich,
assistant, "Technology of cellulose and woodworking"
Tashkent chemical-technological institute
Email: mardonovasror@mail.ru

STUDY OF THE SORPTION RATE OF COMPOSITION PAPER SAMPLES OBTAINED ON THE BASES OF CELLULOSE-BEARING PLANTS CELLULOSE AND BASALT FIBER

Abstract: Composite materials samples have been obtained from cellulose and bazalt fibers based on cellulose-bearing plants. The properties of paper samples have been studied: the amount of cellulose, the amount of ash, water absorption and breaking load. Gained results show that the composite material with the addition of basalt fibers is more durable. Half-finished cellulose fibers obtained from basalt, straw and wastepaper are more porous than ones obtained from cotton plant.

Keywords: basalt fiber, composite material, high-strenght-paper, topinambour, packaging material, heat-insulated material, paper and cardboard samples.

Introduction

It's hard to imagine a place without paper. Worldwide, 339 mln. t. (2003 y), 350 thousand tons in Russia (2000 y). According to the 2009 year data, paper produced in Uzbekistan provides 10% of the demand for this product. The rest of the paper is imported from foreign countries.

In recent years, paper production has been expanding from year to year. About 75% of annual paper produced in the world is produced in the People's Republic of China, and the country meets 50% of its own demand for paper with paper obtained from annual plants.

Uzbekistan has a very large source of raw materials (guza-paya and rice straw, straw, hemp, etc.) to obtain paper from annual plants.

Nowadays, as the demand for paper and paper products is rising, it has called us to obtain other types of paper products. For this purpose, a series of investigations have been carried out.

Cellulose-containing wastes, annual plants cellulose and other ingredients can be obtained from different compositional properties. The composition of the cellulose solution, the one-dimensional mixtures, is a mixture of acrylamide ingredients, which is characterized by the formation of any

trimmed compositions. Among these local raw materials in our Republic is basalt fiber with heat stability and durable properties. Basalt fiber tends to crystallize more easily than other glass fibers. It is resistant to heat, chemical effects and combustion and is highly durable. Therefore, it is used to produce composite plastics instead of asbestos, which is a concentrate (conserogen). We have chosen the basalt fiber extracted in Asmosoy, our Republic, for the experiment. The fluid temperature of this fiber is 1250° C, which is much lower than the one in other places.

Objects and methods. We obtained paper samples on the bases of annual composite materials based on the annual cellulose and basalt fibers and studied their properties. The main purpose of the work is to increase the strength of the paper, reduce its burning and moisture absorbing.

We have obtained five different composite materials containing cellulose and basalt fibers. As a raw material, the following materials were used to prepare cellulose compositions: basalt, topinambur, cotton lint, cellulose derived from guza-paya. The composition of the humid composition composite material was made in the laboratory by mixing basalt fiber with cellulose from each of them separately, in equal quantity. The prepared mass was diluted for 1–1.5%, and the paper was pulled into the paper-making machine. When the cylinder of the apparatus is gently lifted together with the net, at the end of the water, the wet cellulose layer is formed. The generated cellulose layer is brought together with a net and dehydrated at a drying pad for 105–110° C up to 75–80% moisture. Then it is press (fig. 1) on the press until the desired thickness is reached and kept in the press for 30 minutes.

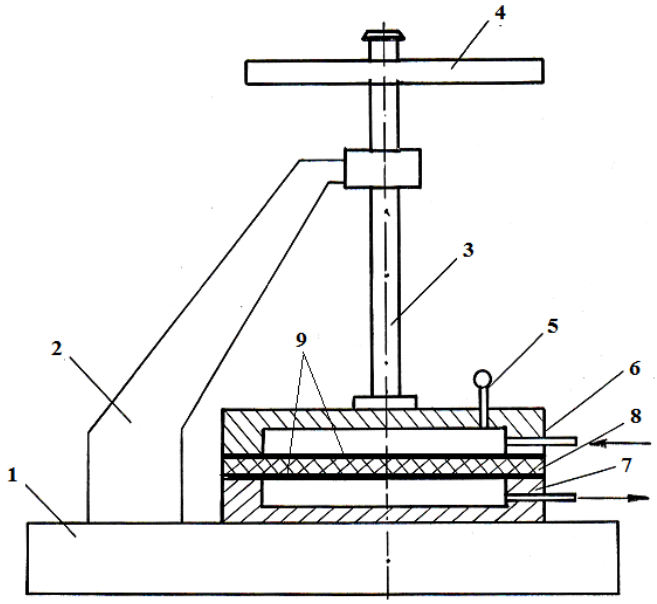

Figure 1. Laboratory filter-press: 1 – base; 2 – handle; 3 – screw; 4 – screwer; 5 – monometer; 6 – movable plate; 7 – unmovable plate; 8 – wet cardboard; 9 – metal disk

The sample is dried again up to 5–6% moisture. It is cut by 6 x 6 cm and the mass is determined with the analytical weights. The thickness of the sample is measured using a shaft. All samples were molded in the same manner. After drying, the technical parameters of the samples are determined and other physicochemical and heat conductivity and thermal parameters are determined. In this article we basically examine the absorption degree of composite paper samples. The mass of the molded samples has been determined.

The next step is to determine the sorption degree of the composition. Methods for determining the samples sorption degree:

1. Take 1 g of samples to determine the swelling degree and is swelled in the water for 30 minutes. Then the mass of excess water is determined by rotating the water over time and then turning the centrifuge to 5,000 times per minute.

2. Samples are kept in the water for 30 minutes and then put the two pieces of pulp between disks and the excess water is 2 kg. The mass is determined removing the excess water with power.

3. To determine the mass after storage for 24 hours generating a relative humidity with 70% in the concentrated soda ash state.

We studied the sorption properties of the obtained materials. This job has been completed according to the above-mentioned methodical instructions. For this purpose, soaking samples in the water, the amount of absorbed water, the sagging rate and the degree of absorption of relative humidity by 70%. The absorption rate of samples is shown in the table below.

Table 1.– The absorption rate of composite paper samples is shown in the table below

№	Name	Weight, g		Absorption rate,%
		dry	wet	
1.	The paper obtained on the basis of topinambour cellulose	1.0	1.70	70
2.	The paper obtained on the bases of basalt fibre and topinambour cellulose	1.0	1.40	40
3.	The paper obtained on the basis of poplar cellulose	1.0	1.76	76
4.	The paper obtained on the bases of basalt fibre and poplar cellulose	1.0	1.40	40
5.	The paper obtained on the basis of cotton lint cellulose	1.0	2.15	115
6.	The paper obtained on the bases of basalt fibre and cotton lint cellulose	1.0	1.60	60
7.	The paper obtained on the basis of wheat straw cellulose	1.0	2.40	140
8.	The paper obtained on the bases of basalt fibre and wheat straw	1.0	1.71	71
9.	The paper obtained on the bases of guza-paya cellulose	1.0	2.11	111
10.	The paper obtained on the bases of basalt fibre and guza-paya cellulose	1.0	1.70	71
11.	The paper obtained on the bases of basalt fibre	1.0	1.16	16

As it can be seen from the table, the composition of the composition paper sample based on topinambur and cotton linter cellulose and basalt fiber is about 40–60%, which is a positive result. Our goal is to introduce paper-based composite paper into different industries. At the next stage of our experiments, we investigated the degree of sorption of moisture from relative humidity by about 70% of the composition paper sample.

As it can be seen from the table, the sorption of moisture from air depends on the composition of samples. In this table, the composition paper sample based on topinambour and cotton lint cellulose and basalt fiber constitutes about 3% of the amount of moisture absorption. These figures describe the structure of the paper samples. The more samples absorb moisture, the more likely the cellulose fibers will be in the porosity. Therefore, paper samples obtained from the poplar, straw and stalks of cellulose and basalt fibers are stiffer than paper samples obtained from cotton lint and topinambur cellulose.

Table 2.– The sorption degree of moisture from air with relative humidity of 70% of composition paper

№	Name	Weight, g		Absorption rate,%
		dry	wet	
1.	The paper obtained on the basis of topinambour cellulose	1.0	1.6	160
2.	The paper obtained on the bases of basalt fibre and topinambour cellulose	1.0	1.03	103
3.	The paper obtained on the basis of poplar cellulose	1.0	1.5	150
4.	The paper obtained on the bases of basalt fibre and poplar cellulose	1.0	1.04	104
5.	The paper obtained on the basis of cotton lint cellulose	1.0	1.6	160
6.	The paper obtained on the bases of basalt fibre and cotton lint cellulose	1.0	1.03	103
7.	The paper obtained on the basis of wheat straw cellulose	1.0	1.7	170
8.	The paper obtained on the bases of basalt fibre and wheat straw	1.0	1.04	104
9.	The paper obtained on the bases of guza-paya cellulose	1.0	1.6	160
10.	The paper obtained on the bases of basalt fibre and guza-paya cellulose	1.0	1.04	104
11.	The paper obtained on the bases of basalt fibre	1.0	1.01	101

At the next stage, we blended the annual plants cellulose and basalt fibers in different composition and obtained the paper samples and studied their properties. We've presented the results in the table below.

Table 3.– The sorption rate of paper obtained on the bases of basalt fiber and topinambour cellulose

№	The name and content of composition	Weight, g		Absorption rate,%
		dry	wet	
1.	The paper obtained on the bases of basalt fibre and topinambour cellulose, 25:75	1.0	1.69	69
2.	The paper obtained on the bases of basalt fibre and topinambour cellulose, 50:50	1.0	1.40	40
3.	The paper obtained on the bases of basalt fibre and topinambour cellulose, 75:25	1.0	1.29	29
4.	The paper obtained on the basis of basalt fibre, 100	1.0	1.16	16

Table 4.– The sorption rate of paper obtained on the bases basalt fiber and wood cellulose

№	The name and content of composition	Weight, g		Absorption rate,%
		dry	wet	
1	*2*	*3*	*4*	*5*
1.	The paper obtained on the bases of basalt fibre and wood cellulose, 25:75	1.0	1.71	71

1	*2*	*3*	*4*	*5*
2.	The paper obtained on the bases of basalt fibre and wood cellulose, 50:50	1.0	1.40	40
3.	The paper obtained on the bases of basalt fibre and wood cellulose, 75:25	1.0	1.33	33
4.	The paper obtained on the basis of basalt fibre, 100	1.0	1.16	16

Table 5.– The sorption rate of paper obtained on the bases of basalt fibre and cotton lint cellulose

№	The name and content of composition	Weight, g		Absorption rate,%
		dry	wet	
1.	The paper obtained on the bases of basalt fibre and cotton lint cellulose, 25:75	1.0	1.87	87
2.	The paper obtained on the bases of basalt fibre and cotton lint cellulose, 50:50	1.0	1.60	60
3.	The paper obtained on the bases of basalt fibre and cotton lint cellulose, 75:25	1.0	1.41	41
4.	The paper obtained on the basis of basalt fibre, 100	1.0	1.16	16

Table 6.– The sorption rate of paper obtained on the bases of basalt fibre and wheat straw cellulose

№	The name and content of composition	Weight, g		Absorption rate,%
		dry	wet	
1.	The paper obtained on the bases of basalt fibre and wheat straw cellulose, 25:75	1.0	1.90	90
2.	The paper obtained on the bases of basalt fibre and wheat straw cellulose, 50:50	1.0	1.71	71
3.	The paper obtained on the bases of basalt fibre and wheat straw cellulose, 75:25	1.0	1.47	47
4.	The paper obtained on the basis of basalt fibre, 100	1.0	1.16	16

Table 7.– The sorption rate of paper obtained on the bases of basalt fibre and guza-paya cellulose

№	The name and content of composition	Weight, g		Absorption rate,%
		dry	wet	
1.	The paper obtained on the bases of basalt fibre and guza-paya cellulose, 25:75	1.0	1.89	89
2.	The paper obtained on the bases of basalt fibre and guza-paya cellulose, 50:50	1.0	1.71	71
3.	The paper obtained on the bases of basalt fibre and guza-paya cellulose, 75:25	1.0	1.45	45
4.	The paper obtained on the basis of basalt fibre, 100	1.0	1.16	16

As it can be seen in the tables above, that the more the basalt fibre is added into the content of composition, the more the sorption rate of composition paper decreases. It is also worth mentioning

that the most optimal variant of our paper, based on basalt fiber and topinambour cellulose. Below you will find examples of composition paper through experiments.

The paper obtained on the bases of basalt fibre and wheat straw cellulose (1:1)

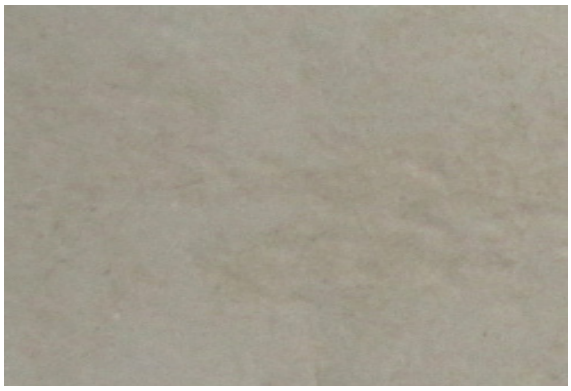

The paper obtained on the bases of basalt fibre and cotton lint cellulose (1:1)

The paper obtained on the bases of basalt fibre and poplar cellulose (1:1)

The paper obtained on the bases of basalt fibre and guza-paya cellulose (1:1)

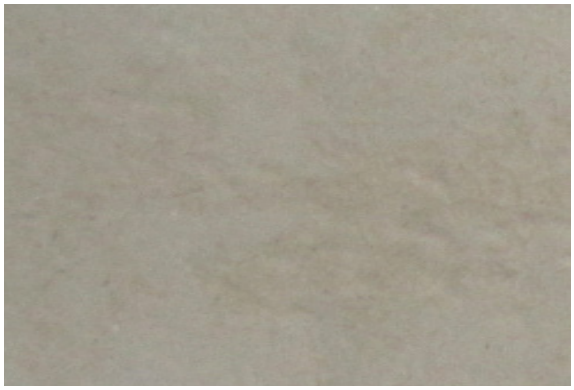

The paper obtained on the bases of basalt fibre and topinambour cellulose

References:

1. Рахмонбердиев Г.Р Целлюлоза, полученная из топинамбура «Иктисодиёт ва иновацион технологтялар» илмий электрон журнали. – Тошкент,– 2011.– № 2.

2. Кадыров Б. Г., Ташпулатов Ю. Д., Примкулов М. Т. Технология хлопкового линта, целлюлозы и бумаги.– Ташкент: Фан,– 2005.– 172 с.
3. Волкова Г. П. и др. Бумага из базальтового волокна / Бумажная промышленность.– Москва,– 1965.– № 6.– С. 31–32.
4. Дерикот Л. З. Зависимость коэффициента теплопроводности базальтовой ваты от обьемного веса / В сб: Теплофизические свойства веществ.– Киев.– 1966.– С. 141–143.
5. Джигирис Д. Д., Махова М. Ф. Основый производства базалбтовых волокно изделий.– М.: Каменный век.– 2002.– С. 200–211.

Section 6. Chemistry

Nguyen Thi Huong, Vo Hoang Phuong,
Institute for Chemistry and Material,
Vietnam Academy of Military Science and Technology, VN
E-mail: Nguyenhuong0916@gmail.com
Tran Hong Con, Le Thanh Son,
Faculty of Chemistry, Hanoi University of Natural Science, VNU
Dang Thi Uyen,
Military Institute of Chemistry and Environment, VietNam

REMOVAL POSIBILITY OF BENZENE VAPOUR IN THE AIR BY ZEOLITE HY COMPOSITE

Abstract: The zeolite composites were synthesized by seft assembly trom tributyl phosphate or tricresyl phosphate and zeolite HY in n-hexane at 70 °C for 3 hours contacting. The structural characterization and the porosity of the material were studied by Field Electronic Scanning Emission Microscope (FESEM), X-Ray Difraction (XRD) and Brunauer-Emmett-Teller (BET) adsorption method. Chemical bondings were characterized by Fourier Transform Infrared Spectroscope (FT-IR). The synthesized materials were studied on their adsorption ability of benzene in the air. Adsorption of benzene vapor in fixed-bed columns of zeolite composite materials was investigated at low vapor concentrations. The effects of empty bed contact time (EBCT), factors influencing on the dynamic equilibrium absorption capacity of the zeolite composties, such as inlet concentrations of benzene vapor (20 ppmv to 60 ppmv), working temperature (30° C and 40° C), gas flow rate (0.15 L/min to 0.60 L/min) were studied. The results showed that these composite absorbents were suitable for application of benzene vapour treatment in the air environment.

Keywords: Tributylphosphate, Tricresylphosphate, Benzene, Zeolite HY, Zeolite Composite.

1. Introduction

Benzene is one of highly toxic agents of volatile organic compounds (VOCs) upon human and animal. When the human body is benzene poisoned, it will directly affect the structure of cells, or alter the development of cells and hold-back the enzymes which are related to the process of forming blood cells. The above processes would cause diseases related to anemia, lack of leukemia and related to bone marrow diseases, as well as cancer (Stanley E. Manahan, 2003); Suleeporn Sangrajang, 2008); Robert Snyder, 1993); Ernest Hodgson, 2004). So, there are many studies concerning to adsorption of benzene vapor in the air used zeolite HY as a benzene adsorbent, showing the benzene adsorbed on zeolite HY formed a fairly durable compound of HY-benzene. However, this adsorption process is mostly physical with low binding energy. In this process there are two types of binding between benzene and H atoms in the zeolite, it is result of the interaction of

Van der Waals forces of benzene inside 12-T or 4-T of zeolite. According to Shuai Ban, the process of benzene adsorption of zeolite HY started at 10 kPa, and rising fast when the pressure increases, the adsorption is less variable at high pressure. With low pressure, the adsorbability of benzene on zeolite HY depends greatly on temperature (Shuai Ban, 2009). The benzene adsorption on the zeolite HY mainly depends on the interaction of benzene with 4 hydroxyl groups of 4 faces in a zeolite cell unit, normally these H groups can be determined through IR spectrum measurement (Shuai Ban, 1995). However, the studies showed that the number of hydrogen group types in the cell unit is different. According to Jirák, in a cell unit were found 21.1 ± 5.5 H (1), 30.9 ± 7.0 H (3), without the presence of H (2), H (4). Czjzek et al. found 28.6 ± 1.0 H (1), 15.0 ± ± 1.0 H (3), 9.5 ± 1.0 H (2) and also did not find the presence of H (4) (Mirjam Czjzek et al., 1992). Meanwhile, Vitale with his group found that all four types of hydrogen were found in the cell unit of the zeolite HY (G. Vitale et al., 1995). The study results of Fabien Jousse et al. have launched an interactive model of benzene in zeolite HY with Si/Al ratio of 2.43; where are 4 types of hydrogen interaction with benzene appeared, including H(2) – Benzene; H(1) – Benzene; 2 H(1) – Benzene and W – Benzene (Fabien Jousse et al., 2000). According to Siricharn S. Jirapongphan et al., benzene adsorption on zeolite HY occurs in the following 6 types of H1, H2, 2H1, W and two types of U6 and U4 (Siricharn S. Jirapongphan et al., 2006).

Currently, in order to increase the selective adsorption of volatile organic compounds agents, as well as benzene of zeolite, some research groups have modified zeolite by organosilicone agents, with the aim to bring more aromatic cyclic groups on zeolite surface and to create interaction between the electron π of benzene with eπ agents of the aromatic cyclic group (Qin Hu et al., 2009).

This article presents the method of preparation and properties of materials based on organic phosphorus and zeolite HY and study on their adsorbability of benzene vapour in the air.

2. Material and methods

2.1. Zeolite composite preparation

The typical synthesis of a zeolite composite is according to procedure as below: To a 1 g of zeolite HY (HS-320, Wako-Japan; SiO_2/Al_2O_3: 5,5 mol/mo/; crystal size: 0,3 μm; pore aperture: 0,8 nm) in the reflux reactor, was added 50 ml of n-hexane and the mixture was continuously stired; then 50 ml of n-hexane containing 0.1 g tributyl phosphate (TBP 0.979 g/ml, Aldrich) or tricresyl phosphate (TCP 1.16–1.175 g/ml, Aldrich) was slowly added and stirring for 3 hours at 70 °C. The synthesis process was performed in closed reaction system to avoid evaporation of n-hexane. The n-hexane (the solvent) in the product sample was then removed by vacuum distillation and finaly, the sample was dried at 110 ° C for one hour, cooled and stored in a desiccator. The zeolite composite samples were signed as CY_{TBP} and CY_{TCP} for tributylphosphate and tricresylphosphate respectively.

The chemical bonding characteristics of CY_{TBP} and CY_{TCP} materials were evaluated by Fourier Transform Infrared Spectroscope (FT-IR, GX-Perkin Elmer, USA), the materials structure was determined by Field Emission Scanning Electron Microscope method (FESEM, Jeol 6610LA, Japan). Nitrogen adsorption — desorption isotherms were performed at 77 K in Tristar 3000-Micromeritics equipment, USA, using static adsorption proceduce. Samples were degassed at 150°C and 10^{-6} Torr for minimum 12 h prior to analysis. BET surface areas were calculated from the linear part of BET plot according to IUPAC recommendation. Pore size distributions of the samples were calculated via the conventional BJD model.

2.2. Adsorption of benzene vapor

2.2.1. Adsorption column preparation:

— *Quartz sand in mixture with zeolite composite samples:* Quartz sand with diameter of 0.4–0.5 mm was washed and soaked in HCl of 0.1 M for 24 hours.

Then the sand was washed again to pH 7, dried and heated at 550–600°C for 3 h to completely remove organic impurity.

— *Adsorption column:* 0.5 g of zeolite composite and 2.0 g of sand were mixed well together then filled into 1.0 cm diameter quartz column. The length of adsorption material columns after filling was 3.5–3.7 cm. In two ends of the column were blocked by layers of glass fiber. For experimental performance, the column was inserted into the themostate room as shown in Figure 1.

* *The research equipment:*

— Figure 1 is diagram of the equipment for organic solvent vapor adsorption investigation with themostate room seting temperature with vibration of ± 0.1°C.

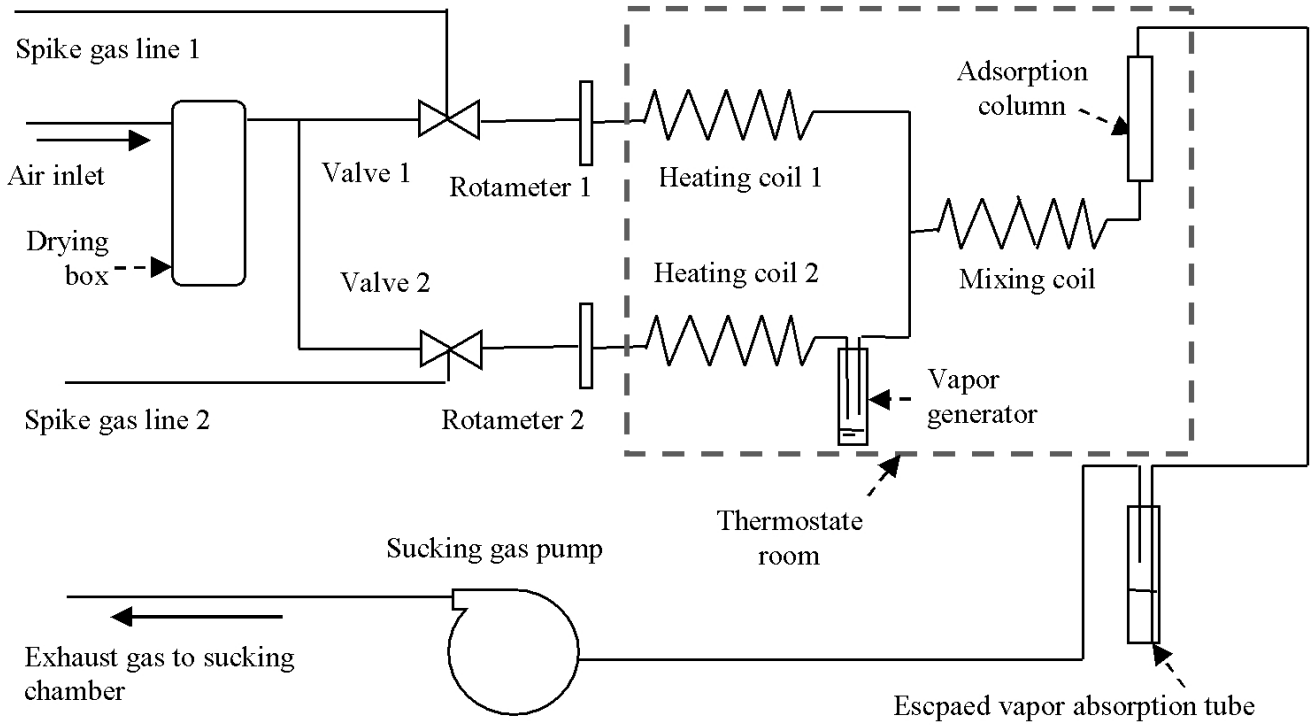

Figure 1. Diagram of vapor adsorption research equipment

* *Benzene concentration determination* (Abulrahman Bahrami et al., 2011; L. Zoccolillo et al., 2001): The inlet and outlet benzene vapor concentrations were determined through analysis of benzene adsorbed in acetonitrile — water mixture with volume ratio of 3:1 before and after adsorption respectively by the HPLC Mode HP 1100, using column C18-Zobax and DAD detector series. The content of adsorbed benzene vapro on the column over the time was calculated by the formular:

$$m_B = m_I - m_t \ \text{(mg)};$$

In which: m_I is the amount of input benzene vapor (mg); m_t is the amount of output benzene vapor (mg) in the time *t*.

The equilibrium adsorption capacity of material is calculated according to the formula:

$$q = \frac{m_B}{m_Z} \ \text{(mg/g)}$$

In which m_B is the amount of adsorbed benzene vapor (mg), m_Z is the adsorption material mass (g).

3. Results and discussion

3.1. Characteristics of zeolite composite materials

The infrared spectrum of CY_{TBP} and CY_{TCP} is shown in Figure 2.

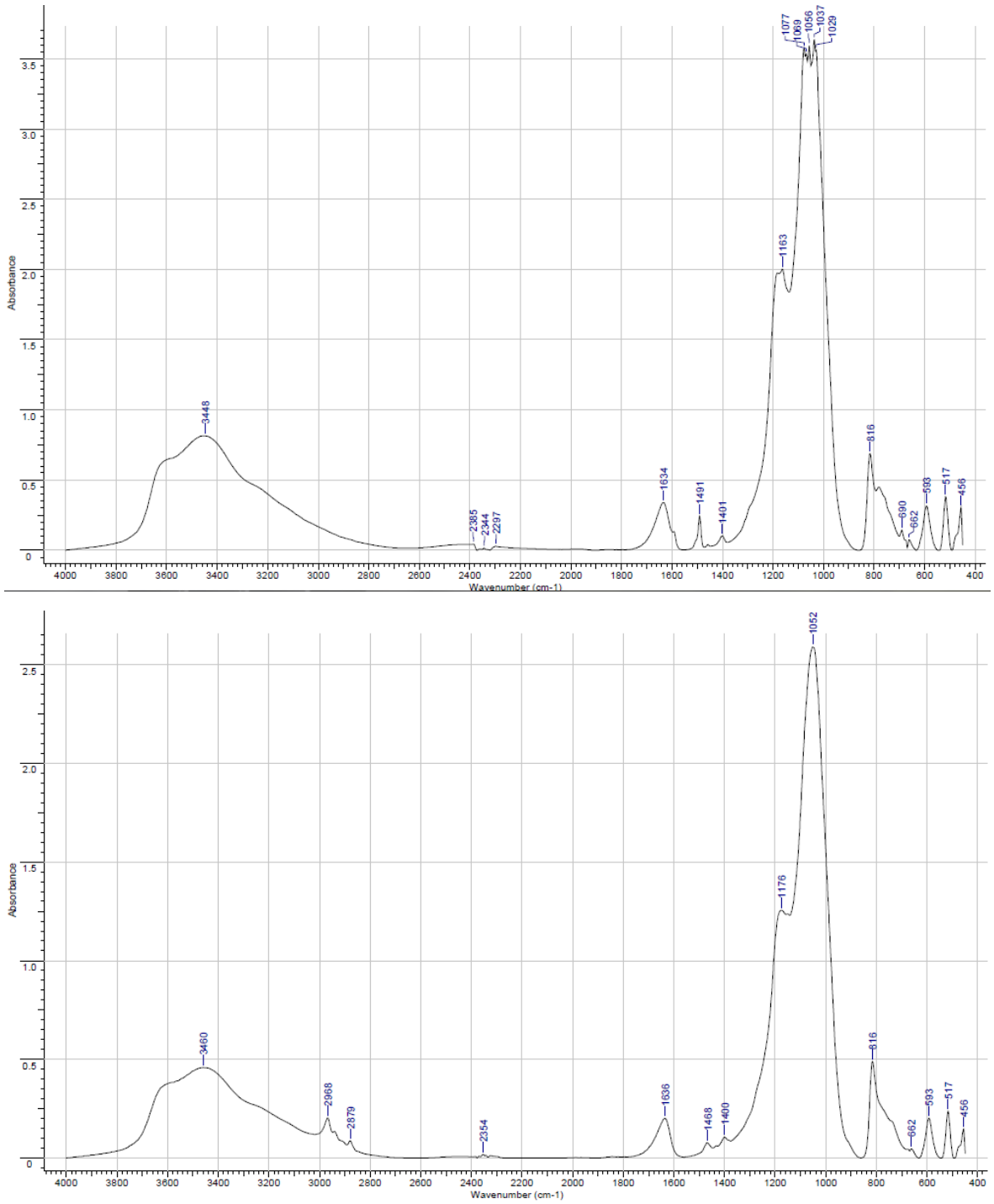

Figure 2. Infrared spectrum of CY_{TCP}, (a) and CY_{TBP} (b)

The infrared spectrum diagram of samples showed the presence of the peak at wave number from 3448 cm^{-1} to 3460 cm^{-1} with wide base, characterized the vibration of the OH group of the zeolite. However, the peak intensity is weak due to the presence of physical adsorbed H_2O on the surface of zeolite, so the hydrogen bridge bonds between oxygen in water and the OH group covered the O-H bond of the zeolite surface. It was also demonstrated where presence of peak at wave number 1638 cm^{-1} (CY_{TBP}) and 1634 cm^{-1} (CY_{TCP}) (H. Robsin, 2001). The peaks at wave number 2879 cm^{-1} and

2968 cm^{-1} characterize the vibration of C-H bond in CH_3 group in the tributylphosphate in CY_{TBP} sample, while in CY_{TCP} sample there is no appearance of these peaks at these wave numbers. And the CY_{TCP} has peaks appeared at wave number 1491 cm^{-1} and 1401 cm^{-1} with stronger intensity than peak at wavenumber 1468 of CY_{TBP}. This shows that in the CY_{TCP} there is a characteristic vibration of aromatic cyclic structure. Notably, both samples have the appearance of peaks at wave number from 1178 cm^{-1} to 1163 cm^{-1} and from 1077 cm^{-1} to 1050 cm^{-1}, with the strong to moderate intensity characterized the vibration of Si-O-Si and Si-O-C bonds. The above characteristics of the material show that there was interaction between zeolite surface and organic components.

In the wave numbers from 1200 cm^{-1} to 400 cm^{-1}, there appeared characteristic peaks for frame structural bonds of zeolite, both samples have the appearance of three smaller peaks around wave number 600 cm^{-1}, characterized the vibration of frame structure and distortion vibration of group O-T-O of zeolite. In which, the presence of the peak at wave number 583 cm^{-1} (CY_{TCB}) and 593 m^{-1} (CY_{TCB}) characterize asymmetrical and symmetrical vibration of the four-sided ring, which is also the characteristic of distortion vibration of the double ring in the frame structure of zeolite type Faujasite (H. Robsin, 2001; Wtodzimierz Mozgawa et al., 2011). In addition, both materials have the appearance of two peaks at wave number characterized the valence vibration of group P-O aliphatic for CY_{TCB} (1150 cm^{-1}; 816 cm^{-1}) and P-O aromatic for CY_{TCB} (1163 cm^{-1}; 1037 cm^{-1}). These two groups indicate the presence of phosphate functional group in the structure of the zeolite composite samples. Surface morphology of samples HY, CY_{TBP}, CY_{TCP} is expressed in FE-SEM image (Figure 3).

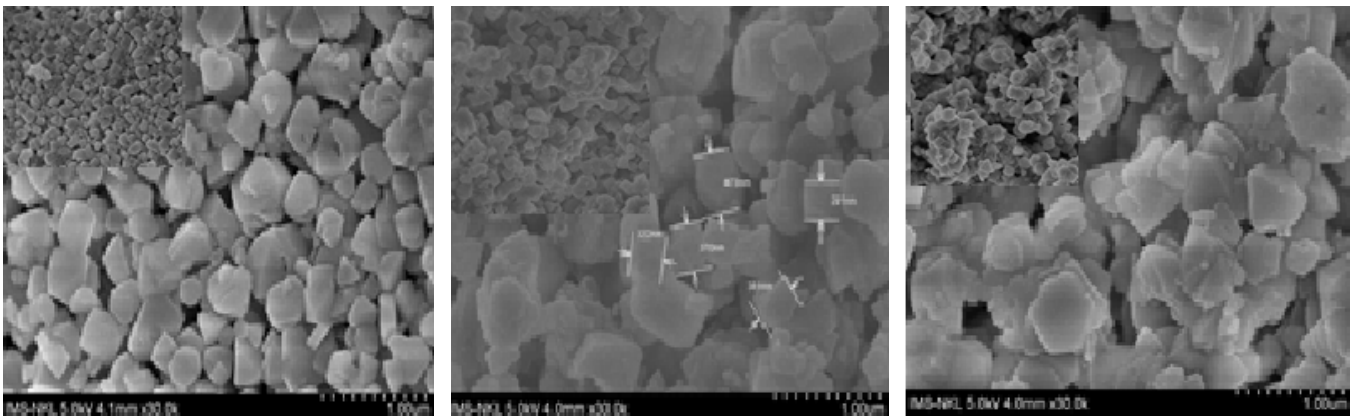

Figure 3. The FE-SEM image of sample HY, CY_{TBP} and CY_{TCP}

As what is seen at the FE-SEM images, the original zeolite structure consists of almost unconected grains with the form of rectangular blocks and the size of several μm to dozens μm. While the composite of organophosphorous and zeolite showed that in the grains surface likely appeared covered sticky layer. However, the surface and grains size of all three materials are almost the same as that of original zeolite. But the materials covered organic agents hopefully increase ability of VOCs separation and absorption of materials, because organic agents have the role of both absorber and conductor in interaction with VOCs.

For better understanding the changes in the structure of the material, proceed to determine the structure of capillary and the surface area of sample by the the nitrogen isothermal adsorption method and size distribution of capillary is implemented. The results are presented in Figure 4.

Study on the surface properties of zeolite composite materials, based on the BET method shows that the nitrogen isothermal adsorption-desorption

line of all three samples was of type IV and has hysteresis loop type H2 (as sorted by IUPAC). The properties belong to materials have medium capillary with hollow both ends cylinders, and corresponding to the Barret-Joyner-Halenda (BJH) hole size distribution.

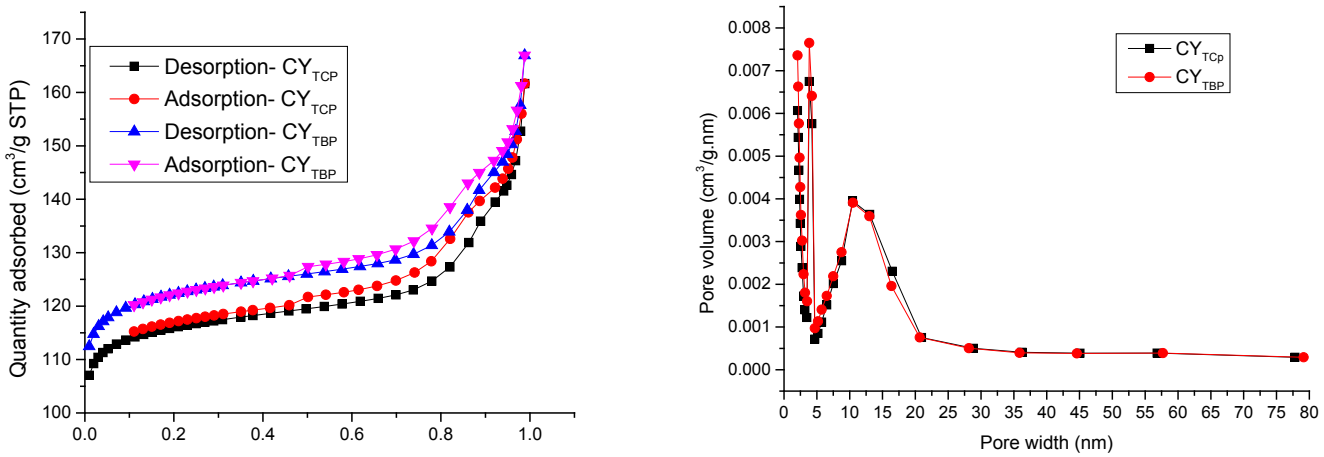

Figure 4. Diagram of the nitrogen isothermal adsorption-desorption line and capillary size distribution of CY_{TBP} and CY_{TCP}

Figure 3 also shows that desorption line of the samples were relatively smooth, in which the two samples has the nitrogen isothermal adsorption-desorption line started condensation in the relative pressure P/P_o about 0.5–0.95, demonstrates that the material has a relatively large capillary diameter. As for the two samples CY_{TBP}, CY_{TCP}, they have the condensation in the earlier relatively pressure P/P_o, and have a capillary diameter greater than the capillary diameter of original zeolite sample. According to the BJH survey, all three samples have capillary distribution ranging from 0.8 nm to 80 nm, in which the current pore data of the two samples CY_{TCP}, CY_{TBP} are 2.46 nm and 2.42 nm respectively.

Thus, the difference in the average capillary size of samples is result of spatial effects of organic agents used in zeolite composite, as well as their interaction with zeolite created larger capillaries than original zeolite sample. The specific surface area of CY_{TBP} and CY_{TCP} are 409.34 m^2/g and 388.17 m^2/g respectivelysmaller than those of original HY (550 m^2/g). This again confirms that in CY_{TBP} and CY_{TCP} samples, the organophosphorous components were linked and obstructed the spatial part of the pore on the original zeolite surface. However, when comparing the results with zeolite composite specimens modified by silicified muscle compounds, it shows that these samples have larger specific surface area (Le Thanh Son et al., 2016).

3.2. Adsorption ability of benzene vapor on zeolite composite materials

3.2.1. Influence of contact time

Empty bed contact time is known as the time required for a adsorbate element moving through the length of the adsorbent layer in the case of empty column. Empty bed contact time is one of the important parameters of an adsorption system. Assuming the flow is ideal, the empty bed contact time is calculated by the following formula (William F. Naylor et al., 1995; Chaiwat Rongsayamanont et al., 2007):

$$EBCT = \frac{V}{f}$$

where EBCT is Empty bed contact time, s

V is Empty bed volume of the column, L.

f is The gas flow rate through the column, L/s

The study was conducted with the gas flow rate from 0.15 L/min to 0.60 L/min at 40°C; the inlet benzene concentration is 21.8 ppmv, the bed volume of the material is 2.9 mL. The results are given in table 1 and Figure 5.

Table 1.– Influence of gas flow rate to the content of adsorption of CY_{TBP}, CY_{TCP}

No.	Gas flow rate (L/min)	Contact time (s)	Adsorption capacity of CY_{TBP} (mg/g)	Adsorption capacity of CY_{TCP} (mg/g)
1	0.15	1.16	1.0038	1.8224
2	0.30	0.58	1.0235	1.8970
3	0.60	0.29	0.9070	1.7446

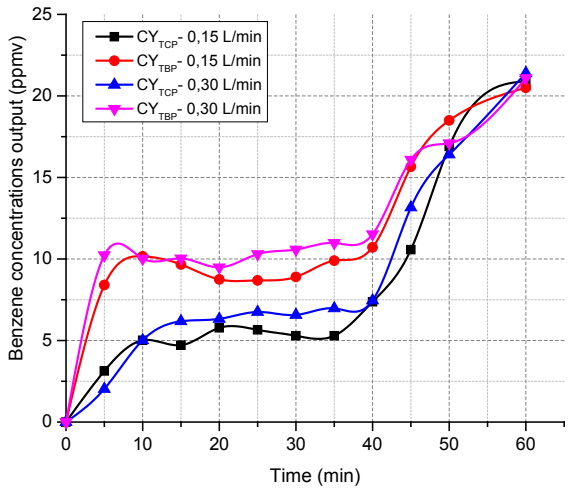

Figure 5. Breakthrough curve of benzene vapor through zeolite composite column at 40°C

As results showed in table 1, with the same inlet benzene concentrations, but with lower contact time (about 0.29 s), the adsorption capacity began decrease. It demonstrates the rate of gas flow really affecting on adsorption capacity, particularly, when the contact time is too short, it shall not guarantee that gas molecules can diffuse through the absorbed material surface. From the above review, we conducted the survey of benzene vapor adsorption process of the materials in the two flow rate 0.15 L/min and 0.30 L/min.

The results also showed that at the flow rate of 0.15 and 0.30 L/min, the adsorption capacity of the materials varied not so much. However, adsorption breakthrough curve is different. The breakthrough curve at a flow rate of 0.30 L/min is more sloping than those of 0.15 L/min. However, the difference of adsorption capacity appeared by the different organophosphorous component in the material. The composte material with tributylphosphate showed higher adsorption capacity than those with tricresylphosphate.

3.2.2. The influence of temperature

The investigation was carried out at 30 °C and 40 °C; the initial benzene concentration was 12.6 ppmv and 21.8 ppmv; air flow rate 0.30 L/min; the adsorption fractions were measured after every 5 min, the cumulative curves of benzene vapor on the zeolite composite waere given in Figures 6.

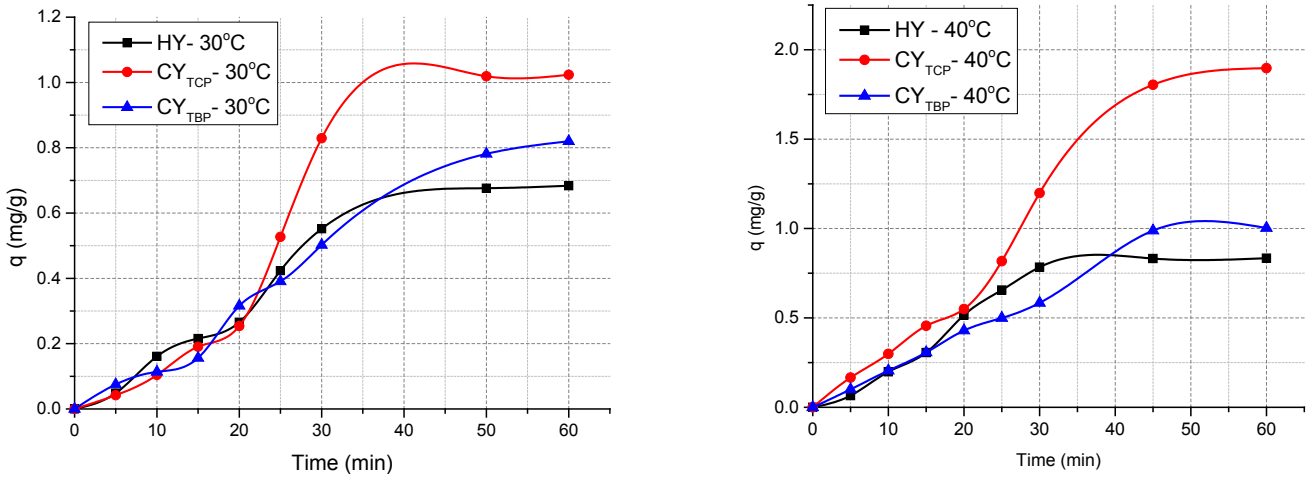

Figure 6. Cumulative curves of benzene vapor on the zeolite composites at 30°C and 40°C

The results showed that, increasing of temperature from 30°C to 40°C, the adsorption capacity of CY_{TBP} and CY_{TCP} increased, and after maximum 60 min contacted the adsorption process of all materials reached equilibrium state. The dynamic equilibrium adsorption capacity of CY_{TBP} reached 0.8206 mg/g and 1.0235 mg/g, and those of CY_{TCP} were 1.0822 mg/g and 1.8970 mg/g respectively. This phenomenon seems unaccordant to the adsorption kinetics (temperature increased, decreased the adsorption capacity). In this case, it can be explained by better diffusion of benzene through organophosphorous layer to zeolite core in high temperature and holed in zeolite structure. But actualy, the threshold of higher temperature was not determined yet.

The adsorption capacity of benzene vapor on CY_{TCP} was better than that on CY_{TBP} and original zeolite. The reason can be explained by that, kinetic diameter of benzene is 5.85 Å which is much smaller than capillary size of original zeolite and composite system of zeolite and organophosphorous agents which have average capillary diameter determined by the BET method (Figure 3). In particular, the IR study showed that the CY_{TCP} has interaction of benzene ring in the TCP agent with benzene vapor, so the dynamic equilibrium adsorption capacity of this material was greater than that of CY_{TBP}. The results also showed that benzene adsorption process of zeolite HY formed a fairly durable compound like HY-benzene, however it still belonged to physical adsorption type. There are able two main compounds created by links of benzene with H in zeolite and by Van der Waals interaction of benzene inside 12-T or 4-T of zeolite (Shuai Ban, 2009). According to Qin Hu (Qin Hu et al., 2009), the presence of aromatic cyclic agent in the material, its adsorption ability changed, and this was explained by the interaction of electron-π of benzene or phenyl when studied adsorption of benzene on different materials.

4. Conclusion

Zeolite composite materials (CY_{TBP} and CY_{TCP}) prepared from zeolite HY with tributylphosphate and tricresylphosphate have a high surface area (409 m^2/g and 388 m^2/g respectively), grain size of materials from several μm to dozens μm, the current pore data around 2.46 nm to 2.42 nm. The IR spectra of the zeolite composite showed strong interaction between zeolite base and organophosphate substances.

Zeolite composite materials have high adsorption capacity of benzene vapor in quite low concentration (from 20 ppmv to 50 ppmv) and the adsorption time of 0.29 s to 1.16 s. The dynamic equilibrium adsorption capacity of CY_{TCP} was 1.0822 mg/g and 1.8970 mg/g and those of CY_{TBP} was 0.8206 mg/g and 1.0235 mg/g corresponding with 30 °C and 40 °C in the adsorption conditions of gas flow rate of 0.30 L/min; input benzene concentration of 21.8 ppmv and temperature of 30°C and 40°C.

References:

1. Stanley E. Manahan., – 2003. Toxicological chemistry and biochemistry, CRC, – P. 288–307.
2. Suleeporn Sangrajang., – 2008. Toxicological review of benzene: cancer aspect, Thai cancer journal, – Vol. 28. – No. 2. – P. 93–100.
3. Robert Snyder. – 1993. The toxicology of benzene, Environmental health perspectives. 100, – P. 293–306.
4. Ernest Hodgson. – 2004. A textbook of modern toxicology, Jonh Wiley & Sons, – P. 70–110.
5. Shuai Ban. – 2009. Computer Simulation of zeolites- Utrecht University, Utrecht, Netherlands: Adsorption, diffusion and dealumination, – P. 52–62.
6. Dombrowski, Jürgen Hoffmann, Johanna Fruwert. – 1995. Infrared spectroscopic investigation of Hydroxy-group siting in H Faujasites, J. Chem. Soc., Faraday Trans. 1(82), – P. 2257–2281.
7. Mirjam Czjzek, Hervé Jobic. – 1992. Direct determination of proton positions in D-Y and H-Y zeolite samples by neutron powder diffraction, J. Phys. Chem. 96, – P. 1535–1540.

8. Vitale G., Bull L. M., Powell B. M., Cheetham A. K. – 1995. A neutron diffraction study of the acid form of zeolite Y and its complex with Benzene, J. Chem.Soc., Chem. Com. – P. 2253–2254.
9. Fabien Jousse, Scott M. Auerbach, Daniel P. Vercauteren. – 2000. Adsorption sites and diffusion rates of benzene in HY zeolite by force field based simulations, J. Phys. Chem. B, 104, – P. 2360–2370.
10. Siricharn S. Jiraponghan, Juliusz Warzwoda, David E. Budil, Albert Sacco Jr. – 2006. Simulation of benzene adsorption in zeolited HY using supercage – based docking, Microporous and Mesoporous Materials. 94, – P. 358–363.
11. Qin Hu, Jin Jun Li, Zheng Ping Hao, Lan Dong Li, Shi Zhang Qiao. – 2009. Dynamic adsorption of volatile organic compounds on organofunctionalized SBA-15 materials, Chemical engineering journal. 149, – P. 281–288.
12. Abdulrahman Bahrami, Hosien Mahjub, Marzieh Sadeghian, Farideh Golbabaei. – 2011. Determination of Benzene, Toluene and Xylene concentrations in Air using HPLC developed method compared to Gas chromatography, International Journal of Occupational Hygiene. – Vol. 3. – No. 1. – P. 12–17.
13. Zoccolillo L., Alessandrelli M., Felli M. – 2001. Simulataneous determination of Benzene and total aromatic fraction of Gasoline by HPLC-DAD, Chromatographia. – Vol 54. – P. 659–663.
14. Robsin H. – 2001. Verified synthesis of zeoliteic materials, Elsevier Science B.V, – P. 69–71.
15. Wtodzimierz Mozgawa, Magdalena Król, Katarzyna Barczyk. – 2011. FT-IR studies of zeolites from different structural groups, CHEMIK. 65(7), – P. 667–674.
16. Le Thanh Son, Tran Hong Con, Nguyen Thi Huong, Vo Hoang Phuong. – 2016. Influence of Y Zeolite content of zeolite composite material. VNU Journal of Science: Natural science and Technology. – Vol . 32. – No. 3. – P. 141–146.
17. William F. Naylor, Dennis O. Rester. – 1995. Determining activated carbon performance, Pollution Engneering, – P. 28–29.
18. Chaiwat Rongsayamanont, Khaornak Sopajaree. – 2007. Modification of synthetic zeolite pellets from Lignite Fly Ash B: Treatability study, World of coal ash, Covington Kentucky-USA. – May 7–10.

Abdurakhmonov Eldor,
Junior researcher, Laboratory of Elemental Analysis
of Institute of General and Inorganic Chemistry of Uzbekistan Academy of Sciences
E-mail: eldor8501@mail.ru
Rakhmatkariev Gairat,
Dr in chemistry, Prof., Head of Laboratory of Elemental Analysis
of Institute of General and Inorganic Chemistry of Uzbekistan Academy of Sciences;
Rakhmatkarieva Feruza,
Ph D., Researcher, Head of Laboratory of Elemental Analysis
of Institute of General and Inorganic Chemistry of Uzbekistan Academy of Sciences
Ergashev Oybek,
Ph D., Teacher, Namangan Engineering-Technological Institute
Ministry of the higher and secondary special education of the republic of Uzbekistan

ADSORPTION-MICROCALORIMETRIC INVESTIGATION OF BENZENE CONDITION AND DISTRIBUTION IN THE ZEOLITE LIY

Abstract: Differential heats, isotherms, the differential entropies and thermokinetics of benzene adsorption in the zeolite LiY at 303K have been measured using the method of adsorption calorimetry. Differential molar entropy and free energy of adsorption were calculated. The isotherms of adsorption were quantitatively reproduced on the basis of three-term VOM theory. These data formed the basis for identifying the detaled mechanism of benzene adsorption in LiY zeolite.

Keywords: Ion-molecular complexes, LiY zeolite, benzene, differential heats, isotherms, the differential entropies, thermokinetics, adsorption calorimetry.

Introduction

Zeolite [1] is microporous crystals possessing wide application in chemical and petrochemical industries as catalysts and sorbates [2; 3]. Method of adsorptive calorimetry is widely used in our practice ensuring detailed researches host-guest interaction in the systems adsorbent-adsorbate in wide space equilibrium pressure. The results these studies were confirmed such complementary methods as powder X-ray diffraction, NMR spectroscopy and computer modeling [4]. Before benzene adsorption was mainly studied in Na form zeolites type X and Y [5–7]. We were set a goal to reveal detailed mechanism of benzene adsorption in the zeolite LiY based on results energy investigations.

Objective: to study isotherms and main thermodynamic characteristics of adsorption and the mechanism of adsorption of benzene in zeolite of Y type with exchangeable Li^+ cations.

Subjects and Methods. Adsorption studies were carried out with zeolite Li Y. As adsorptives of benzene molecule were selected. Adsorption-calorimetric method used in this paper provides a high-precision molar thermodynamic characteristics of adsorption systems and through them to reveal the mechanism of adsorption processes occurring in the adsorbent. As a calorimeter the microcalorimeter Tian-Calvet-type, with high accuracy and stability was used [11; 12].

Results and discussion. Changing the differential heat of adsorption (Q_d) benzene in the zeolite LiY depending on the amount of adsorption (a -amount of benzene per 1/8 of the unit cell

(C_6H_6 / (1/8) unit cell) or one supercages) shown in Fig. 1. The dashed line in the figure shows the heat of condensation of benzene ΔH_v. The adsorption heats in ~ 2.3 times exceed the heat of benzene condensation. Change of the differential heats of adsorption is singular as well.

Heats begin from 108 kJ/mol and reduced sharply to 73.5 kJ/mol at 0.21 C_6H_6/(1/8) unit cell, then double pass through a maximum, more pronounced in the range of adsorption, *a* 0,21–0.49 C_6H_6/(1/8) unit cell and less pronounced 0,49–0,78 C_6H_6/(1/8) unit cell. Further the heat are reduced wavy to 75.21 kJ/mol at ~ 2 C_6H_6/(1/8) unit cell, then grow to a maximum of 82.28 kJ/mol at 4 ~ C_6H_6/(1/8) unit cell.

Entering into the cavity of the third and fourth molecules leads to an increase of the heat of adsorption due to the contribution to the total energy, the energy of interaction between adsorbate-adsorbate. Location four C_6H_6/Li^+ complexes is close to the tetrahedral and a cluster fills almost all the space supercages. The fifth entry of the molecule leads to a wavelike decrease of heat at first insignificant, then sharply in the range of 4.36–4.85 C_6H_6/(1/8) unit cell.

In accordance with the wavelike Qd it can be divided into the following sections: 0,78–1,41; 1,41–1,92; 1,92–2,44; 2,44–3,08, 3,08–3,73, 3,73–4,36 and 4,36–5,00 C_6H_6/(1/8) unit cell, which complete curve and small segment in the range of 5,00–5,18 C_6H_6/(1/8) unit cell.Total LiY zeolite adsorbs 5.18 of benzene molecules per 1/8 unit cell or one supercages.

On 1/8 unit cell investigated by us the zeolite there is an average of 6.87 cations of Li^+. All of them, in accordance with [7; 8; 9], should be distributed HN on sodalite (SI position ‘, adjacent to the hexagonal ring that separates the sodalite cavity from the hexagonal prism) and supercages (SII position adjacent to the undivided surface of sodalite cavity). If the position SII, whose number is 4, fully settled by cations, the remaining 2.87 cations are distributed on positions SI ‘, whose number is also 4.

So far sodalite cavity with diameter of the input six -membered oxygen window ~ 0.25 nm have not been available for a relatively large molecule of benzene. Therefore, we exclude from consideration of adsorption centers in these cavities. Consequently, adsorption mainly proceeds in Supercages. High-energy area (up to *a* = 0.21 C_6H_6/(1/8) unit cell) refers to adsorption on the cations of Li^+, are in supercagess in SIII position ‘. These open positions are more accessible to the adsorbed molecules and therefore have the greatest energy of a specific interaction, reaching to 110kJ/mol.

The ability of the adsorbed molecules in supercages to extract small size of the cations of Li^+ from sodalite cells, was shown by us in the adsorption of polar H_2O and quadrupole CO_2 molecules [10]. Two sections 0,21–0,49 and 0,49–0,78C_6H_6/(1/8) unit cell at ~ 77 kJ/mol, we refer to benzene adsorption on the lithium cations are in the 4-membered oxygen rings (SIII).

A cation of Li^+, located in SII positions due to the small size is immersed in the 6-membered oxygen ring. Therefore, the benzene molecule adsorbed on the cation of lithium in the SII position, cannot be focused more favorably as cation and a negatively charged oxygen atoms forming 6-membered oxygen ring. After the adsorption of benzene on the Li^+ in the SIII ‘ position has begun its adsorption on the Li^+ in SIII position. The further mixed adsorption of C_6H_6 0.63/(1/8) unit cell benzene occurs on lithium cations in the positions of the SII and SIII (0,78–1,41C_6H_6/(1/8) unit cell).

It is only two sections 1,41–1,92 1,92–2,44 and C_6H_6/(1/8) unit cell by 0.5 C_6H_6/(1/8) unit cell are responsible for the benzene adsorption exclusively on SII lithium cations. The rest of the section is per 0.64 C_6H_6/(1/8) unit cell each reflects adsorption on the SIII and SII. If each of these sections to subtract a portion of responsible for adsorption on SII, 0,50 C_6H_6/(1/8) unit cell, the residue corresponding to adsorption SIII, equals 0.144 C_6H_6/(1/8) unit cell. Such sections are 5, therefore, within

these sections adsorbed 0.72 C_6H_6/(1/8) unit cell (5 x 0.144 = 0.72). And 0.72 + 0.57 = 1.29 C_6H_6/(1/8) unit cell is adsorbed just taking into account SIII on the second and third sections. With reference to adsorption on SII, 2.5 C_6H_6 / (1/8) unit cell (5 x 0.5 = 2.5) are adsorbed in accordance with the five sections in these centers and plus 1 C_6H_6/(1/8) unit cell (2 by 0,5C_6H_6/(1/8) unit cell of 5 and 6 sections). A total of 3.5 C_6H_6/(1/8) unit cell adsorbed in the SII.

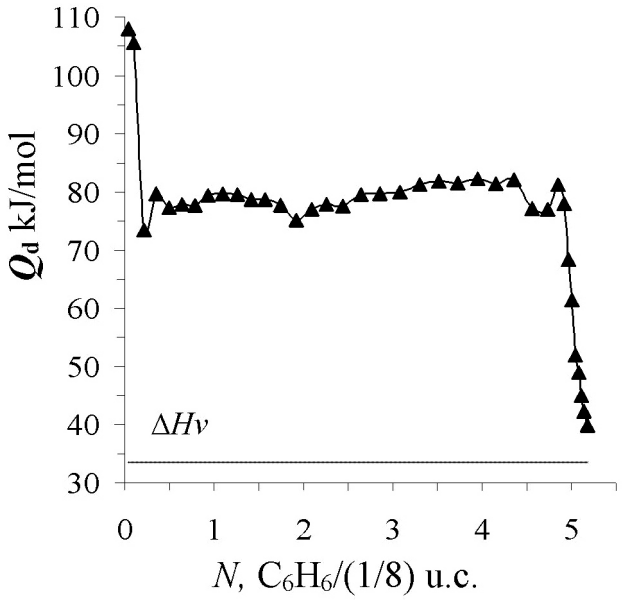

Figure 1. The differential heat of benzene adsorption in the zeolite LiY at 303K. The horizontal dashed line is heat benzene condensation at 303K

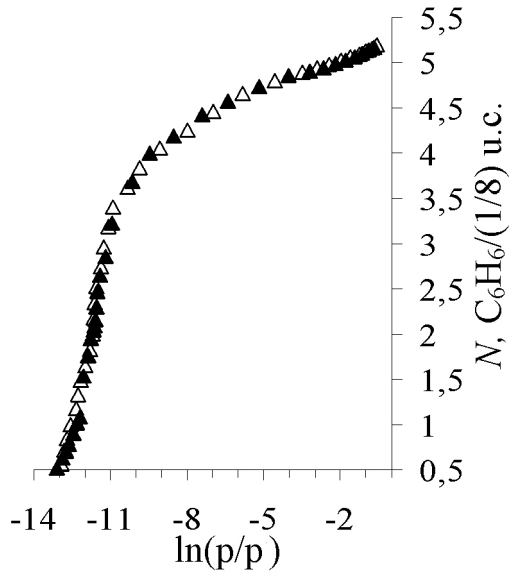

Figure 2. Benzene adsorption isotherm in the zeolite LiY at 303K
Δ – experimental data
Δ – estimating data by VOM

Thus, at saturation of LiY zeolite cavities by 0.21C_6H_6/(1/8) unit cell adsorbed on cations in the SIII', 1,29 C_6H_6/(1/8) unit cell adsorbed on SIII and 3,5 SII. From 6.87 of lithium cations per 1.8 unit cell in the adsorption process involved 5. In the last section, after adsorption of 4.36 C_6H_6/(1/8) unit cell heat begins to decreas from 82.1 to 77.1 kJ/mol, as is usual at the end of the adsorption process. However, the redistribution of the adsorbed molecules to create more densely packed adsorbate molecules allow to decreased more 0,64 C_6H_6/(1/8) unit cell, adsorption which leads to a sharp rise of heat of adsorption to the level of 81.3 kJ/mol. Redistribution of benzene begins after adsorption of 4 C_6H_6/(1/8) unit cell. In the issue of the redistribution, the fifth molecule of benzene per 1/8 unit cell is displaced to a new the center of W in the 12 -membered oxygen rings. The small "tail" on the curve Qd at culminating stage of benzene adsorption (*a* from 5 and 5.18 C_6H_6/(1/8) unit cell with a heat falling from 61 to 40 kJ/mole) is determined by adsorption in mesopores.

The adsorption isotherm was determined by volumetric method at a temperature of 303K. Control of adsorption equilibrium carefully performed with the thermo-kinetic curves. Figure 2 shows the adsorption isotherm (a) of benzene in the zeolite Li Y. Isotherm was built in semilogarithmic coordinates, allowing you to visually present the adsorption of *a* in the entire range of equilibrium pressures.

There are identified the adsorption point, the blackout point processed VOM equation in Fig. 2. It is observed that a satisfactory agreement between the experimental and calculated points in the initial and final adsorption areas.

The molar differential entropy of adsorption (ΔSd) of benzene in the zeolite LiY calculated by the

Gibbs-Helmholtz equation of the isotherms and differential heats of adsorption [11–12] and is shown in Figure 3.The initial part of the curve rises from area of the low and negative entropy (–125kJ/mol * K), pointing to a strong localization of benzene adsorbed on Li^+ cations in the open position of SIII ', then passes through a maximum (–30kJ/mol * K) and at first slowly up to N = 2 C_6H_6/(1/8) unit cell, then decreases sharply and at 4.9 C_6H_6/(1/8) unit cell it becomes two times lower than the solid benzene entropy, is123 J/mol * K), which demonstrates the growing inhibition of translational and rotational motions of benzene molecules with the gradual filling of the adsorption space.

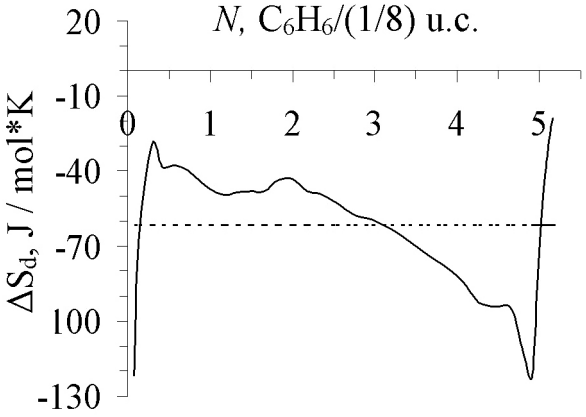

Figure 3. The differential entropy of the benzene adsorption in the zeolite LiY at 303K. Entropy of liquid benzene is taken as zero. The horizontal dashed line – mean molar integral entropy

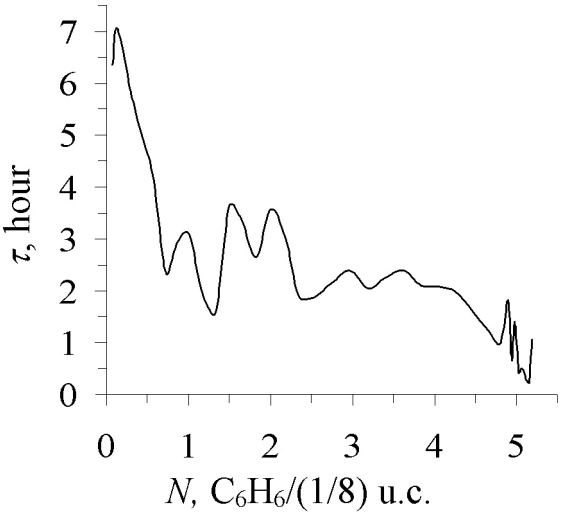

Figure 4. The set-time of the adsorption equilibrium, depending on the size of the adsorption of benzene in the zeolite LiY at 303K

It is interesting that, when N = 4,26 C_6H_6/(1/8) unit cell entropy decrease sharply interrupted and the curve forms a step with a length of 0.4 C_6H_6/(1/8) unit cell in the range of 4.26–4.66 C_6H_6/(1/8) unit cell at 92.6 J/mol* K. However, further the entropy decreases sharply up to 123.1 J/mol *K at 4.9 C_6H_6(/ 1/8) unit cell. The adsorption entropy confirms the data heats of adsorption indicating that in this area there is a redistribution of the benzene molecules benzene and formation of densely packed of benzene molecules. The curve sharply rises in the direction of liquid benzene entropy passing through a minimum. Mean molar integral of the entropy of adsorption close to entropy of solid benzene and is equal to –61.4 J/mol*K, which generally indicates the solidlike state of benzene molecules in the zeolite matrix.

After two adsorption of C_6H_6/(1/8) unit cell τ is accelerated and equilibrium is established in average for 2–2.5 hours. Accelerate of the adsorption smoothes the waves, but if the rest of the curve divided into sections from the maximum to the maximum, that is got a section with length of 1.0 C_6H_6/(1/8) unit cell and three at 0.63 C_6H_6/(1/8) unit cell. The first section corresponds to the adsorption of benzene on the Li^+ in the SII positions (2 by 0.50 C_6H_6/(1/8) unit cell) and three sections reflect adsorption on mixed positions of SIII and SII (at 0.63 C_6H_6/(1/8) unit cell). Reducing heat in the adsorption is more than 4 C_6H_6/(1/8) unit cell. It leads to accelerate the process, but benzene redistribution and the appearance of new centers dramatically slows down and the curve τ passes through maximum at 4.9 and 4.98 unit cell.

The study shows that, along with the isotherm and differential heats of adsorption, entropy and thermo kinetics of adsorption reflects the specifics

of the formation of the ion / molecular complexes in the zeolite matrix. The mechanism of adsorption, established on the basis of the heats of adsorption and isotherms, fully confirmed. Benzene molecules in the zeolite matrix are strongly localized and their state closes to solidlike. The migration of cations from the sodalite cavities in the supercages flows with a strong slowdown in the adsorption process.

References:

1. Meier W. M., Olson D. H. // Atlas of Zeolite Structure Types. Butterworth. London.– 1987.
2. Breck D. W. // Zeolite molecular Sieves. Wilunit cell. New York.– 1974.
3. Barrer R. M. // Zeolites and Clay Minerals as Sorbent and Molecular Sieves. Academic Press. London.– 1978.
4. Klyachko A. L., Brueva T. R., Mishin I. V., Rubinstein A. M. Calorimetric study of the adsorption of bases on zeolites. // Proceedings of the IV National Conference on the adsorbents. L:. Publishing House. "Nauka": Adsorbents, preparation, properties and applications.– 1978.– P. 125–129; Bosachek V., D. Froyde, Kretschmer R. G., and others. There are same.– P. 35–40.
5. Angell C. L., Howell M. V. Infrared spectroscopic investigation of zeolites and adsorbed molecules. J. Phys. Chem // – 1969.– 73 (8).– P. 2551–2554.
6. Coughlan B., Carroll W. M., O' Mallunit P. cell, Nunan J. Benzene in hydrogen zeolites. Infrared spectroscopic and catalytic investigation of variously exchanged hydrogen Y systems. J. Chem. Soc. Faraday Trans. I. // – 1981.– V. 177.– P. 3037–3047.
7. Herden N., Einicke W-D., Schollner R., Mortier W. J., Gellens L. R. and Uytterhoeven B., Location of Li-ions in synthetic zeolite X and Y. // Zeolites.– 1982.– V. 2.– P. 131–134.
8. Forano C., Slade R. C.T., Krogh Andersen E., Krogh Andersen I. G., and. Prince E. Neutron Diffraction Determination of Full Structures of Anhydrous LiX and LiY Zeolites. J. Solid State Chem // – 1989.– V. 82.– P 95–102.
9. Herden H. Einicke W-D and Schollner R., Dyer A. Investigations of the arrangement and Mobility of Li ions in X- and Y-zeolites and the Influence of mono- and Divalent Cations on It. J. Inorg. Nucl. Chem // – 1981.– V. 43.– No. 10.– P. 2533–2536.
10. Rahmatkariev G. U., Rahmatkarieva F. G., Abdurahmonov E. B. Isotherm and differential heat of benzene adsorption in the zeolite LiY // Uzb. Chem. Journal.– 2013. 1.– P. 13–17.
11. Mentzen B. F., Rakhmatkariev G. U., Host/Guest interactions in zeolitic nonostructured MFI type materials: Complementarity of X-ray Powder Diffraction, NMR spectroscopy, Adsorption calorimetry and Computer Simulations // Узб. хим. журнал.– 2007.– No. 6.– С. 10–31.
12. Rakhmatkariev G. U., Mechanism of Adsorption of Water Vapor by Muscovite: A Model Based on Adsorption Calorimetry // Clays and Clay Minerals,– 2006.– Vol. 54.– P. 423–430.

Mammadova Salima Huseyn,
PhD., student, the Faculty of Chemical Engineering
Azerbaijan State Oil and Industry University
E-mail: bvl_ok@rambler.ru
Garaybayli Samira Aslan,
Engineer, the Faculty of Chemical Engineering
Azerbaijan State Oil and Industry University
Baghiyev Vagif Lachin,
Professor, department of chemistry
and chemical materials engineering
Azerbaijan State Oil and Industry University
E-mail: Vagif_bagiev@yahoo.com

THERMODYNAMIC EVALUATION OF ETHANOL CONVERSION ROUTES

Abstract: The work is devoted to the thermodynamic study of ethanol conversion routes. It was shown that the reaction of dehydrogenation of ethanol to ethyl acetate is exothermic and proceeds with a volume increasing. It was found that for the selective conversion of ethanol to ethyl acetate. the dehydrogenation reaction must be carried out in the temperature range 200–250 ° C.

Keywords: thermodynamics. ethanol. acetone. ethylene. ethyl acetate.

In recent years. an increasing number of chemical compounds are derived from ethanol in the industry [1; 2; 3]. This is because ethanol is produced in large quantities from biomass and in the future. it will be one of the main sources of raw materials for the chemical industry. One of the possible ways of converting ethanol is the reaction of its dehydrogenation to form ethyl acetate. Various undesirable reactions can also take place with the formation of ethylene. acetone. etc. In order to identify possible optimal conditions for obtaining ethyl acetate. we carried out thermodynamic calculations of the reaction of dehydrogenation of ethanol to ethyl acetate. as well as possible reactions of formation of undesirable side reactions.

Method of calculation

Calculation of the change in the isobar of the chemical reaction was carried out according to the Temkin-Shvartsman equation:

$$\Delta G_T^0 = \Delta H_{298}^0 - T(\Delta aM_0 + \Delta bM_1 + \Delta cM_2 + \Delta c^{/}M_{-2})$$

To conduct thermodynamic calculations. we took from the reference tables the values of the standard thermodynamic functions at a temperature of 298K. We took thermodynamic functions for the initial reactants and reaction products for example changes in the enthalpy of formation of the substances ΔH_0. absolute entropies S_0 and also the values of the coefficients entering into the equations describing the temperature dependence of the heat capacity of the substance.

Results and discussions

The dehydrogenation of ethanol to ethyl acetate proceeds according to the following reaction.

$$2C_2H_5OH = CH_3COOC_2H_5 + 2H_2$$

The formation of reaction by-products. namely acetone. ethylene and acetic aldehyde. proceeds according to the following reactions.

$$2C_2H_5OH + H_2O \rightarrow CH_3COCH_3 + CO_2 + 4H_2$$

$$C_2H_5OH = C_2H_4 + H_2O$$

$$C_2H_5OH = CH_3CHO + H_2$$

The values of thermodynamic quantities dependence of the chosen for calculations (enthalpy ΔH_0. absolute entropies S_0 values of the heat capacity temperature coefficients) are given in Table 1.

Carried out calculations showed that the value of changing in the enthalpy of the reaction is –9430 J. i.e. the reaction is exothermic. and since the reaction proceeds with an increase in the number of moles. an increasing in pressure leads to a shift of the reaction to the left.

Table 1.– The thermodynamic values of the initial reactants and reaction products

Substance	ΔH_{298}	S_{298}	Cp = f(T)			
			a	$b*10^3$	$c'*10^{-5}$	$c*10^6$
C_2H_5OH	–234800	281.38	10.99	204.70	0	–74.20
CH3COOC2H5	–479030	259.41	8.67	303.1	0	–115.8
C_2H_4O	–166000	264.20	13.00	153.50	0	–53.70
C_2H_4	52300	219.45	11.32	122.01	0	–37.90
CH_3COCH_3	–217570	294.93	22.47	201.80	0	–63.50
CO_2	–393510	213.66	44.14	9.04	–8.54	0
H_2	0	130.52	27.28	3.26	0.50	0
H_2O	–241810	188.72	30.00	10.71	0.33	0

Carried out calculations showed that the value of changing in the enthalpy of the reaction is –9430 J. i.e. the reaction is exothermic. and since the reaction proceeds with an increase in the number of moles. an increasing in pressure leads to a shift of the reaction to the left.

The calculated Gibbs energy values are shown in (Table 2) below. It is seen that as the reaction temperature increases. the Gibbs energy for the reaction of ethyl acetate formation increases from 3.3 kJ at 300 K to 14.9 kJ at 600 K. It should be noted that the Gibbs energies for the acetone formation reaction in the entire studied temperature range have a negative value. Gibbs energy of other products as seen from table 2 decrease and at temperatures above 550 K have negative values. This indicates that at these temperatures high yields of acetone. acetic aldehyde and ethylene should be observed. A comparison of the Gibbs energy values for all reactions suggests that in order to reduce the yields of ethylene. acetone and acetic aldehyde. the dehydrogenation of ethanol must be carried out at temperatures below 500K or up to 250 ° C.

Table 2.– Thermodynamically calculated values of Gibbs energy for the reaction of formation of ethyl acetate. ethylene. acetic aldehyde and acetone.

Reactions of alcohol conversion into:	Gibbs Energy. ΔG. кj.						
	300	350	400	450	500	550	600
ethyl acetate	3.3	5.3	7.3	9.2	11.1	13.0	14.9
acetic aldehyde	34.8	29.1	23.2	17.3	11.3	5.2	–.90
Acetone	–185.2	–193.8	–202.8	–212.0	–221.6	–231.5	–241.5
ethylene	7.2	0.9	–5.6	–12.1	–18.6	–25.2	–31.8

Conclusions

1. The reaction of dehydrogenation of ethanol to ethyl acetate is exothermic and proceeds with increasing volume.

2. For the selective conversion of ethanol to ethyl acetate. the dehydrogenation reaction must be carried out in the temperature range 200–250 ° C.

References:

1. Dapeng Liu, Yan Liu, Eileen Yi Ling Goh, Christina Jia Ying Chu, Chuandayani Gunawan Gwie, Jie Chang. Armando Borgna. Catalytic conversion of ethanol over ZSM-11 based catalysts. Applied Catalysis – A: General.– Volume 523.– 2016.– P. 118–129.
2. Hala R. Mahmoud. Highly dispersed Cr2O3–ZrO2 binary oxide nanomaterials as novel catalysts for ethanol conversion. Journal of Molecular Catalysis A: Chemical.– Volume 392.– 2014.– P. 216–222.
3. Filek U., Kirpsza A., Micek-Ilnick A., Lalika E., Bielański A. Ethanol conversion over cesium-doped mono- and bi-cationic aluminum and gallium H3PW12O40 salts. Journal of Molecular Catalysis A: Chemical.– Volume 407.– 2015.– P. 152–162.

Ravshanov Dilshod,
Tashkent chemical-technological institute, researcher
Kadirov Yuldoshxon,
Tashkent chemical-technological institute, professor
E-mail: Ulug85bek77@mail.ru

PERFECTION OF TECHNOLOGY OF PROCESSING OF COTTON SOAPSTOCKS

Abstract: It can be seen that the process of processing soapstoks in general and cotton in particular has not been sufficiently studied. In addition, in the present study, new approaches have been taken to studies of the process of neutral fat digestion, containing in a co-abbreviated fat mixture, by the stepwise application of concentrated sulfuric acid and catalysts. To determine the influence of dilution of soapstock on the process of decomposition of soapstock on the process of decomposition of its soap part, experiments were carried out with varying the amount of water in the 0; 50; 75 and 100% of the total weight of the soapstock. The optimal regimes of the non-reactive cleavage of the cotton saopstock fat mixture are established: the amount of reaction water in the ratio of fat: water 1: 1.

Keywords: technology, soapstocks, physicochemical parameters, sulfuric acid, decomposition-splitting, Quality indicators.

One of the important stages in the new technology of processing soapstocks is the stage of sulfuric acid treatment of soapstock, because the choice of optimal conditions for this process depends on: a) the completeness of the decomposition of the soap portion of the soapstock: b) the maximum removal of non-fat substances from the fat mixture; (coloring agents, phosphatides, etc.); c) the normal flow of subsequent processes (splitting, distillation); d) improvement of the quality of fatty acids and glycerin.

In the literature there are contradictory information about the process of decomposition-splitting of soapstocks in general and sulfuric acid treatment of soapstocks in particular, for example, in some sources [1; 3] it is indicated that the best decomposition-splitting occurs at a temperature of 80–90°, even 100 °C, and others [2] give preference to the conduct of the decomposition-splitting process at a temperature of 60–70 °C. In addition, some believe that sulfuric acid treatment should be carried out without additional dilution of the initial soapstock with water [3; 4] and others with such a treatment are recommended to conduct with liquefied (water) soapstock [2], in order to improve the flow of decomposition of the soap portion of the soapstock. The question of the behavior of non-fatty substances in the sulfuric acid treatment of soapstocks and the degree of their removal from the fat mixture is completely unclear.

Finally, there is no reduction in the consumption of concentrated sulfuric acid necessary for the stepwise decomposition-splitting of the soap portion of the cotton soapstock, its neutral fat and the non-fat complex.

It can be seen that the process of processing soapstoks in general and cotton in particular has not been sufficiently studied. Therefore, we carried out research to find conditions for the decomposition-splitting of cotton soapstocks and the production of co-abdominal fat and glycerin waters, with a minimum content of foreign impurities of a group of non-fatty substances. In addition, in the present study, new approaches have been taken

to studies of the process of neutral fat digestion, containing in a co-abbreviated fat mixture, by the stepwise application of concentrated sulfuric acid and catalysts.

During the day of conducting laboratory experiments, the cotton soapstocks of JSC "Kokand-fat-oil" were initially used with the following indicators (Table 1).

Table 1.– Physicochemical parameters of cotton soapstock

Image numbers	Composition of cotton soapstock in %					
	Total content of fatty acids	neutral fat	soap	non-fatty substances	humidity	Color
1.	58.45	21.55	31.15	5.48	24.05	Dark
2.	55.60	24.01	37.94	8.05	26.81	Dark brown
3.	59.24	18.95	33.51	6.84	25.41	Dark brown
4.	61.48	20.44	33.14	5.48	24.88	Dark brown

The consumption of sulfuric acid for the decomposition-splitting of soapstock varied widely, depending on the amount of soap and neutral fat contained in it.

In this connection, the content of soap, neutral fat and non-fatty substances was determined in each batch of soapstock.

The decomposition of cotton soapstocks was carried out on a laboratory installation. Stirring was carried out by a mechanical stirrer making 100–150 rpm; the reaction mass was heated in a water bath. After the introduction of the components of the reaction medium, the process lasted for 2 hours, and then the mass was left for stratification, which resulted in three layers: the bottom was concentrated in the water layer, the upper layer of fat, and at the interface between the aqueous and fat phases, an emulsion layer (a resinous layer of non-fatty substances)

To determine the optimum conditions for carrying out the process of sulfuric acid treatment of sopstocks of various compositions, the following effects were investigated:

– additionally introduced water for liquefaction of soapstock;
– excess of concentrated sulfuric acid;
– temperature of the reaction mass;
– is the amount of catalyst.

To determine the influence of dilution of soapstock on the process of decomposition of soapstock on the process of decomposition of its soap part, experiments were carried out with varying the amount of water in the 0; 50; 75 and 100% of the total weight of the soapstock.

The amount of concentrated sulfuric acid necessary for the decomposition of the soap portion of the soapstock, the maintenance of the corresponding strongly acidic reaction medium, the partial cleavage of the neutral fat, and the decomposition-splitting of the non-fatty substances of the soapstock was calculated on the basis of the content of soap in copulation with 30% excess.

The experimental conditions and results are shown in the (Table 2).

The data of (Table 2) shows that, when the water (distilled) is introduced into the reaction mass in the ratio-co-liquor: water = 1:1, 1:0.75, the decomposition proceeds normally, the mixture separation takes of a very long time (experiment 1–5). The intermediate layer (emulsion and resinous substances) in all experiments has a brown color.

In experiments 8–10 (without introducing additional water into the soap), the process of mixing the mass was difficult.

In experiments 6, 7 (the ratio of co-liquids: water 2:1) plus added 3 g of sulfuric acid dramatically improved the decomposition process, it passed normally, the corresponding phases were clearly separated in a short time. The intermediate layer (the emulsion layer)

Table 2. – Influence of the condition of conducting experiments on the process of decomposition-splitting of soapstocks

№	Amount g			Duration a min.		The temperature of the decomposition process, °C	Sludge of the reaction mass in hours	Number of intermediate layer (layer, emulsion) g	Output of the soap oil mixture		Containing sulfuric acid in acidic waters,%	Separation of the reaction mixture	Characteristics of the intermediate layer (emulsion)
	soapstock	water	sulfuric acid with 30% excess	input of concentrated sulfuric acid	The process of decomposition-splitting				g	%			
1.	500	500	34.0	15	120	88–92	12	101	245	76.0	0.68	A very long time	Brown color
2.	500	500	34.0	15	120	88–90	12	121	244	76.0	0.51	–	–
3.	500	500	34.0	15	120	90–95	10	113	248	76.0	0.58	–	–
4.	500	500	34.0	15	125	90–93	10	118	227	70.0	0.63	–	–
5.	500	375	34.0	15	120	90–92	2	123	221	69.0	0.71	The rapid seeding was parted.	–
6.	500	250	34.0+3.0	15	120	90–91	2	84	300	92.7	1.59	–	Color dark brown layer more dense
7.	500	250	34.0+3.0	15	125	90–92	1h 50m	79	300	92.0	1.50	–	–
8.	500	300	34.0+3.0	15	125	90–93	1h 50m	Poor separation	Undefined	–	1.68	–	–
9.	500	300	34.0+3.0	15	120	90–93	4	–	–	–	1.65	–	–
10.	500	250	34.0+3.0	15	120	90–92	4	–	–	–	1.65	–	–

was more dense and in a smaller amount, compared with previous experiments. The color of the intermediate layer is dark brown. Therefore, it was decided to carry out subsequent experiments according to the experimental regime No. 6, No. 7, but with a variation in the excess of the input concentrated sulfuric acid.

Thus, we studied the process of upgrading cotton soapstock by an improved method that allows us to save scarce caustic soda while manufacturing fatty acids from sapstocks and to exclude the use of table salt. Without reactive cleavage of the soap-oil fat mixture was carried out on a specially made 1.4-liter cameral autoclave. Splitting of the fat mixture was conducted in two phases with a duration of 6 hours each at a temperature of 225 ° C and a pressure of 2.2–2.4 MPa (22–24 kg / cm^2).

Cotton soapstock fat mixture before loading into the autoclave was thoroughly washed with hot water to remove traces of sulfuric acid. In this case, of course, partially washed and sulfate. The presence of sulfuric acid in the fat is not allowed, since it destroys the effect on the material of the autoclave. Distilled water was used for both phases during the cleavage.

In the first and second phase of the cleavage, the amount of fat mixture of distilled water and pressure in the autoclave was constant, respectively, 450 and 440 g, respectively; 450 and 400 g; 22 MPa, and when studying the effect of the amount of reactive water on the cleavage process, these amounts were equal to 450 and 440 g; 390 and 340g; 22 MPa.

The results of the study of the process of the non-reactive cleavage of cotton sapostock fat mixture are presented in (Tables 2 and 3).

At the end of the first phase of the cleavage, the mass was set aside. After the first glycerin water was drained, the second phase of decomposition was carried out. The separation of aqueous phases occurred normally without the formation of an emulsion.

From the data of (Table 2) shows that when the ratio of the fat blend to water phase I at 1:1, in phase II of 1:0.9 and with the duration of the degradation process until 6 watch is best depth equal splitting 93.4–94.1% (experiments 1 / 61–2 / 61). Subsequent reduction of the duration of the cleavage process up to 4 hours (I phase), 3:00 (II phase) already affected the depth cleavage soapstock fat, reducing it to 91.1%. Further decrease in the duration of the cleavage process up to 3 hours (phase I) and 3 hours (II phase) still lowered the depth of fat splitting to 84.0%.

Also, the acid numbers from 183.1 mg KOH to 179.6 mg KOH decreased. After the first phase of cleavage, the content of glycerin in water was 6.5–7.4%, after the second phase 2.0–4.1%.

Table 4 shows the results of a study of the effect of the amount of introduced reaction water on the process of the reactive cleavage of the cotton copolymer mixture.

In order to clarify the possibility of concentration of the first glycerin water in the case of no-reactive cleavage, an attempt was made to reduce the ratio of the amount of water introduced to the fat of 0.87:1 in the first cleavage phase and 0.77: 1 in the second cleavage phase. As shown by the data obtained, the decrease in the amount of water affected the decrease in the depth of splitting of the sap grease mixture both in the 1st phase and in the second cleavage phase (the cleavage depth after the II phase fluctuated within 85.4–89.0% at acidic number of crude fatty acids in the range of 176.0–181.0 mg KOH, although the concentration of glycerol waters increased somewhat) after the II phase – up to 4.3%.

It follows that when splitting the co-paste fats of cotton soapstock in a non-reactive way, it is not recommended to reduce the amounts of reactive water below the ratio of fat: water 1: 1 and 1: 0.9.

For purification and processing, glycerin water, obtained after both cleavage phases, was mixed and processed into glycerol. It was purified by neutralization with milk of lime. Glycerin water from all experiments obtained by the method of hydrolysis of a cotton soap fat mixture by a reactive method (using sulfuric acid, a sulfonol catalyst) and without a reactive method was purified, neutralized, evaporated and analyzed.

Table 3.– Effect of the duration of the process on the depth of the split of the cotton fat mixture

№ of experiment	I Phase of the cleavage				II Phase of the cleavage					
	Continuing resident. process, h	Temperature of the mass, 0C	Glycerin water		Continuingprocess, h	Temperature of the mass, °C	Glycerin water		The splitting depth%	CN crude oil. Acidity, mg KOH
			Color	Concentration,%			Color	Concentration,%		
1/61	6	220	yellow. green	7.2	4	220	yellow	4.0	93.4	183.1
2/61	6	219	–	7.4	4	220	–	4.1	94.1	183.6
3/61	4	218	–	6.8	3	220	yellow	2.6	91.1	181.5
4/61	4	220	yellow	6.9	3	220	–	2.8	90.8	180.8
5/61	3	220	yellow	6.5	3	220	yellow	2.0	85.1	180.0
6/61	3	220	yellow	6.6	3	220	yellow	2.3	84.0	179.6

Table 4.– Effect of reactive amounts of water on the process of splitting the fat blend of cotton

№ of experiment	I Phase of the cleavage					II Phase of the cleavage								
	Continuingresident. process, h	Temperature of the mass, °C	Pressure. in an autoclave, MPa	Glycerin water		Fat mixture, g	Distilled water, g	Continuingprocess, h	Temperature of the mass, °C	Pressure. in an autoclave, MPa	Glycerin water		The splitting depth%	CN crude oil. Acidity, mg KOH
				Color	Concentration,%						Color	Concentration,%		
7/61	6	220	22	yellow	7.1	440	340	4	218	22	yellow	4.3	89.0	180.5
8/61	6	220	22	–	7.0	440	340	4	219	22	–	4.2	88.4	181.0
9/61	4	220	22	yellow	6.5	440	340	3	220	22	–	3.8	85.4	176.0
10/61	4	220	22	yellow	6.3	440	340	3	220	22	–	3.6	85.4	176.0
11/61	3	219	22	yellow	6.1	435	340	3	218	22	–	3.1	86.1	177.5
12/61	3	219	22	yellow	6.8	440	340	3	219	22	–	3.0	85.5	176.1

When the mixture of glycerin waters was settled, some quantities of fatty acids appeared on their surface and were removed by depletion.

To neutralize water containing sulfuric acid and free fatty acids, it was treated with milk of lime.

Lime milk was prepared by quenching calcined lime, as well as diluting the calcareous creeper with tap water.

Neutralization of acidic glycerol waters after the reactive cleavage of the co-abbreviated fat mixture was carried out with lime milk by stirring with a mechanical stirrer making 65 rpm. At a temperature of 70–83 ° C – until a slightly alkaline reaction (by titration).Neutralization is completed, if 3–5 liters of 0.01 N hydrochloric acid are consumed while titrating 25mm of neutralized glycerin water. This corresponds to an excess of alkali 0.003–0.005% in terms of calcium oxide.

The neutralized glycerol water from all the experiments was then defended, a layer of floating foam, calcium soaps separated, filtered and allowed to evaporate in vacuum at a residual pressure of 10 mm Hg. During the evaporation, sodium sulfate was separated in the flask, from which glycerin was separated by decantation. After cooling at room temperature, some more sulfate was separated from the glycerin, after which all the resulting glycerol batches were filtered and then analyzed.

The glycerin waters of the non-reactive cleavage of co-abstained fatty mixtures contained less organic and mineral impurities, they were neutralized with lime milk, defended, filtered and evaporated in vacuum. During the evaporation of sulfate, the separation was significantly less than when working with glycerol water after cleavage with sulfuric acid and sulphonol.

Since the glycerol water produced by splitting cotton sapstock fat mixtures turned out to be dirtier than the glycerin water obtained in the cleavage of pure triglycerides, it was necessary to develop special processing regimes for treating these contaminated glycerol waters. For this purpose, the following technological regimes for treating co-pumped glycerol waters are proposed.

1. Primary treatment

The combined glycerol waters after the I and II cleavage phases at 80–84 C were neutralized with lime milk until a slightly alkaline reaction, then filtered and evaporated in vacuum with periodic separation of sodium sulfate. However, the resulting glycerin was of low quality and therefore subjected to additional secondary processing.

2. Secondary treatment

Glycerin water after the primary treatment was again neutralized with lime milk, filtration and subsequent treatment at a temperature of 80–82 ° C and agitation with alumina. At the end of the introduction of alumina, glycerol water was mixed for another 1.5–2 hours then defended and filtered.

The excess of alumina was qualitatively determined by adding a small amount of alumina solution to the filtered sample of glycerol water. The absence of a deposit of alumina hydrate indicates that alumina is added to glycerol water in sufficient quantity.

The filtered weakly acidic waters were neutralized with lime, they were defended for another 1.5 hours. and then concentrated by evaporation to 25–30%. The semi-evaporated products were treated with activated carbon at 55–60 ° C and stirred by a mechanical stirrer for 2–2.5 hours. The amount of activated carbon varied widely and was determined depending on the color of the glycerol waters obtained after purification and the quality parameters of the finished glycerin. The purified glycerol water after filtration was finally evaporated in vacuum to a concentration of about 88%.

The results of the studies are presented in (Tables 5 and 6).

In all experiments, the yield of glycerin is about 7% of the weight of neutral fat contained in the cotton soapstock.

In order to study the quality of the glycerol obtained, depending on the methods of treating glycerol waters, separate experiments were performed for the non-reactive cleavage of cotton saphonic fatty mixtures.

Table 5. – Quality indicators of the obtained batches of glycerol depending on the methods of treatment of glycerol waters

Name of glycerol waters after splitting		Glycerin water after primary processing, filtration and partial evaporation			Glycerin after the secondary water treatment, filtration and residue		
№ of ex.	Concentration of glycerol waters to processing	Concentration%	Content,%		Concentration%	Content,%	
			Non volatile organic remnant	ashes		Non volatile organic remnant	ashes
64	9.2	15–20	11.4–11.8	12.5–13.01	83.04	3.85–3.90	3.7–3.8
65	9.6	21.5	12.5–12.7	13.15–13.41	87.10	4.15–4.16	3.91–4.01
66	9.5	19–20	11.1–11.4	12.1–12.3	84.15	4.20–4.48	4.04–4.21
67	10.4	19.5	10.4–11.5	11.0–12.1	83.50	3.95–3.99	3.95–4.31
68	11.0	24.0	11.0–11.1	12.1–12.5	85.10	4.45–4.80	4.11–4.40
69	10.1	20.0	12.0–12.1	11.5–12.5	86.15	4.50–5.01	4.10–4.50
70	9.8	19.0	12.0–12.8	12.0–13.0	84.25	4.14–4.28	4.08–4.15

Glycerin water had a concentration in the range of 6.81–7.4% after the first phase of the cleavage. Glycerin water after the I phase and 3.31–4.50% after the II phase of the cleavage. Glycerin water after the appropriate primary treatment and filtration (see above) were light yellow, and after final filtration and evaporation – light brown. The qualitative characteristics of the products obtained during the splitting and the composition of the treated glycerol waters are shown in (Table 5).

The data in (Table 5) show that, with a non-reactive cleavage of a cotton soapostock fat mixture, the depth of the fatty mixture is achieved to 94.18% and the glycerol water concentration is up to 7.4%.

The glycerin obtained after filtration, secondary processing and evaporation had a concentration of 88.97% and contained a non-volatile organic residue up to 3.65% and ash to 1.49%. According to these indicators, the glycerin obtained corresponded to the requirements of the standard for commercial grade 2 glycerin.

Thus, the expediency of the non-reactive cleavage (hydrolysis) of cotton saphonic fatty mixtures and the production of crude fatty acids and glycerol is shown. At the same time, the depth splitting of the fat mixture 93,4–94,1%, acid number of crude fatty acids 181,5–183,6mg KOH corresponding to the standard TU Uz86–6–98.

Table 6. – Qualitative indicators of glycerin

Soapstock fat, g		Depth splitting		Concentration glycerol water		Glycerol obtained after filtration, secondary processing of glycine. the water of their residue		
Phase I	Phase II	After Phase I	After Phase II	After Phase I	After Phase II	Glycerol at recalculation 88%-percent	Con tent,%	
							Non-volatile organic remnant	ashes
450	425	89.75	93.85	6.81	3.31	86.97	2.56	1.04
450	420	88.70	94.01	7.40	3.41	88.5	2.57	1.49
450	430	88.75	93.15	6.95	4.11	88.0	3.59	1.14
450	425	89.40	94.18	7.01	4.50	88.6	3.65	1.11

The optimal regimes of the non-reactive cleavage of the cotton saopstock fat mixture are established:

– the amount of reaction water in the ratio of fat: water 1: 1;

– The temperature of the process of splitting of the I phase – 6h., Phase II – 4h.

– The pressure in the autoclave is about 2.4 MPa (24 kgf / cm^2).

References:

1. Rukovodstvo po tehnologii polucheniya i pererabotki rastitel` nyih masel i zhirov. VNIIZH,– 1961.– T 3.– 67 s.
2. Kasparov G. N. i dr. "Nepreryivnyiy process razlozheniya soapstokov sernoy kislotoy" MZHP,– 1966.– No. 7.– 14 s.
3. Racional` nyie metodyi ochistki glicerinovyih vod v proizvodstve glicerina – M. CINTI Pisheprom,– 1968.– S. 32–34.
4. Mad T. K. Continous Acidulution of Soapstock and Recovery of Asid oil J. A. O. Ch, Soc.,– 1983.– No. 5.– P. 1008–1011.

Hashimova Esmira Nazim,
Phd., student, the Faculty of Chemical engineering
Azerbaijan State Oil and Industry University,
E-mail: esmira.hashimova@mail.ru
Abilova Ulviya Murshid,
Scientific researcher, the Faculty of Chemistry
Baku State University,
E-mail: u.abilova@mail.ru
Chiraqov Famil Musa,
Professor, the Faculty of Chemistry
Baku State University,
E-mail: Ciraqov@mail.ru

INVESTIGATION OF DETERMINATION OF PALLADIUM (II) ION BY CONCENTRATION WITH NN′-DIPHENYL GUANIDINE FRAGMENTED CHELATE FORMING SORBENT

Abstract: The new sorbent was synthesized from maleic anhydride-styrene copolymer modified by the addition of NN′ – diphenylquanidine and formaldehyde. The method of fixation of palladium (II) ion with a new synthesized sorbent has been developed. The optimum condition has been determined by the sorption and desorption of Pd (II) ions over obtained sorbent.

Keywords: palladium (II), concentration, sorbent, sorption, photometry.

In modern age determination of traces amount of noble metals in geological objects, on magmatic mountain rocks by concentration with natural and synthetic polymer sorbents are widely used. However, it is well known from the literature that the chelate sorbents have great importance in the concentration of noble metals [1, 243; 2, 256]. It is known that for concentration of elements are used polystyrene-based modified complex sorbents, silica gel, porous glass, poly acryl nitrile fibers and modified complex reagents. However, in the literature there is little information about the determination of Pd (II) ions by the sorbents obtained based on maleic anhydride-styrene copolymer. For this purpose, the new sorbent was obtained based on the maleic anhydride styrene copolymer and modified by formaldehyde and NN′ – diphenyl guanidine.

Experimental

The solution of Pd (II) ion of 1000 mg/l was prepared from $PdCl_2$ salt and was clarified by comparison with standards. The equilibrium concentration of the Pd (II) ion in the solution was determined by the spectrophotometric method with using pyrogallol based 2,2,3,4-tetrahydroxy-3′-sulfo-5′-chlorazobenzene reagent. The KCl salt solution was used to form the required value of the ionic force. Ammonium-acetate buffer solution (pH 3–11) and HCl fiksanal (pH 0–2) were used to maintain the pH constant. The KOH solution was prepared by dissolving the calculated mass of KOH in distilled water and then its concentration determined by titration with standard HCl solution. The optical density of the solutions was measured by KFK-2 type photo colorimeter. The pH of the solution was controlled by pH-25 glass electrode ionomer. The

FTIR – spectrum of sorbent was studied in the Varian 3600.

The new NN′– diphenyl guanidine fragmented chelate forming polymer sorbent was synthesized. For this purpose, the known methodology was carried out with radical copolymerization of maleic anhydride and styrol in benzene solution and at water bath (75–80 °C). Benzoyl peroxide was used as an initiator. The obtained copolymer was dried in vacuum. The calculated amount of the formaldehyde and NN′– diphenyl guanidine was added over obtained copolymer. The reaction was carried out for 2 hours without interruption in the water bath at 65–70 °C. The obtained sorbent was washed with water and dried to a constant weight in vacuum at 50 °C. A photometric method was used to determine the absorbed amount of Pd (II) ion. For this purpose, the complexion of Pd (II) ion with 2,2,3,4-tetrahydroxy-3-sulfo-5/-chlorazobenzene was determined by the maximum absorption of the light on the reactive background of the complex λ = 490 nm.

Sorbent identification. The obtained sorbent was identified by the IQ spectroscopy method. In the FTIR spectra of obtained sorbent there are range of absorption band at 3600–3100 cm^{-1} (valent dances of the – OH group in the carboxyl group), 3400–3200 cm^{-1} (valent dance of the –NH group), 1750–1710 cm^{-1} (valent dances of the group –C = O in the carboxyl group), 1570–1550 cm^{-1} (–CH valent dance and deformed dance of – NH group), 1610–1510 cm^{-1} (C–C valent dance in benzene) and 710–680 cm^{-1} (CC deformation dance in benzene).

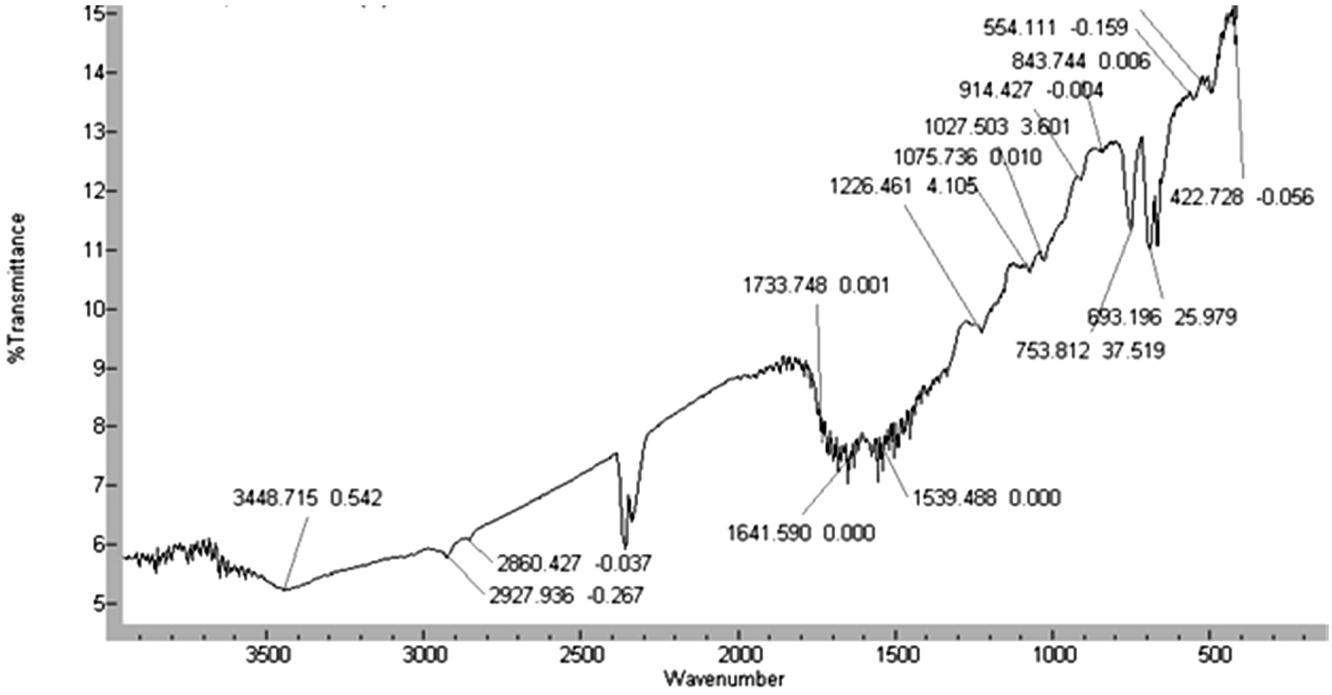

Figure 1. FTIR spectrum of sorbent

Potentiometric titration of sorbent was made by known method. In order to determine the ionization constants the exact static sorption capacity of K+ ions was determined by the potentiometric titration. Based on the results of the titration, a differential curve was constructed (figure 2).

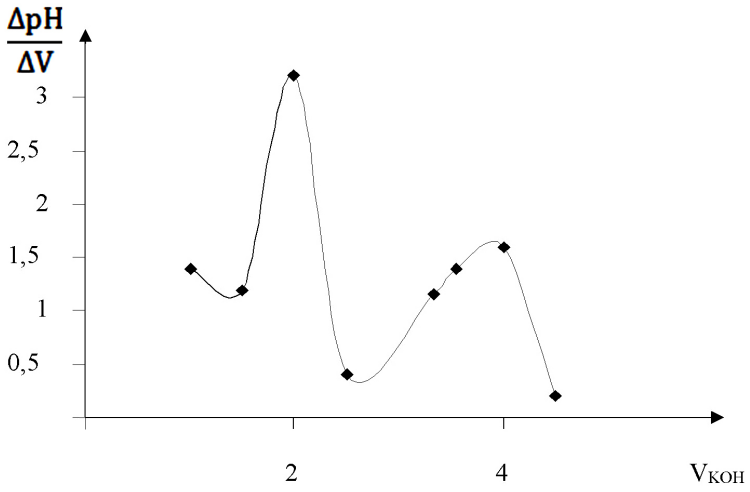

Figure 2. Differential titration curve

Thus, the ionization process of the purchased polymer sorbent will occur in two stages:

$H_2R \leftrightarrow HR^- + H^+$

$HR^- \leftrightarrow R^{2-} + H^+$

During titration, the amount of alkaline used to obtain the first peak is pK1 and the amount of alkaline used to obtain the second peak characterizes pK2. Based on the potentiometric titration, the cost of ionization constants is calculated by the modifier equation of Henderson-Hasselbach. It is known that in a wide range of *a* dependence $pH - \ell g\frac{\alpha}{1-\alpha}$ is a line, and this linear dependence is determined by the graph and calculation of ionization constants of ionogenic groups in sorbent sleeves. The results needed to calculate the ionization constant are shown in Table 1. Investigation of sorption properties was carried out in static conditions.

Table 1.– Determination of sorbent ionization constants ($m_{sorb.}$ = 100.000 mq, C_{KOH} = 0.1M, $p\overline{K}_1 = 4.07$, $p\overline{K}_2 = 8.53$)

α	$\frac{\alpha}{1-\alpha}$	$\lg\frac{\alpha}{1-\alpha}$	V_{KOH},ml	pH	pK_1	α	$\frac{\alpha}{1-\alpha}$	$\lg\frac{\alpha}{1-\alpha}$	V_{KOH},ml	pH	pK_2
0.1	0.(1)	–0.954	0.13	2.87	6.23	0.1	0.(1)	–0.954	1.41	7.78	9.74
0.2	0.25	–0.602	0.26	3.07	5.40	0.2	0.25	–0.602	1.52	7.90	9.27
0.3	0.43	–0.368	0.39	3.29	4.84	0.3	0.43	–0.368	1.63	8.06	8.96
0.4	0.(6)	–0.176	0.52	3.58	4.39	0.4	0.(6)	–0.176	1.74	8.26	8.70
0.5	1.00	0.000	0.65	3.97	3.97	0.5	1.0	0.000	1.85	8.47	8.47
0.6	1.5	0.176	0.78	4.53	3.55	0.6	1.5	0.176	1.96	8.71	8.24
0.7	2.(3)	0.368	0.91	5.21	3.10	0.7	2.(3)	0.368	2.07	8.98	7.98
0.8	4.0	0.602	1.04	6.00	2.54	0.8	4.0	0.602	2.18	9.30	7.67

The effect of pH on the Pd (II) ion in the sorption process was studied by NN/-diphenyl guanidine fragmented chelate sorbent. Experimental data shows that in the investigated heterogeneous system the value of Pd (II) ions distribution coefficient is increased from the acid environment to the weak acid environment and then to neutral environment. The low value of the pH in the fluid phase (pH 0–3) is because the functional groups in the macromolecules are in protonated form and that the polymer sorbent is inflated. The aqueous solution is present in the form of hydroxocomplexes along with the metal ions shown in the pH-4 range. The optimal sorption of the investigated metal ions at the pH range of 4–6

indicates that the sorption mainly goes to the ionized form (HR^-, R^{2-}).

In static conditions, the optimum pH environment (pH-4) was experimented with a constant rate of ionic force, and the aliquot fraction from the liquid phase at different time intervals determined the concentration of metal ion in the solution. Experiments shows that the sorption balance over NN/-diphenyl guanidine fragmented chelate-forming sorbent based on maleic anhydride styrene copolymer forms within 1–2 hours.

The dependence of the sorption process on the ionic force was investigated. Increasing the ionic force of the fluid phase to 0.8 mol/l does not have a significant effect on the degree of sorption. The subsequent increase in ionic force leads to a reduction in Pd (II) ions' sorption rate.

When the concentration of Pd (II) ion is 800 mg/l, the sorbent's sorption capacity is maximal. Effects of the absorbed Pd (II) ion of the various solids ($HClO_4$, HNO_3, H_3PO_4, HCl) and their concentration were investigated from the polymer sorbent desorption. Experience shows that $HClO_4$ acid has better desorption capability. Desorption experiments have been performed in different layers of perxloric acid to determine the optimum condition of desorption. The obtained results are shown in

Table 2. – Effect of acid concentration and volume to desorption of Pd (II) from polymer sorbent

Density and volume of $HClO_4$	**Desorption degree (%)**
0.5 M, 5 ml	96.81
1 M, 5 ml	98.32
1.5 M, 5ml	98.40

Thus, it has been established that the determination of the palladium (II) ion can be accomplished by using sorption-photometric methods in rocks, electrodes, standard alloys.

References:

1. Blok H., Morse R. D., Twaites B. L. Comparison of analysis techniques for gold // J. Geochem. Explor.– 1986.– V. 25.– No. 1–2.– P. 243–244.
2. Hall G. E.M., Bonham C. G.F. Review of methods to determine gold, platinum and palladium in production oriented geochemical laboratories with application of a statistical procedure to test for bias // J. Geochem. Explor.– 1988.– V. 30.– No. 3.– P. 255–289.

Contents